ABSTRACT

SCHULZ, TAYLOR CRAIG. Catalytic Conversion of Cyanobacteria Fatty Acids to Alkanes for Renewable Jet Fuel. (Under the direction of Harold Henry Lamb).

The overall goal of this project was the catalytic conversion of cyanobacteria-derived fatty acids (CBFAs) to hydrocarbons for renewable jet fuel. A freshwater cyanobacterium, *Synechocystis* sp. PCC 6803, was genetically modified to secrete free FAs, specifically lauric acid (LA), into the growth medium, by the Vermaas Lab at Arizona State University (ASU). *Synechocystis* sp. PCC 6803 was grown phototrophically at ASU in bench-top carboys using artificial light and a growth medium that excluded an organic carbon source. Crude CBFAs were adsorbed from the cultures onto polymer resin beads and recovered by elution with methanol and other eluents.

In semi-batch experiments, the model compound LA was deoxygenated via decarbonylation and decarboxylation (DCO) to *n*-undecane (*n*-C_{11}) using a 5 wt. % Pd/C catalyst at 300°C and 15 bar under 1-20% H_2 and at initial concentrations of 4-46 mol. %. Gas-phase products were analyzed using an on-line quadrupole mass spectrometer (QMS), and liquid-phase products were analyzed off line by gas chromatography (GC). Higher H_2 mole fractions in the purge gas resulted in lower CO + CO_2 and *n*-C_{11} yields and CO_2 selectivities. The initial decarboxylation rate and batch productivity increased at lower H_2 partial pressures. The initial decarbonylation rate was independent of H_2 mole fraction in the purge gas. Increasing the initial LA concentration suppressed the initial decarboxylation rate and lowered batch productivity. In contrast, the initial decarbonylation rate increased linearly with LA concentration before saturating at 46 mol. %. Comparison of these data with deoxygenation results for myristic and palmitic acids shows that the initial

decarbonylation rate is independent of FA chain length. In contrast, the initial decarboxylation rate increases significantly with FA alkyl chain length; the initial decarboxylation rate quadruples from LA to palmitic acid.

Methyl laurate (ML), ethyl laurate (EL), methyl stearate (MS), and ethyl stearate (ES) were deoxygenated over 5 wt. % Pd/C at 300 °C and 15 bar under 5 vol. % H_2. These fatty acid esters (FAEs) were shown to be deoxygenated via a two-step process involving hydrogenolysis to either methane or ethane and the corresponding FA followed by FA deoxygenation (via DCO) to a *n*-alkane. ML deoxygenation was demonstrated to follow Langmuir-Hinshelwood kinetics. Changing the ester moiety from methyl to ethyl increased the apparent 1^{st}-order rate constant. For ML, this change nearly doubled the apparent rate constant. The increase in FA chain length from ML to MS also caused the apparent 1^{st}-order rate constant to increase.

CBFAs were deoxygenated over 5 wt. % Pd/C at 300 °C and 15 bar under 5 vol. % H_2. The CBFAs were recovered by adsorption using an anion exchange resin and a hydrophobic resin. GC analysis of the CBFAs determined that LA was the main constituent (~80 wt. %). Activated carbon decolorization, alkaline hydrolysis, acid hydrolysis, precipitation, and C18 adsorption chromatography were all used as purification methods for CBFAs. Semi-batch CBFA deoxygenation over Pd/C determined that adsorption chromatography and alkaline hydrolysis were able to reduce the sulfur concentration below 20 ppm—the empirical threshold for achieving >90% CO_2 selectivity and >80% *n*-alkane yield. β-hydroxymyristic acid (BHMA) was identified as a CBFA constituent using liquid chromatography-mass spectrometry (LC-MS). Semi-batch deoxygenation experiments with reagent-grade material demonstrated that BHMA was converted to *n*-tridecane (*n*-C_{13}), 2-

tridecanone (2-C_{13}-ONE), and 2-tridecanol (2-C_{13}-OH) over 5 wt. % Pd/C. Moreover, addition of BHMA inhibited LA DCO, and this was attributed to preferential adsorption of BHMA on the Pd catalyst.

The model compound *n*-undecane (*n*-C_{11}) was hydroisomerized using bifunctional Pt/zeolite catalysts (Pt/HY, Pt/CaY and Pt/NaY) at 300°C and 500 psig (initial H_2 pressure) in the liquid-phase. Pt/CaY converted *n*-C_{11} with the highest *i*-C_{11} yield at moderate to high conversions. For example, at 89.8% *n*-C_{11} conversion, the *i*-C_{11} yield was 55.1%. For comparison, Pt/HY produced an *i*-C_{11} yield of only 42.8% at a conversion of 89.6%. Alkanes derived from CBFAs via deoxygenation over Pd/C in semi-batch and fed-batch mode were isomerized over Pt/CaY in the liquid-phase at 300°C. Three out of four isomerization reactions reached conversions between 20 and 30%, with isomer selectivities between 86 and 95%. The successful isomerization of *n*-alkanes over Pt/CaY was the last step in demonstrating of an integrated catalytic process for producing synthetic paraffinic kerosene (jet fuel sans aromatics and cycloalkanes) from biorenewable CBFAs.

Catalytic Conversion of Cyanobacteria Fatty Acids to Alkanes for Renewable Jet Fuel

by
Taylor Craig Schulz

A dissertation submitted to the Graduate Faculty of
North Carolina State University
in partial fulfillment of the
requirements for the degree of
Doctor of Philosophy

Chemical Engineering

Raleigh, North Carolina

2014

APPROVED BY:

_____	_____
H. Henry Lamb Committee Chair	Steven W. Peretti
_____	_____
Fanxing Li	Jerry L. Whitten

BIOGRAPHY

Taylor was born April 29, 1988 in Longmont, CO to Brian and Kathy Schulz. After having lived in Colorado and Montana, the family settled in State College, PA. Taylor graduated from State College Area High School in 2006, where he was a member of cross-country team, as well as the concert band. He graduated from the Pennsylvania State University in 2010 with a B.S. in Chemical Engineering and a minor in Economics.

ACKNOWLEDGMENTS

First and foremost, I would like to thank my family for their continuous support over the past 26 years. I'd also like to thank them for instilling in me the value of persistence and resilience. I would not have gotten this far without them. Mom, thank you for blessing me with your sense of humor and for supporting my many passions. To my father, your continued pursuit of your own degree inspires me. Kara, you have become my best friend and a constant source of positivity.

I'd also like to thank Dr. Lamb for his mentoring over the past four years. Working in your lab has been an invaluable experience. I'd like to thank you for challenging me as a scientist, and I plan to use the skills I've acquired during the course of my work to further our understanding of heterogeneous catalysis.

I'd like to thank my group members (past and present) for all of the knowledge they have provided me with. Jeff Ford, I would like to thank you for training me on the liquid-phase reactor system. Dr. Keyi Sun, thank you for your collaboration. Simon Thompson, thank you for answering the questions I wanted to ask no one else.

To the staff, thank you for all that you do to make this department run as smoothly as it does.

My friends, whether near or far, deserve to be recognized as well. They have provided me with experiences and friendship that cannot be replaced. To Adria, Dennis and Simon ("The Band"), I'd like to thank you for taking time out of your schedules to play music with me. I'd like to thank "The Crew" for keeping in touch and keeping me laughing. To Diana, Matt, etc., our many weekend reunions were a necessity.

TABLE OF CONTENTS

LIST OF TABLES

LIST OF FIGURES

LIST OF EQUATIONS

CHAPTER 1: Introduction

The economic and environmental impacts of fossil fuels have been studied for decades and are relevant now more than ever. A primary economic concern associated with the use of fossil fuels is the assumed finite supply of these fuels. In 1956, M. King Hubbert introduced the idea of "peak oil," which is when production of crude oil reaches a maximum. Along with the idea that production of oil would reach a maximum and never recover, Hubbert also stated that this would occur somewhere between 1965 and 1970, which was quasi-confirmed with a decline in production in the early 1970s [1, 2]. This situation was further compounded by the oil embargo of 1973, which caused a short-term non-equilibrium in the oil market and subsequent price increases [2]. To alleviate this massive price increase, the United States became a major importer of petroleum. Further aiding the idea of peak oil is an economic inefficiency involved in the extraction of crude oil from the Earth, which presents itself in two fashions. The first of these is the increased price required to recover oil from smaller reserves, making it economically unfeasible to do so. According to "Sustainability Science" by John Ayers at Vanderbilt University, approximately 85% of all crude oil comes from nearly 5% of all oil fields [1]. This economic inefficiency also shows itself in the form of increased cost and energy involved in extracting a large percentage of the reserve from each field, no matter the size. Primary extraction techniques remove anywhere from 25-40% of the reserve [1, 2]. Controlling the reservoir pressure by injecting other gases and liquids into the reservoir can increase recovery efficiency only to 50-60%, leaving much of the crude oil untouched [1]. Proponents of the peak oil theory have pointed to the decline in discovery of new fields as evidence that Hubbert was indeed correct. Peak oil opponents

point to the fact that most new oil comes from additional exploration of already proven reservoirs [2]. Peak oil, and its effect on the price of crude oil, is still being fiercely debated.

While the debate over the global supply of oil may be important, the demand for fossil fuels, and its effect on the environment, is possibly the more important problem. This demand seems to be driven mainly by the development of new economies and an overall growth of the world economy [3]. When discussing the environmental impact of trade, the concept of the "Environmental Kuznets Curve" must first be explained. The "Environmental Kuznets Curve," named by Grossman and Krueger in 1993, is the relationship between income per capita and environmental damage and takes the form of an inverted "U." At very low levels of income, there is almost no damage to the environment, presumably because there is very little industrial activity. This environmental damage sharply increases as the income per capita increases. Once an income per capita threshold has been met, the environmental damage levels off. Continuing increases in income per capita cause a large drop in environmental damage, mainly because countries with such a large income per capita finally have the means to enact meaningful environmental legislation. For SO_2, the income threshold was determined to be between $5,000 and $6,000, which still exceeds the income per capita of many developing countries. The "Environmental Kuznet Curve" also holds for NOx emissions and particulate matter. This relationship was thought not to hold for CO_2, as it appeared that the amount of CO_2 emitted to the atmosphere accelerated with the level of economic growth. This was later shown to be false, with CO_2 indeed following the same "Environmental Kuznets Curve."

The Kyoto Protocol, and the wealthy countries involved in its formation, may have been the reason that CO_2 followed this trend. However, it was concluded that atmospheric CO_2 levels are heavily influenced by trade [4]. Between 1990 and 2000 CO_2 emissions increased at a rate of 1% per year, but between 2000 and 2008 that rate was almost triple at 3.4% per year. Most of the increase in emissions since 1990 has been due to emerging economies in developing countries, many of which do not abide by the standards set forth by the Kyoto Protocol. Shifts in advanced economies from manufacturing to services and an increase in international trade have been identified as the major source of CO_2 emissions increases in developing countries not adhering to the Kyoto Treaty. China, specifically, has been a main contributor to the increase in CO_2 emissions since 1990. In 1990, 16% of all Chinese CO_2 emissions were due to exportation of goods, with this number jumping up to 30% by 2005. In the United States, national emissions jumped by 6% between 1997 and 2004. However, emissions due to import of international goods have jumped 17% over the same time period [3]. It should also be noted that while the United States was instrumental in the formation of the Kyoto Protocol and has signed it, it has no intention of ratifying the document [5]. The most recent global economic recession caused the rate of CO_2 emission to drop to 2.0% for 2007 and 2008. In a 2009 paper published in Nature Geoscience, using the IMF prediction for a drop in global GDP and the decrease in carbon intensity for world GDP, the rate of CO_2 emission was expected to drop by nearly 2.8% [3].

Biorenewable liquid fuels are one method for relieving environmental stresses caused by fossil fuel demand. The first generation of biorenewable liquid fuels was focused on bioethanol and biodiesel, which are produced by sugar and starch fermentation and

triglyceride esterification, respectively [6]. First-generation biorenewable liquid fuels encounter three major problems: the "food vs. fuel" dilemma, low energy content and poor chemical stability. The "food vs. fuel" dilemma is encountered when feedstocks used for renewable fuel are also used as a food source, both for humans and the animals that they consume. Corn ethanol, is a prime example of a renewable fuel with a feedstock that encroaches on the "food vs. fuel" dilemma. Between 1999 and 2011, the total amount of corn produced in the United States increased by about 30%, from a little less than 10 billion bushels to almost 12.5 billion. Over that same time period, corn used for ethanol production increased from 0.6 billion bushels to 5 billion bushels, an increase in the proportion of corn used for ethanol from 6% to 40%. The total amount of corn and amount used for ethanol production dropped in 2012 due to drought conditions, but the proportion of corn used for ethanol remained near-constant [7]. Government and mandates, such as the Renewable Fuel Standard and tariffs on sugarcane ethanol imports, have fueled the recent increase in biofuel production and have made the United States the largest biofuel producer in the world [8, 9]. In a paper published for the World Bank in 2011, it was determined that increases in biofuel production were responsible for 20% of the corn price increase between 2001 and 2007 [9]. This number has also been reported as high as 60% [8]. These increases in domestic corn prices are extremely important to the world market. The United States exports the most corn in the world, which actually only accounts for 15% of the demand for U.S. corn. The relatively small impact of global corn demand on the U.S. market has created a situation in which the international community has had to adjust their prices based on the U.S. market [10]. The increase in demand for corn for ethanol, and the corresponding price increase, will

most likely leave importers, which are mainly developing countries, facing prices they may not necessarily be able to pay.

The high oxygen content in many first generation biofuels contributes directly to two problems listed above, lower energy density and decreased chemical stability. Ethanol and methanol have especially low energy densities relative to gasoline and diesel fuels. Methanol, which is mainly produced from natural gas, has an energy density between 57,000 and 65,000 Btu/gal has almost half the energy density of gasoline and diesel, which have energy densities between 116,000 and 124,000 Btu/gal and 128,000 and 137,000 Btu/gal, respectively. Ethanol has an energy density between 76,000 and 84,500 Btu/gal, which is still quite low compared to traditional transportation fuels [7]. Other fossil fuels used for transportation, which include jet fuel, have similar energy densities to gasoline and diesel. Jet-propulsion fuel 5 (JP-5) has an energy density of about 120,000 Btu/gal. Jet-propulsion fuel 8 (JP-8) has an energy density of approximately 119,000 Btu/gal [11]. Biodiesel is one of the first generation biofuels that actually has a comparable energy density to fossil fuels with a value between 120,000 and 128,000 Btu/gal [7]. While the oxygen content in biodiesel may not diminish its energy density, it does cause chemical stability problems. Regular diesel fuel has a shelf life of almost a year, but biodiesel has a shelf life of nearly half that at 6 months. Beyond these six months, the biodiesel is expected to have a decrease in quality and must be mixed with a stabilizer to lengthen its shelf life [12]. This six month window appears to be true for soy and canola-based biodiesel. Biodiesel produced from palm oil and animals fats usually lasts for almost nine months without additives [13]. The oxygen content in biodiesel also causes a major problem when trying to use the fuel in colder

climates. This problem is a gelling, or even solidification, of the fuel at lower temperatures, which seemingly limits the climates in which biodiesel can be used. The cloud point is the temperature at which the very first crystals appear in the fuel. This is followed by the cold filter plugging point, which is where the lines and filters in the automobile become clogged with the fuel. The final stage of biodiesel solidification is called the pour point, which is the lowest temperature at which the fuel will flow. The biodiesel cloud point is also dependent on the source of the feed triglycerides, with more saturated fats having a higher pour point. This gelling problem can effectively be mitigated by blending the biodiesel into petroleum diesel in concentrations up to 5% [14].

Second-generation biofuels were designed with the aim of avoiding the "food vs. fuel" debate and increasing land usage efficiency. Lignocellulosic biomass and other non-edible plant residues/biomass are used as feedstocks for second-generation biofuels [6]. The Centia™ process is one example of a second-generation biofuels process that could supplant first-generation biofuels as the main source of alternative transportation fuel. This process includes three steps: hydrolysis of the triglycerides (TAGs) to produce fatty acids (FAs), deoxygenation of the FAs to alkanes, and then hydroisomerization of the resulting alkanes [15]. This technology is especially important for two reasons. The first of these was mentioned in the previous paragraph, and that is that the resulting fuel can be used in already-existing transportation infrastructure. The second of these reasons is that fat from nearly any source can be converted to fuel. Waste cooking oil, which is notoriously dirty, can be used in this process. The ability to use waste oil is beneficial on two levels: it is

economically responsible as waste oil is much cheaper than a virgin feedstock and it also avoids competing with a food source [16].

While the Centia™ process is an improvement on many of the first-generation fuels, it also can be improved on, *i.e.* other technological improvements can eliminate steps in the Centia™ process. Recent advancements in the genetic modification of cyanobacteria has all but eliminated the triglyceride hydrolysis step of the Centia™ process. Lipid and FA production from marine and freshwater cyanobacteria has been studied for decades. One study showed that lipid yield from four freshwater cyanobacteria strains (*Anabena cylindrica*, *Anacystis nidulans*, *Nostoc canina*, and *Nostoc muscorum*) was extremely low, around 10-12% by weight. The FA profiles from these same strains were also determined to contain both saturated and unsaturated C_{16} and C_{18} TAGs [17]. Studies with other strains of freshwater and marine cyanobacteria showed that the FA profiles associated with the TAGs were in that same chain length range. *Synechocystsis* sp. PCC6803 and PCC6308, freshwater cyanobacteria strains, were shown to have FA profiles that included C_{14}, C_{16} and C_{18} FAs [18, 19]. The genetic code for *Synechocystis* sp. PCC 6803 has been thoroughly documented, making *Synechocystis* sp. PCC 6803 a prime candidate for further genetic modification and experimentation [20, 21]. This genetic modification was done with the intention of solving two problems involved with implementing TAGs derived from microalgae and bacteria as possible biofuel feedstocks: the intense energy required for extracting lipids from biomass and the environmental stresses required to coax the cyanobacteria into producing TAGs. One major advancement in algal biofuel production was the genetic modification of *Synechocystis* sp. PCC6803 to promote cell lysis in the presence of $NiSO_4$ [22]. This provided a simple

way to collect biofuel feedstocks from cyanobacteria. One major drawback of this study was that the cyanobacteria were killed during the collection process. Further work by this same group aimed to avoid this problem altogether. In a subsequent study, the same strain of Synechocystis was modified to overproduce FAs and then secrete them through the cell membrane into the growth medium, thus avoiding the problem of killing the cyanobacteria in order to harvest the desired product. This work also broadened the chain length range of FAs being produced by the cyanobacteria. The bacteria produced fully saturated C_{10} FAs and C_{12} FAs, which are ideal for producing jet fuel range hydrocrabons [23].

In the past few years, FA deoxygenation over heterogeneous precious metal catalysts has become the focus of intense research. The general landscape of fatty acid deoxygenation has been established in a short time: a number of metals and supports have been tested for their efficacy in FA deoxygenation, the reaction pathways have been established, and a number of process variables have been explored. In order to understand exactly how the metals and supports were judged for their FA deoxygenation efficiency, the deoxygenation pathways must first be understood. There three pathways through which FA deoxygenation happens: decarboxylation, decarbonylation and hydrogenation/dehydration. Decarboxylation occurs when CO_2 is removed from the FAs and a fully saturated hydrocarbon is produced. Decarbonylation occurs when CO is removed from the FAs and H_2O and a terminal alkene are produced. This alkene can then potentially be hydrogenated to an alkane, depending on the metal used for deoxygenation. The third pathway for FA deoxygenation is a hydrodeoxygenation reaction by which oxygen is removed on the form of water and no

carbon-carbon bonds are broken. These reactions are shown below in Equations 1.1-1.3. R represents a saturated alkyl product, and R' represents an unsaturated alkyl product.

Equation 1.1: Decarboxylation $R - COOH \rightarrow R - H + CO_2\ (g)$

Equation 1.2: Decarbonylation $R - COOH \rightarrow R' - H + CO\ (g) + H_2O\ (g)$

Equation 1.3: Hydrodeoxygenation $R - COOH + 3\ H_2\ (g) \rightarrow R - CH_3 + 2\ H_2O\ (g)$

Decarboxylation and decarbonylation are the two main pathways for FA deoxygenation over Pd [24, 25]. The preferred pathway is the decarboxylation pathway, as it does not produce CO, which is a known noble metal catalyst poison, and it does not produce an unsaturated hydrocarbon product, which would consume hydrogen upon saturation. There is a debate in catalysis community as to whether these two main pathways are independent or not. This uncertainty stems directly from the fact that precious metals that are active for FA deoxygenation are also active for the water-gas shift (WGS) reaction, which is shown below as Equation 1.4.

Equation 1.4: Water-gas shift $CO\ (g) + H_2O\ (g) \rightleftharpoons CO_2\ (g) + H_2\ (g)$

When the WGS reaction is combined with the decarbonylation and alkene hydrogenation reactions, the resulting reaction products are the same ones produced by the decarboxylation reaction. Supported Pd catalysts are active for the WGS reaction, making it

nearly impossible to discern how much of the CO_2 produced during FA deoxygenation is due to decarboxylation and how much is due to the WGS reaction [25, 26]. A study from 2010 explored the role of the WGS reaction in FA deoxygenation and found that the WGS reaction could not account for the high CO_2 selectivity during stearic acid (C18:0, SA) over 5 wt. % Pd/C. SA deoxygenation over Pd/C exhibited a 95% CO_2 selectivity. Using the Gibbs free energy, the equilibrium CO_2 yields under the test conditions were determined to be all above 98%. The CO_2 yield from the WGS reaction over did not exceed 70%, which is well below both the aforementioned SA CO_2 selectivity and equilibrium WGS CO_2 yields. This fact led to the conclusion that the WGS alone could not account for the high CO_2 selectivity shown during SA deoxygenation [25].

As stated previously, quite a few metals have been tested for their FA deoxygenation ability. Pd is by far the most widely studied precious metal for this reaction [24, 25, 27-33]. Deoxygenation studies with Pd have shown that Pd can efficiently convert FAs, fatty acid esters (FAEs) and TAGs to fully deoxygenated alkane products. Platinum (Pt) has also been shown to be active for FA, FAE and TAG deoxygenation [32, 34, 35]. SA deoxygenation over Pd and Pt exhibited high conversion and high selectivity for n-heptadecane (n-C_{17}) [36]. Though Pd and Pt are effective for producing alkanes from FAs, their high cost is prohibitive to using them in a large-scale FA deoxygenation plant. The need for a cheaper metal has spurred research into other metals. Both nickel (Ni) and copper (Cu) have been tested for their ability to deoxygenate FAs. Ni was found to be much less active for SA deoxygenation than Pd and Pt. It was also much less selective to n-C_{17} than Pd and Pt, with a large percentage of the product distribution coming from alkane cracking [36, 37]. 5 wt. % Cu/γ-

Al_2O3 was used to deoxygenate SA under an inert atmosphere. The catalyst exhibited 96% conversion and 21% selectivity to paraffinic products. 61% of the products from this reaction were olefins [37]. Ruthenium (Ru) supported on magnesium oxide was also shown to be active for SA deoxygenation, but the reaction was exclusively selective to a dimer product unlike FA deoxygenation over Pd and Pt [36].

The metal is not the only part of the catalyst that influences how the reaction proceeds. Catalysts supports are used to stabilize the active metal nanoparticles and maximize the number of available active sites [38, 39]. These supports can also be highly influential in determining how active a catalyst is and how selective it is for a desired product. This support effect has explored over a few metals in great detail. The support used to disperse Ru was shown to be extremely influential in the deoxygenation of SA. Holding the active metal content constant for each catalysts, it was determined that MgO is the most effective support. SA deoxygenation over Ru/MgO reached a conversion of 96%. Neither Ru/SiO_2 nor Ru/C reached a conversion exceeding 15% [37]. This support effect has also been illustrated with supported Pd catalysts. Semi-batch SA deoxygenation was conducted over 5 wt. % Pd/C, $PdSiO_2$ and Pd/Al_2O_3 under 5% H_2 at 300 °C at 15 atm. SA deoxygenation reached near full conversion over all three catalysts. Though the level of conversion did not seem to be affected by the support, the CO_2 selectivity was high influenced by the support, with the order appearing as follows: $Pd/C>Pd/Al_2O_3>Pd/SiO_2$. All three catalysts were tested via N_2 physisorption for their BET surface area, total pore volume and micropore volume. Pd/C exhibited a surface nearly four times that of Pd/SiO_2 and Pd/Al_2O_3. The micropore volume of Pd/C was also one to two orders of magnitude larger

than that of Pd/SiO_2 and Pd/Al_2O_3. The only metric tested where Pd/C did not exceed the others was in total pore volume, where the trend was determined as follows: Pd/SiO_2>Pd/C>Pd/Al_2O_3. The difference in CO_2 selectivity was concluded to be determined by the difference in surface area and micropore volume [28]. Though carbon seemed to be the best support for FA decarboxylation over Pd, other supports have also shown to be quite effective for this reaction. MgO is one of these supports. Pd/MgO was determined to be a highly effective FA decarboxylation catalyst. Oleic acid (C18:1, OA) decarboxylation over Pd/MgO to n-C_{17} at high liquid-phase yield (94%) was demonstrated for over 150 hours [40]. Though other supports are just as effective for metal dispersion and enhance FA decarboxylation activity, carbon is generally preferred due to its ease of separation from the active metals. This attribute makes catalyst recycling a much more efficient process [38].

The type of carbon used to support the catalyst may also have an effect on how the catalyst behaves during reaction. Carbon supports fall into two categories: carbon black (CB) and activated carbon (AC). CB is produced by the pyrolysis of hydrocarbons. AC is generated through two different processes: chemical and physical activation of carbonaceous material. Chemical activation is the simultaneous carbonization and activation of a raw material with H_3PO_4 or $ZnCl_2$ at 600-800 °C. Physical activation is the process of exposing an already carbonized material to either steam or CO_2 at 800-1100 °C [38]. These activation processes cause the AC to exhibit much higher specific surface areas and pore volumes than CB [38, 41]. Both types of carbon supports have the same surface functional groups, which are postulated to consist mainly of strong acidic carboxyl groups, weakly acidic carboxyl groups, phenolic hydroxyl groups, and carbonyl groups [38, 42]. The structural differences

between the two types of carbon supports dictate what reactions each support can be used for. CB-supported catalysts has been shown to be an effective catalyst for hydrogenation of dinitrotoluene and as electrocatalysts for fuel cell applications [38]. AC-supported catalysts have proven to be efficient for hydrogenation of halogenated nitroaromatic compounds, glucose oxidation, and the isomerization of polyunsaturated fatty acids [38, 39]. These carbon supports can also be pretreated to enhance the activity of the catalyst. Addition of oxygenated groups to the carbon supports via exposure of the support to HNO_3 or oxygen can increase the dispersion of the catalyst and the rate of reaction [41, 43].

Modification of carbon supports such as multi-walled carbon nanotubes (MWNTs) and carbon nanofibers (CNFs) with oxygenated groups has shown that these modifications can slow reaction kinetics for certain reactions. In one study, the effects of oxygenating MWNTs impregnated with Pt was examined. One batch of MWNTs was merely impregnated with Pt and used as the control. The MWNTs also treated by refluxing in HNO_3 overnight. Part of this batch was then heated in He in order to remove all of the surface oxygen groups. Both of these supports were also impregnated with Pt. Test reactions included aqueous phase reforming (which produces H_2 and CO_2 from ethylene glycol), decalin and cyclohexane dehydrogenation, and gas phase reforming of ethylene glycol. It was determined that the HNO_3 treatment increased the surface area and the metal dispersion of the catalyst. The catalyst turnover frequency for the aqueous phase reforming and dehydrogenation reactions dropped when the MWNTs were modified via HNO_3 [44].

Another study tested a surface modification process with SA deoxygenation over Pd. CNFs were oxygenated via HNO_3 treatment, and Pd was deposited on these CNFs. Surface

oxygen groups were removed from a sample of these CNFs to determine how the lack of surface oxygenated groups would affect the deoxygenation of SA. The Pd/CNF samples that had their surface oxygen groups removed were treated once again with HNO_3. However, this second treatment was done in the gas phase. It was found that Pd/CNFs with no oxygenated groups on the surface and Pd/CNFs that had been treated with gas phase HNO_3 had the same Pd dispersion, but very different levels of SA deoxygenation activity. Both catalysts exhibited Pd particles around 7 nm. At 250 °C, Pd/CNFs that had been modified with gas phase HNO3 reached an *n*-C_{17} yield of 60% at a reaction time of 70 h. Pd/CNFs that had not been modified only reached an *n*-C_{17} yield of approximately 10% over the same reaction time. The data also showed that the activation energy for SA deoxygenation dropped by a little over 40% (from 140 kJ/mol to 80 kJ/mol) due to the surface modifications made by HNO_3 treatment. It was posited that this increased activity stems from increased polarity due to surface modification, which in turn changed the way that the SA interacted with the CNF surface. This was illustrated in this published study and is shown below as Figure 1.1. When the surface oxygen content was high, it was inferred that the polar head of the SA molecule interacted with the support, facilitating interaction with the Pd particle. It was inferred that the aliphatic chain of SA selectively adsorbed to the CNF surface when the oxygen content was low, thus slowing the interaction of the carboxylic acid group with the Pd nanoparticle [45].

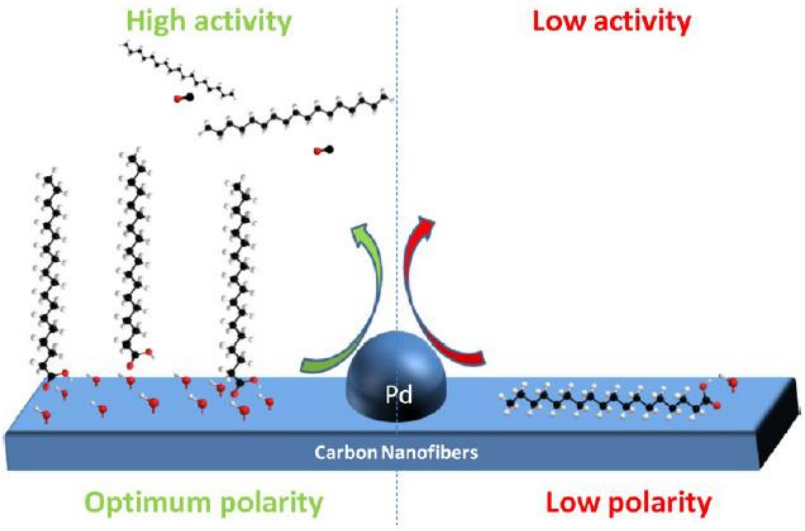

Figure 1.1: Adsorption of SA onto CNF surface at high surface oxygen content (left) and low to no surface oxygen content (right) [45].

This study showed that while the activation energy dropped and the total product yield increased with surface modification with oxygen groups. However, this work did not further the understanding of how modification of the carbon surface affected the deoxygenation pathway.

Factors other than active metal and support also influence how the catalyst deoxygenates FAs. These factors include, but are not limited to, the following: H_2 partial pressure, solvent and FA concentration. The same study that elucidated the support effect of SA deoxygenation over Pd also studied the effect of H_2 partial pressure on the system over the Pd/SiO_2 and Pd/C samples. Gas feed streams with 5% and 10% H_2 by volume were used to test this effect. Under both conditions, near full conversion was achieved over the course of the four hour reaction. While the increase in H_2 partial pressure did not lower the

conversion, it significantly decreased the reaction CO_2 selectivity. For the SiO_2-supported samples, the CO_2 selectivity dropped from 50-66% to 3-17% when the H_2 partial pressure was doubled. The carbon-supported sample was less affected by the H_2 partial pressure increase, but the change was still substantial with CO_2 selectivity dropping from 95% to 77% [28]. SA deoxygenation over Pd/C under an inert atmosphere has also been studied. When under He, SA is deoxygenated to full conversion via decarboxylation and yields a mixture of n-C_{17} and n-heptadecene. By the end of the reaction, the selectivity of the reaction to n-C_{17} was at 98%, which was explained by a transfer of hydrogen from the alkane solvent to the alkenes. This study also showed that although the initial rate of decarboxylation was higher under He, n-C_{17} was produced at a much faster rate under 10% H_2 [24]. This difference in n-C_{17} production rate indicates that hydrogen transfer from the solvent to the alkene is a relatively slow process. This H_2 effect was also studied for lauric acid (C12:0, LA) deoxygenation over Pd/C with pure hydrogen and pure argon as reaction atmospheres. It was shown that deoxygenation produces fully saturated hydrocarbons much faster in the presence of H_2, even at an extreme concentration.

The effect of H_2 partial pressure on the semi-batch deoxygenation of LA and two related compounds, lauryl alcohol and lauryl aldehyde has also been studied. In this work, 100 mL of 0.05 M LA solution was deoxygenated in semi-batch mode under pure Ar and pure H_2 over 100 mg Pd/C. The carbon used as a support was Sibunit, which is a synthetic mesoporous carbon [46, 47]. Initially, the reaction under Ar was more active than the reaction under H_2. After the 5 h reaction time, the experiment involving pure H_2 reached a LA conversion of 65%, while the reaction involving Ar reached a LA conversion of 43%.

The reaction involving pure H_2 also produced a much higher *n*-C_{11} selectivity, which is expected [46]. Deoxygenation of SA over Pd/C (E117) under He and 10% H_2 showed that the initial rate of deoxygenation was much higher under He, but that the rate slowed substantially due to formation of unsaturated hydrocarbons. Both reactions reached full conversion by the end of the 5 h reaction time [24]. The drop in conversion with the decrease in H_2 partial pressure in the Pd/Sibunit work appears to directly conflict with what is shown above. However, this difference is most likely due to a difference in the carbon support structure. The Pd/Sibunit C catalyst had a surface area of 357 m^2/g [46].

The commercial catalyst used in the work shown above, and previous FA deoxygenation studies, had a surface area of 800 m^2/g [24, 28]. Pd supported on activated carbon has the ability to spill hydrogen atoms onto the support surface, which is promoted by the support oxygenated functional groups [48]. The decrease in surface area means a decrease in the ability to store H_2. The nature of the synthetic carbon structure may have also reduced the number of hydrogen atoms that were able to be stored on the support surface. It is unknown if or how this Sibunit carbon was activated, which means that it is possible that the support could have had no surface oxygen groups at all. During LA deoxygenation over Pd/Sibunit under Ar, it is likely that all surface hydrogen was used early in the reaction and that the catalyst became severely deactivated.

The solvent used to suspend the catalyst and dissolve the feedstock can be highly influential in determining which deoxygenation pathway will occur. In the same paper that explored the H_2 effect of SA deoxygenation over Pd/C, the effect of the solvent used was also elucidated. Dodecane (C_{12}) and n-C_{17} were both explored as solvents for SA

deoxygenation. Under 10% H_2, it was found that SA decarboxylation happened nearly six times faster when the catalyst and FA were in the C_{12} solvent. This was attributed to the low partial pressure of the n-C_{17} solvent, which increased the H_2 partial pressure in the reactor [24]. The aliphatic chain length of the FA also has a large influence on the decarboxylation rate and overall CO_2 selectivity of the reaction. Every even numbered FA between decanoic acid (C10:0, DA) and SA was deoxygenated over Pd/C. SA exhibited a CO_2 selectivity nearly 10 percentage points higher than DA and was decarboxylated at a rate nearly 20 times that of DA. This difference was attributed interactions between the FAs and the activated carbon support, with longer chain FAs more readily adsorbing to the support surface [28].

FA concentration also has the ability to determine which pathway is used and how fast these pathways occur. Palmitic acid (C16:0, PA) at four different concentrations (6, 12, 24 and 48 wt. %) was deoxygenated over 5 wt. % Pd/C. The CO_2+CO yields, pentadecane (*n*-C_{15}) yield and CO_2 selectivity decreased as the PA concentration was increased. Between 6 and 24 wt. % the decline in all three of these metrics was only slight. Once the initial PA concentration reached 48 wt. %, all three of these dropped off significantly. One metric that increased with the increase in PA concentration was the hourly batch productivity of the catalyst, which is the number of moles of CO and CO_2 produced per gram of catalyst per hour that the reactor was at the reaction temperature of 300 °C. This batch productivity increased when the initial PA concentration was increased from 23.5 at 6 wt. % to 43.1 at 24 wt. %. When the PA initial concentration was increased to 48 wt. %, this batch productivity dropped to 19.4, below any of the other values. The initial decarboxylation rate dropped

from 71 mmol/g_{cat}-h to 20 mmol/g_{cat}-h across the concentration series, while the initial decarbonylation rate increased from 2 mmol/g_{cat}-h to 20 mmol/g_{cat}-h [49].

The effect of weight-hourly space velocity (WHSV) and initial LA concentration in continuous LA deoxygenation over powder Pd/C under N_2 was also studied. WHSV is defined as the reactant mass flow divided by the catalyst mass. A mixture of LA and C_{12} (0.22 mol/L LA) was pumped to the reactor in different volumetric rates to test the effect of increasing WHSV. It was found that the overall rate of deoxygenation decreased exponentially to a steady state as the WHSV was increased by a factor of ten. The final deoxygenation rate was only a half of its original value. The effect of LA concentration was tested by injecting three LA/C_{12} solutions with different LA concentrations (0.22 mol/L, 0.35 mol/L and 0.44 mol/L) over the catalyst bed at the same volumetric flow rate. This experiment showed that the deoxygenation rate reached a maximum at a concentration of 0.35 mol/L [50].

Deoxygenation of FAEs over Pd catalysts has mainly involved ethyl stearate (ES). It has been shown that ES is deoxygenated to *n*-C_{17} and *n*-heptadecene with an SA intermediate product [27, 51]. It was also shown that FAEs exhibit lower conversions over the same reactions times than FAs [51]. It was also shown that gas phase products from ES deoxygenation include CO, CO_2, and ethane (C_2H_6) [52].

The objective of this project was to convert photosynthetically derived fatty acids into hydrocarbons for bio-jet fuel. This process is considered carbon-neutral, as the CO_2 that is produced during the fatty acid (FA) deoxygenation process and the combustion of the fuel mixture is then used in photosynthesis to create more FAs. A freshwater cyanobacterium,

Synechocystis sp. PCC 6803, that had been genetically modified to secrete free FAs, specifically lauric acid (LA), into the growth medium were grown in the Vermaas Lab at Arizona State University (ASU). *Synechocystis* sp. PCC 6803 was grown phototrophically in bench-top carboys using artificial light in a growth medium that did not include an organic carbon source. After recovery and purification, the FAs produced by *Synechocystis* sp. PCC 6803 were deoxygenated over Pd/C and the resulting alkane product was subsequently hydroisomerized over Pt/CaY to produce an alkane product similar to jet fuel.

References

[1] J. C. Ayers, "Sustainability Science," ed, 2011.

[2] D. Yergin, "There Will Be Oil," ed, 2011.

[3] C. Le Quere, M. R. Raupach, J. G. Canadell, G. Marland, L. Bopp, P. Ciais, *et al.*, "Trends in the sources and sinks of carbon dioxide," *Nature Geoscience*, vol. 2, pp. 831-836, Dec 2009.

[4] J. Frankel, "Environmental Effects of International Trade," ed, 2009.

[5] (2014). Available: http://unfccc.int/kyoto_protocol/items/3145.php

[6] P. S. Nigam and A. Singh, "Production of liquid biofuels from renewable resources," *Progress in Energy and Combustion Science*, vol. 37, pp. 52-68, Feb 2011.

[7] (2013). *Alternative Fuels Data Center-Fuel Properties Comparison*. Available: http://www.afdc.energy.gov/fuels/fuel_comparison_chart.pdf

[8] X. G. Chen and M. Khanna, "Food vs. Fuel: The Effect of Biofuel Policies," *American Journal of Agricultural Economics*, vol. 95, pp. 289-295, Jan 2013.

[9] G. Hochman, D. Rajagopal, G. Timilsina, and D. Zilberman, "The Role of Inventory Adjustments in Quantifying Factors Causing Food Price Inflation," ed: The World Bank, 2011.

[10] (2014). *USDA ERS - Corn: Trade*. Available: http://www.ers.usda.gov/topics/crops/corn/trade.aspx#.U5OR-_ldWSp

[11] N. R. Council, "Permissible Exposure Levels for Selected Military Fuel Vapors," 1996.

[12] *Managing the Supply Chain*. Available: http://agr.wa.gov/inspection/weightsmeasures/docs/Cerio_National_Biodiesel_Board.pdf

[13] *Biodiesel: Myths versus Facts*. Available: http://www.crimsonrenewable.com/FactVsMyth.pdf

[14] N. B. Board, "Biodiesel Cold Flow Basics," ed: National Biodiesel Board, 2014.

[15] "Centia™ – An Innovative Technology for Converting any Renewable Oil into High-Value Biofuels ", ed.

[16] "Fats into jet fuel -- NC State "green" technology licensed," ed, 2007.

[17] A. K. Sallal, N. A. Nimer, and S. S. Radwan, "LIPID AND FATTY-ACID COMPOSITION OF FRESH-WATER CYANOBACTERIA," *Journal of General Microbiology,* vol. 136, pp. 2043-2048, Oct 1990.

[18] H. Wada and N. Murata, "TEMPERATURE-INDUCED CHANGES IN THE FATTY-ACID COMPOSITION OF THE CYANOBACTERIUM, SYNECHOCYSTIS PCC6803," *Plant Physiology,* vol. 92, pp. 1062-1069, Apr 1990.

[19] M. V. Merritt, S. P. Rosenstein, C. Loh, R. H. S. Chou, and M. M. Allen, "A COMPARISON OF THE MAJOR LIPID CLASSES AND FATTY-ACID COMPOSITION OF MARINE UNICELLULAR CYANOBACTERIA WITH FRESH-WATER SPECIES," *Archives of Microbiology,* vol. 155, pp. 107-113, Jan 1991.

[20] T. Kaneko, A. Tanaka, S. Sato, H. Kotani, T. Sazuka, N. Miyajima, *et al.*, "Sequence Analysis of the Genome of the Unicellular Cyanobacterium *Synechocystis* sp. strain PCC6803. I. Sequence Features in the 1 Mb Region from Map Positions 64% to 92% of the Genome," *DNA Research,* vol. 2, pp. 153-166, 1995.

[21] T. Kaneko, Y. Nakamura, S. Sasamoto, A. Watanabe, M. Kohara, M. Matsumoto, *et al.*, "Structural analysis of four large Plasmids harboring in a unicellular cyanobacterium, Synechocystis sp PCC 6803," *DNA Research,* vol. 10, pp. 221-228, Oct 2003.

[22] X. Y. Liu and R. Curtiss, "Nickel-inducible lysis system in Synechocystis sp PCC 6803," *Proceedings of the National Academy of Sciences of the United States of America,* vol. 106, pp. 21550-21554, Dec 2009.

[23] X. Liu, J. Sheng, and R. Curtiss, III, "Fatty acid production in genetically modified cyanobacteria," *Proceedings of the National Academy of Sciences of the United States of America,* vol. 108, pp. 6899-6904, Apr 26 2011.

[24] J. G. Immer, M. J. Kelly, and H. H. Lamb, "Catalytic reaction pathways in liquid-phase deoxygenation of C18 free fatty acids," *Applied Catalysis a-General,* vol. 375, pp. 134-139, Feb 2010.

[25] J. G. Immer and H. H. Lamb, "Fed-Batch Catalytic Deoxygenation of Free Fatty Acids," *Energy & Fuels,* vol. 24, pp. 5291-5299, Oct 2010.

[26] D. C. Grenoble, M. M. Estadt, and D. F. Ollis, "The Chemistry and Catalysis of the Water Gas Shift Reaction: 1. The Kinetics over Supported Metal Catalysts," *Journal of Catalysis,* vol. 67, pp. 90-102, 1981.

[27] P. Maki-Arvela, I. Kubickova, M. Snare, K. Eranen, and D. Y. Murzin, "Catalytic deoxygenation of fatty acids and their derivatives," *Energy & Fuels,* vol. 21, pp. 30-41, Jan-Feb 2007.

[28] J. P. Ford, J. G. Immer, and H. H. Lamb, "Palladium Catalysts for Fatty Acid Deoxygenation: Influence of the Support and Fatty Acid Chain Length on Decarboxylation Kinetics," *Topics in Catalysis,* vol. 55, pp. 175-184, May 2012.

[29] J. Immer, "Liquid-Phase Deoxygenation of Free Fatty Acids to Hydrocarbons Using Supported Palladium Catalysts," Ph. D., Chemical and Biomolecular Engineering, North Carolina State University, Raleigh, North Carolina, 2010.

[30] W. C. Wang, W. L. Roberts, and L. F. Stikeleather, "Hydrocarbon Fuels From Gas Phase Decarboxylation of Hydrolyzed Free Fatty Acid," *Journal of Energy Resources Technology-Transactions of the Asme,* vol. 134, Sep 2012.

[31] M. Snare, I. Kubickova, P. Maki-Arvela, D. Chichova, K. Eranen, and D. Y. Murzin, "Catalytic deoxygenation of unsaturated renewable feedstocks for production of diesel fuel hydrocarbons," *Fuel,* vol. 87, pp. 933-945, May 2008.

[32] T. Morgan, D. Grubb, E. Santillan-Jimenez, and M. Crocker, "Conversion of Triglycerides to Hydrocarbons Over Supported Metal Catalysts," *Topics in Catalysis,* vol. 53, pp. 820-829, Jul 2010.

[33] L. Boda, O. Gyorgy, H. Solt, L. Ferenc, J. Valyon, and A. Thernesz, "Catalytic hydroconversion of tricaprylin and caprylic acid as model reaction for biofuel production from triglycerides," *Applied Catalysis a-General,* vol. 374, pp. 158-169, Feb 2010.

[34] P. T. Do, M. Chiappero, L. L. Lobban, and D. E. Resasco, "Catalytic Deoxygenation of Methyl-Octanoate and Methyl-Stearate on Pt/Al2O3," *Catalysis Letters,* vol. 130, pp. 9-18, Jun 2009.

[35] J. Fu, X. Y. Lu, and P. E. Savage, "Hydrothermal Decarboxylation and Hydrogenation of Fatty Acids over Pt/C," *Chemsuschem,* vol. 4, pp. 481-486, 2011.

[36] M. Snare, I. Kubickova, P. Maki-Arvela, K. Eranen, and D. Y. Murzin, "Heterogeneous catalytic deoxygenation of stearic acid for production of biodiesel," *Industrial & Engineering Chemistry Research,* vol. 45, pp. 5708-5715, Aug 2006.

[37] A. S. Berenblyum, R. S. Shamsiev, T. A. Podoplelova, and V. Y. Danyushevsky, "The influence of metal and carrier natures on the effectiveness of catalysts of the deoxygenation of fatty acids into hydrocarbons," *Russian Journal of Physical Chemistry A,* vol. 86, pp. 1199-1203, Aug 2012.

[38] E. Auer, A. Freund, J. Pietsch, and T. Tacke, "Carbons as supports for industrial precious metal catalysts," *Applied Catalysis a-General,* vol. 173, Oct 25 1998.

[39] V. Calvino-Casilda, A. J. Lopez-Peinado, C. J. Duran-Valle, and R. M. Martin-Aranda, "Last Decade of Research on Activated Carbons as Catalytic Support in Chemical Processes," *Catalysis Reviews-Science and Engineering,* vol. 52, pp. 325-380, 2010.

[40] P. Ratnasamy, "Process for the Production of Paraffinic Hydrocarbons," 2012.

[41] D. J. Suh, T. J. Park, and S. K. Ihm, "CHARACTERISTICS OF CARBON-SUPPORTED PALLADIUM CATALYSTS FOR LIQUID-PHASE HYDROGENATION OF NITROAROMATICS," *Industrial & Engineering Chemistry Research,* vol. 31, Aug 1992.

[42] H. P. Boehm, W. Heck, R. Sappok, and E. Diehl, "SURFACE OXIDES OF CARBON," *Angewandte Chemie-International Edition,* vol. 3, 1964 1964.

[43] M. Gurrath, T. Kuretzky, H. P. Boehm, L. B. Okhlopkova, A. S. Lisitsyn, and V. A. Likholobov, "Palladium catalysts on activated carbon supports - Influence of reduction temperature, origin of the support and pretreatments of the carbon surface," *Carbon,* vol. 38, pp. 1241-1255, 2000.

[44] X. Wang, N. Li, J. A. Webb, L. D. Pfefferle, and G. L. Haller, "Effect of surface oxygen containing groups on the catalytic activity of multi-walled carbon nanotube supported Pt catalyst," *Applied Catalysis B-Environmental,* vol. 101, pp. 21-30, Nov 22 2010.

[45] R. W. Gosselink, W. Xia, M. Muhler, K. P. de Jong, and J. H. Bitter, "Enhancing the Activity of Pd on Carbon Nanofibers for Deoxygenation of Amphiphilic Fatty Acid Molecules through Support Polarity," *Acs Catalysis,* vol. 3, pp. 2397-2402, Oct 2013.

[46] B. Rozmyslowicz, P. Maki-Arvela, A. Tokarev, A. R. Leino, K. Eranen, and D. Y. Murzin, "Influence of Hydrogen in Catalytic Deoxygenation of Fatty Acids and Their Derivatives over Pd/C," *Industrial & Engineering Chemistry Research,* vol. 51, pp. 8922-8927, Jul 2012.

[47] N. P. Lebedeva, A. S. Booij, I. N. Voropaev, P. A. Simonov, A. V. Romanenko, and V. I. Bukhtiyarov, "Catalyst Structure - Performance Trends for Sibunit Carbon Based Cathodes for Proton Exchange Membrane Fuel Cells," *Proton Exchange Membrane Fuel Cells 9,* vol. 25, pp. 1909-1913, 2009.

[48] D. J. Suh, T. J. Park, and S. K. Ihm, "EFFECT OF SURFACE OXYGEN GROUPS OF CARBON SUPPORTS ON THE CHARACTERISTICS OF PD/C CATALYSTS," *Carbon,* vol. 31, pp. 427-435, 1993.

[49] J. P. Ford, N. Thapaliya, M. J. Kelly, W. L. Roberts, and H. H. Lamb, "Semi-Batch Deoxygenation of Canola- and Lard-Derived Fatty Acids to Diesel-Range Hydrocarbons," *Energy & Fuels,* vol. 27, pp. 7489-7496, Dec 2013.

[50] P. Maki-Arvela, M. Snare, K. Eranen, J. Myllyoja, and D. Y. Murzin, "Continuous decarboxylation of lauric acid over Pd/C catalyst," *Fuel,* vol. 87, pp. 3543-3549, Dec 2008.

[51] E. W. Ping, R. Wallace, J. Pierson, T. F. Fuller, and C. W. Jones, "Highly dispersed palladium nanoparticles on ultra-porous silica mesocellular foam for the catalytic decarboxylation of stearic acid," *Microporous and Mesoporous Materials,* vol. 132, pp. 174-180, Jul 2010.

[52] A. T. Madsen, B. Rozmyslowicz, P. Maki-Arvela, I. L. Simakova, K. Eranen, D. Y. Murzin, *et al.*, "Deactivation in Continuous Deoxygenation of C-18-Fatty Feedstock over Pd/Sibunit," *Topics in Catalysis,* vol. 56, pp. 714-724, Jun 2013.

CHAPTER 2: Experimental Methods

Materials

A 5 wt. % Pd/C catalyst (E117) was purchased from Evonik. A 5 wt. % Pd/C catalyst (BASF Escat 1971) and an activated carbon (AC) were purchased from Strem Chemicals. The following chemicals were purchased from Acros Organics: dodecane (C_{12}, 99%), n-heptadecane (*n*-C_{17}, 99%), myristic acid (MA, 99%), palmitic acid (PA, 98%), stearic acid (SA, 97%), and ethyl stearate (ES, 97%). The following chemicals were obtained from Aldrich: decane (C_{10}, 99%), tridecane (C_{13}, 99%), *n*-pentadecane (*n*-C_{15}, 99%), and 1-heptadecene (1-C_{17}-ene, 99%). Alfa Aesar was the vendor used for 2-tridecanone (2-C_{13}-ONE, 98%), 2-tridecanol (2-C_{13}-OH, >98%), and methyl stearate (MS, 99%). Lauric acid (LA, min. 99%) was purchased from Sigma. TCI America was used to purchase n-undecane (*n*-C_{11}, min 99%). β-hydroxymyristic acid (BHMA, 98% min.) was purchased from Finetech Industry, Ltd. Airgas National Welders was used to procure the He (ultra-high purity), H_2 (ultra-high purity), O_2 (extra dry), and a calibration gas mixture containing 1% CH_4, 5% H_2, 5% CO, and 5% CO_2. Methyl laurate (ML, >98%) and ethyl laurate (EL, >99%) were purchased from TCI. NH_4Y and NaY zeolites were purchased from Zeolyst. NaY zeolite was purchased from Grace Davison.

Catalyst Preparation

Pt/zeolite catalysts for alkane hydroisomerization (HI) were prepared by ion exchange of tetraamineplatinum (II) hydroxide hydrate [$Pt(NH_3)_4(OH)_2$] (58 wt. % Pt) with the zeolite. The Pt/NaY sample was made with the Davison NaY zeolite. A Pt/NH_4Y sample was prepared from the Zeolyst NH_4Y zeolite. The CaY zeolite was made by exchanging the

Zeolyst NaY with Ca^{2+} overnight three times with a $Ca(NO_3)_2$ solution at 80 °C. The following procedure was used to synthesize the Pt/CaY catalyst and is typical of all Pt/zeolite preparations employed in this work. $[Pt(NH_3)_4(OH)_2]$ hydrate (0.0919 g) was dissolved in 9.159 g 18.2 MΩ-cm deionized (DI) H_2O to give the proper Pt loading on the catalyst (1 wt. %). A slurry was made by suspending 5.289 g CaY in 21.286 g DI H_2O. The $[Pt(NH_3)_4(OH)_2]$ solution was added to a burette. The slurry was agitated and heated to 80 °C. After the slurry reached 80 °C, the Pt solution was added dropwise, and the burette was rinsed with 10 mL H_2O, which was added to the slurry. This mixture was held at 80 °C overnight before being cooled. The resulting powder was recovered via vacuum filtration. The filter cake was rinsed three times with DI water (25 mL each) and then dried at 110 °C overnight. Subsequently, the Pt-exchanged zeolite powder (2.0 g) was calcined by heating at 0.5°C/min to 350 °C in flowing extra dry O_2 (600 sccm) and holding for 3 h. This calcination procedure also converted Pt/NH_4Y to Pt/HY.

Prior to use for alkane HI, the Pt/zeolite catalysts were reduced *ex situ*. Catalyst powder (0.36 g) was loaded into a fritted quartz U-tube reactor and purged with He (60 sccm) to remove air. After this purge, the gas was switched to 60 sccm H_2, and the catalyst was heated at 5 °C/min to 400 °C and held for 1 h. After cooling to 25°C in flowing H_2, the reactor was purged with He (60 sccm). Subsequently, the flow was stopped and the fittings holding the U-tube were loosened, allowing air to contact the catalyst very slowly. This allowed for passivation of the catalyst.

Catalyst Characterization

Commercial and lab-prepared catalysts were characterized by N_2 physisorption and volumetric chemisorption using a Micromeritics ASAP 2020c instrument. The Brunauer-Emmett-Teller (BET) method was used to determine the total (physical) surface area. H_2 chemisorption was used to determine the metal dispersion of the Pt/zeolite catalysts. CO chemisorption was conducted for the Pd/C samples, and a CO:Pd stoichiometric ratio of 1.5:1 was used to calculate the dispersion. The relationship between dispersion, as determined via CO chemisorption, and particle size is shown below in Equation 2.1. In Equation 2.1, d_p is the particle diameter (nm) and D is the fractional dispersion of Pd atoms.

Equation 2.1: Dispersion $$d_p = \frac{1.1}{D}$$

Fatty Acid Deoxygenation

The stirred autoclave reactor system used for the fatty acid deoxygenation experiments is shown below in Figure 2.1. The deoxygenation reactions were conducted in an Autoclave Engineers 50 mL MicroClave reactor equipped with a Dispersimax impeller. Gas flow and composition were controlled by Brooks 5850E mass flow controllers (MFCs) that were calibrated with an Agilent Technologies ADM1000 flow meter. Gas was fed through a port in the top of the reactor apparatus, continued through the center of the impeller shaft, and entered the reaction medium through holes in the impeller, ensuring adequate dispersal and mixing of the gaseous reactants. The reactor effluent gas passed through a

condenser to remove organic vapors (e.g., alkanes) from the stream. After the condenser, the effluent gas then passed through a Tescom backpressure regulator (BPR). A small fraction of the effluent gas flow was diverted to a Pfeiffer vacuum system for quantitative analysis. The pumping station was comprised of a MVP035-2 diaphragm pump and TMH 071 P turbomolecular drag pump. Quantitative data was determined by a Prisma QMS 200 quadrupole mass spectrometer (QMS) equipped with a tungsten filament. Flow into the system was controlled by a heated valve and capillary line. QMS data were recorded using Pfeiffer Quadstar 32-bit software. During fed-batch deoxygenation experiments, an ISCO 260D high-pressure syringe pump was used to feed the liquid reactant stream to the reactor. During semi-batch deoxygenation experiments, this syringe pump was disconnected and replaced with a stainless steel plug.

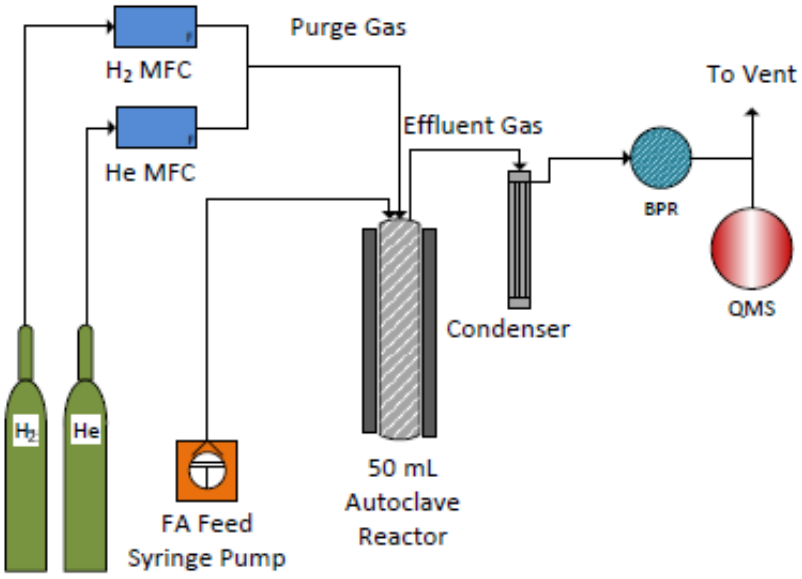

Figure 2.1: Stirred autoclave reactor system used for fatty acid deoxygenation experiments.

Typically, 335 mg Pd/C catalyst was suspended in 22.5 g (approximately 30 mL) (*n*-dodecane) C_{12} via agitation at 240 rpm. After addition of the catalyst and C_{12} solvent, the reactor was purged with 60 sccm He for 5 min. The reactor was then purged with 30 sccm H_2 for 10 min and heated at 5 °C/min to 200 °C. This temperature was held for 1 h. After the reduction was complete, the reactor was cooled to 30 °C and then purged with 60 sccm He for 5 min. Typically, 5.6 mmol of reactant (fatty acid or fatty acid ester) were then added to the reactor, which was purged for 5 min with 60 sccm He after the reactant addition. The gas feed stream was then changed to 5 vol. % H_2 (60 sccm) for 10 min. After this purge, the reactor pressure was increased to 15 bar using the manual BPR. After the reactor had been pressurized, the impeller speed was increased from 240 to 1000 rpm to overcome any mass transfer limitations. A QMS baseline was established requiring from 2-5 h, depending on the reaction. After this pre-reaction baseline was established, the reactor was heated at 5 °C/min to 300 °C and held for a reaction time of 4 h.

The purge gas stream during semi-batch deoxygenation experiments was typically 5 vol. % H_2 at 60 sccm. However, other concentrations of H_2 in the reactor purge gas were used throughout the course of this work. In these experiments, the procedure remained the same up until the point immediately following the addition of the reactant. Once the reactant was added and the reactor had been purged with 60 sccm He for 5 min, the reactor was then purged for 10 min with 60 sccm of the desired reactant gas and pressurized using the manual BPR. The QMS baseline was obtained for the 2-5 h period before heating the reactor to the reaction temperature.

Reactions were carried out with different initial concentrations of fatty acid or ester to examine the effect on the initial deoxygenation rate, CO_2 selectivity, and final conversion. In these reactions, the total liquid mass added to the reactor (solvent mass plus reactant mass) was conserved. The reactant mass (moles) was increased systematically, and the solvent mass was reduced in order to keep the total liquid mass constant.

For fed-batch deoxygenation experiments, typically, 335 mg Pd/C was suspended in 12.5 g C_{12} via mixing at 240 rpm. The reduced solvent mass was used in order to provide extra reactor volume for reaction products that would not be evaporated into the condenser. The reactor was purged with 60 sccm He for 5 min and then 30 sccm H_2 for 10 min. Upon completion of these purges, the reactor was heated at 5 °C/min to 200 °C. This catalyst reduction lasted for 1 h. The reactor was then cooled to 30 °C and purged for 10 min with 60 sccm of the reaction purge gas. The reactor was then pressurized to the reaction pressure (which was typically 15 bar) using the BPR. A QMS baseline was obtained before the reactor was heated at 5 °C/min to 300 °C. When the reactor reached a temperature of 300 °C, injection of the reactant started. Reactant injection rate was controlled using a high-pressure ISCO 260D syringe pump equipped with a heating jacket. The heating jacket temperature was generally set to 10°C above the melting point of the reactant.

Deoxygenation Product Gas-Phase Analysis

The composition of the effluent gas from the stirred autoclave reactor system was monitored via QMS. H_2 (m/z 2), He (m/z 4), CO (m/z 28) and CO_2 (m/z) were the species of interest for the FA deoxygenation experiments. CH_4 (m/z 16) and C_2H_6 (m/z 30) were also monitored for FAE deoxygenation experiments. Response factors for H_2, CO, CO_2 and CH_4

were determined using a calibration gas mixture purchased from Airgas National Welders with the following composition: 1 mol. % CH_4, 5 mol. % H_2, 5 mol. % CO, 5 mol. % CO_2 and balance He. The $CO+CO_2$ yield for each reaction was determined by dividing the total CO and CO_2 moles produced by the reaction by the total reactant moles added to the reactor. The CH_4 yield determined for FAE deoxygenation was determined by dividing the total CH_4 moles produced by the reaction by the total reactant moles. The CO_2 selectivity was determined by dividing the moles of CO_2 produced by the total moles of CO and CO_2 produced during the reaction.

Deoxygenation Product Liquid-Phase Analysis

A Hewlett Packard HP 5890 gas chromatograph (GC) and a Shimadzu GC-2010 Plus were both used to analyze liquid-phase products from the deoxygenation experiments. Each GC was equipped with a flame ionization detector (FID). The HP 5890 GC was equipped with an EconoCap EC-5 capillary column (30 m x 0.32 mm x 1 µm). The column temperature program was as follows: initial temperature of 80 °C, ramp at 5 °C/min to 300 °C, hold at 300 °C for 1 min. A column head pressure of 10 psig and a split ratio of 50:1 were used for these analyses. The Shimadzu GC-2010 plus was equipped with a Restek RTX-5 capillary column (30 m x 0.32 mm x 1 µm). The temperature program for FA and FAE deoxygenation product analyses was as follows: initial temperature at 120 °C, ramp at 10 °C/min to 300 °C, hold at 300 °C for 7 min. Products from BHMA and related compound deoxygenation experiments were analyzed on the Shimadzu GC-2010 plus with the RTX-5 column using the following temperature program: initial temperature at 120 °C, a ramp at 10 °C/min to 195 °C, cooling at 20 °C/min to 157 °C, hold at 157 °C for 3 min, ramp to 300 °C

at 20 °C/min, hold at 300 °C for 7 min. The cooling stage in this temperature ramp was utilized to enhance separation of 2-C_{13}-OH and 2-C_{13}-ONE, which initially appeared as one peak in the chromatogram. Product concentrations were determined using a three-point calibration method with *n*-decane (C_{10}) as an internal standard.

FA and FAE Deoxygenation Initial Rate and Batch Productivity Analysis

The initial rates of decarboxylation and decarbonylation for FAs and FAEs were determined by finding the slope of the initial CO_2 and CO partial pressure curves. These initial slopes were converted to initial rates using the following equation, which has been used previously for initial rate analysis of FA deoxygenation. The derivation of this equation is included in this paper [1]. In Equation 2.2, the constants are defined as follows: V_g is the volume of the reactor head space, W is the mass of the catalyst, R is the gas constant, T is the absolute temperature, t is the reaction time, r_{CO2} is the CO_2 generation rate, and P_{CO2} is the partial pressure of CO_2. CO_2 is specified in Equation 2.2; however, this equation was also used for initial rate analysis of CO and CH_4.

Equation 2.2: Initial Rate Analysis $$(r_{CO_2})_0 = \frac{V_g}{WRT}\left(\frac{dP_{CO_2}}{dt}\right)_0$$

The batch productivity of an experiment was defined as the total amount of moles of CO and CO_2 produced during the reaction per gram of catalyst per hour of reaction (batch) time. The reaction time was determined by drawing a line tangent to the CO_2 curve at a value approximately 50% of the molar flow just before the reaction ended, which was half of

the CO_2 maximum for the reactions involving lower concentrations and half of the quasi steady-state value for reactions involving higher initial concentrations. The reaction time value to make this line intersect with the x-axis was determined. This is illustrated below in Figure 2.2. The red CO_2 trace is from LA deoxygenation at an initial concentration of 4 mol. % and the blue CO_2 trace is from LA deoxygenation at an initial concentration of 27 mol. %. Both of these runs were done over 5 wt. % Pd/C (E117) at 300 °C and 15 bar under 5 vol. % H_2.

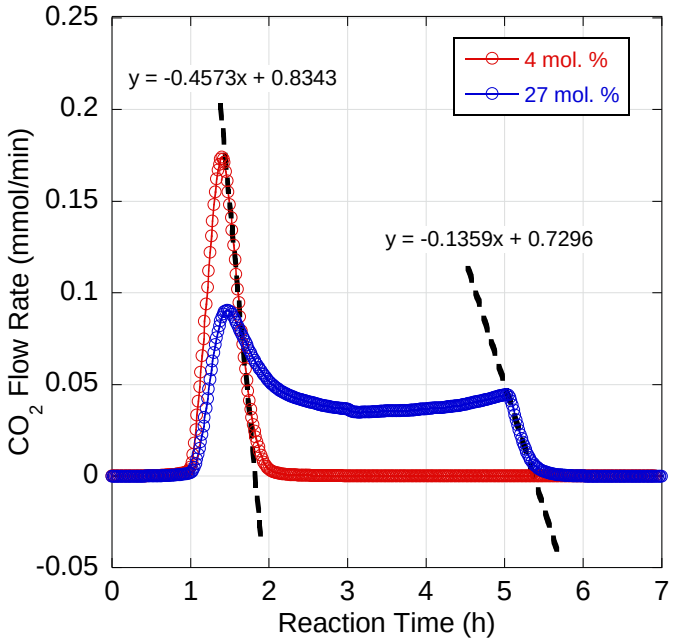

Figure 2.2: Final reaction time analysis for semi-batch LA deoxygenation over 5 wt. % Pd/C at 300 °C and 15 bar under 5 vol. % H_2 at initial concentrations of 4 mol. % (red) and 27 mol. % (blue).

Cyanobacteria-Derived Fatty Acid Recovery and Purification

The Nielsen and Vermaas groups at Arizona State University (ASU) provided the cyanobacteria-derived fatty acid (CBFA) samples. Bench-top growth of *Synechocystis* sp. PCC 6803 at ASU is shown in Figure 2.3.

Figure 2.3: Growth of *Synechocystis* sp. PCC 6803 at ASU.

Upon secretion into the growth medium, the CBFAs were recovered by adsorption onto polymer resin beads. Initially, two resins were used to recover the CBFAs: Lenntech LEWATIT® MonoPlus MP 64 and Dow DOWEX™ OPTIPORE™ L493. The MP 64 resin is an anion exchange resin with a macroporous structure and weak basicity [2]. L493 is a hydrophobic resin with high surface area and capacity for organic compounds [3]. CBFA recovery using a hydrophobic resin column at ASU is shown in Figure 2.4.

Figure 2.4: CBFA recovery over hydrophobic resin.

CBFA samples were extracted from the resins with MeOH, HCl, acetone and C6. A CBFA sample that has been recovered in this fashion is shown in Figure 2.5. The sample shown is representative of most CBFA samples obtained from ASU. The slight yellowish color indicates that the sample is tainted with impurities, since reagent-grade FAs are an opaque white color. Theoretically, FAs that are 100% pure should be completely clear.

Figure 2.5: Recovered and purified CBFA sample FA32.

After recovery, the CBFA samples were purified using a variety of methods to remove the impurities present in crude CBFA samples. Base hydrolysis, acid hydrolysis, adsorption of impurities on activated carbon (decolorization), and adsorption chromatography were explored as purification methods. Combinations of these methods were also used to purify CBFA samples.

Adsorption of impurities on AC (decolorization) was explored as a potential purification method for these CBFA samples with CBFA sample FA03. FA03 was dissolved in approximately 10 g C_{12}, and 0.5 g AC (Strem) was added to the solution. The slurry was then agitated. After the agitation was complete, the AC was separated from the FA03/C_{12} solution via gravity filtration at 60 °C. Figure 2.6 shows this entire process. In Figure 2.6(a), FA03 was dissolved in the minimum amount of C_{12} required. The dark brown color is indicative of high concentrations of impurities. When the rest of the C_{12} solvent was added (shown in Figure 2.6(b)), this dark brown component coalesced into large particles,

effectively separating them from the remaining FA03 solution. However, the sample was still relatively contaminated, as is evidenced by the yellow color. Figure 2.6(c) shows the result of the AC addition and gravity filtration steps. The color of the FA03/C_{12} solution is significantly lighter, indicating a large drop in contaminant concentration.

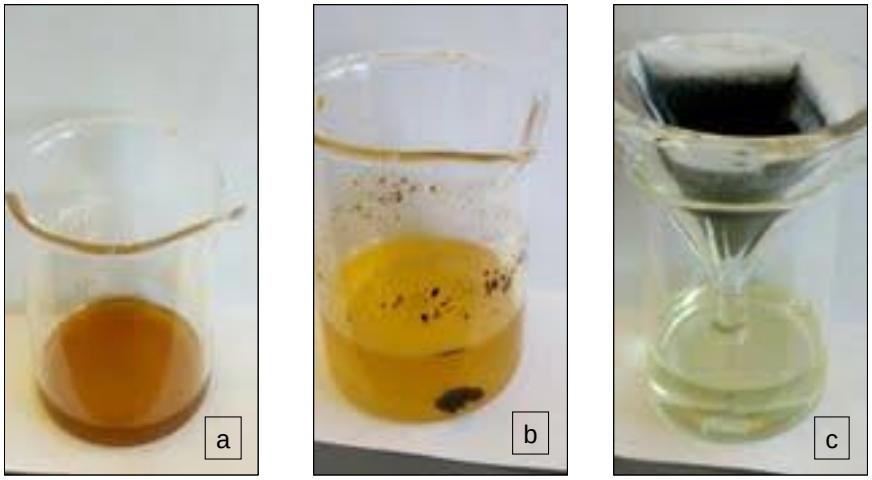

Figure 2.6: Decolorization of FA03 over AC by (a) dissolution in minimum amount of C_{12}, (b) addition of remaining C_{12}, and (c) treatment with AC and gravity filtration.

A combined acid hydrolysis/AC purification method was employed to remove impurities from CBFA sample MFA05. Crude MFA05 (containing 453 ppm S) was subjected to sequential acid hydrolysis and AC decolorization. 1.860 g MFA05 and 75 mL 1 M HCl were added to a three-neck flask, which was purged with N_2 for 10 min. After the purge, the three-neck flask was submerged in a pre-heated H_2O bath. The N_2 flow was continued throughout the experiment. A reflux condenser and bubbler were attached to the

three-neck flask, and the acid hydrolysis mixture was stirred at 500 rpm. The H_2O bath was heated to 100 °C and held for 3 h. Figure 2.7 shows MFA05 before hydrolysis and during hydrolysis at 100 °C.

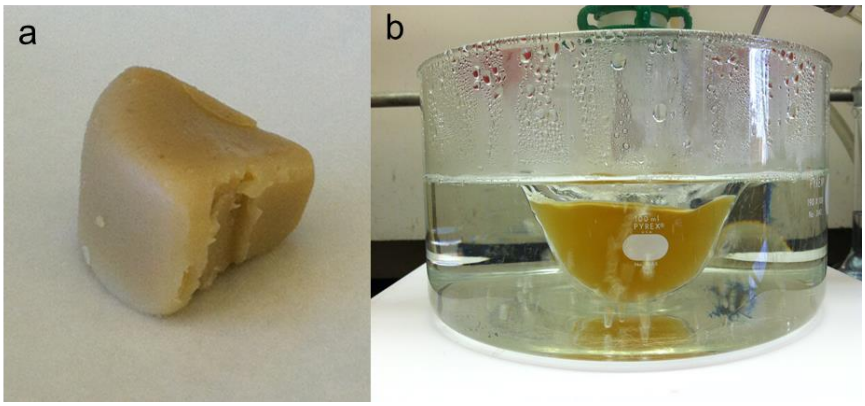

Figure 2.7: Acid hydrolysis of MFA05 at 100 °C in 1 M HCl for 3 h. Crude MFA05 biomass is shown on the right (a). The hydrolysis mixture is shown on the left (b).

After the hydrolysis procedure was completed, the two-phase reaction mixture was transferred to a separatory funnel. Hexanes solvent was added to dilute the MFA05 organic phase. Upon addition of hexanes, a black deposit of biomass debris was observed on the side of the separatory funnel. The aqueous phase and biomass debris were removed, and the remaining organic phase was contacted with 0.1 M HCl, and the aqueous phase was discarded. The final organic phase was transferred to a round-bottom flask, and the hexanes was removed by evaporation with a Büchi Rotavapor R-215. This process is shown in Figure 2.8.

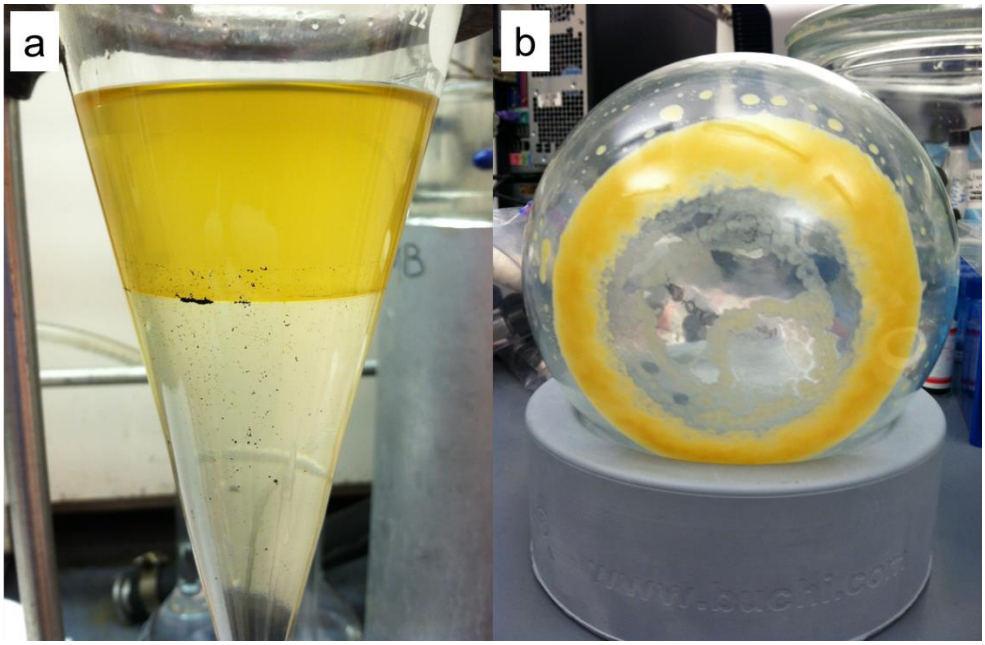

Figure 2.8: (a) Acidification and separation of MFA05 from aqueous HCl. (b) Resultant MFA05 sample after removal of hexanes via Büchi Rotavap.

The post-hydrolysis MFA05 sample was dissolved in 10.5 g C_{12} and transferred to a 50 mL beaker. Strem AC (0.5 g) was added to the solution, which was then agitated for 10 min. The AC was hot filtered from the MFA05/C_{12} solution at 60 °C after the agitation period was over. FA analysis was conducted via GC-FID on samples obtained before and after the AC adsorption process. The AC adsorption process is shown below in Figure 2.9.

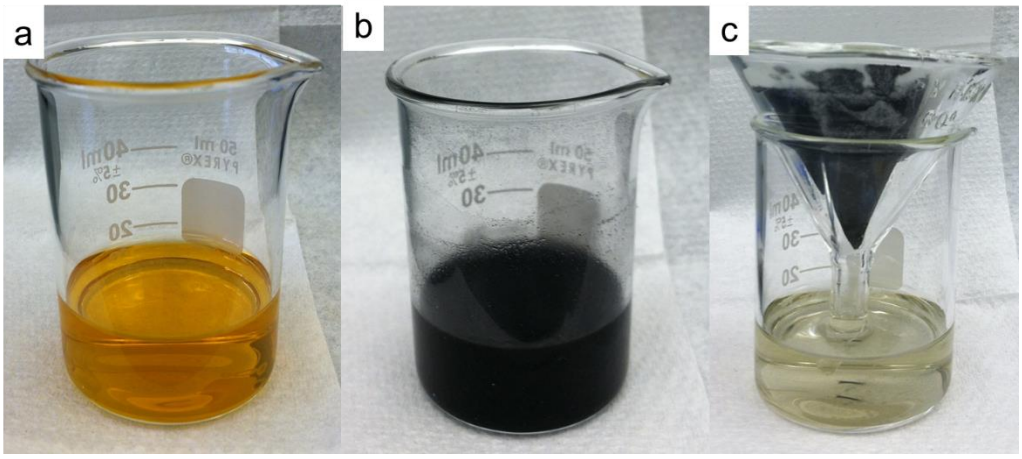

Figure 2.9: (a) Dissolution of post-hydrolysis MFA05 in 10.5 g C_{12}; (b) Adsorption of impurities in MFA05/C12 on 0.5 g Strem AC; (c) Hot filtration of AC from MFA05/C_{12} solution.

Mass balance results for the hydrolysis and decolorization experiment are given in Table 2.1. Most of the biomass loss occurred during the hydrolysis step. Note that two different metrics are used. The first metric is total biomass, and the second is the mass of CBFAs. It is possible that very little CBFA mass was lost in the hydrolysis step, and that the initial FA content of the biomass was only 65-70% (based on historical data). Loss of CBFAs during the AC decolorization and filtration was approximately 20%, including AC adsorption and filtration losses.

Table 2.1: Mass balance for acid hydrolysis and AC decolorization of ASU CBFA sample MFA05 conducted at NCSU.

		Biomass	***Pre-AC/ Filtration***	***Post-AC /Filtration***
	Solution Mass (g)	-	11.683	10.617
GC Results	**GC Mass (g)**	-	0.57	0.571
	FA Mass (g)	-	0.07	0.063
FA Profile Results* (Fraction of Total FAs)	**C12**	-	0.599	0.606
	C14	-	0.083	0.083
	C16	-	0.099	0.078
	C18	-	0.06	0.075
FA Mass (g)	**C12**	-	0.865	0.709
	C14	-	0.12	0.097
	C16	-	0.142	0.091
	C18	-	0.087	0.088
	Total Mass (g)	1.86	1.214	0.984
	Mass Lost (g)	-	0.646	0.229
	% of Biomass Lost (%)	-	34.8	12.3

Analysis of Cyanobacteria-Derived Fatty Acids

Select CBFA samples were sent to Dr. Lisa Dean in the NCSU Food Science Department, where they were analyzed for their FA content by GC-FID after conversion to the fatty acid methyl esters (FAMEs). The analytical method used by Dr. Dean was reported by Bannon, *et al*. and is summarized here [4]. 20-30 mg of FAs was mixed with 1 mL of 0.5 M methanolic KOH in a screw-top tube. The closed vessel was then heated for 5 min in a

water bath at 80 °C. 1 mL BF_3 (14 % in MeOH) was added to the tube after the sample had cooled. The sample was reheated to 80 °C for 10 min. It was then removed from the bath again, and 1 mL H_2O and 1mL hexane were added. The mixture was then vortexed for 30 s. After the vortex step was complete, the sample was let stand so that the organic and aqueous layers could separate. The organic layer was removed and washed with Na_2SO_4 to remove any remaining water. The sample was then analyzed via GC-FID using an SGE BPX70 (30 m x 0.25 mm x 0.25 µm) capillary column.

Inductively coupled plasma optical emission spectroscopy (ICP-OES) was used to determine sulfur concentrations in CBFA samples. ICP-OES analysis was conducted at ASU. CBFAs sent to NCSU were sent to Galbraith Laboratories and Kim Hutchison in the NCSU Soil Science Department for sulfur concentration via ICP-OES.

Alkane Hydroisomerization

Liquid-phase alkane HI reactions over Pt/zeolite catalysts were conducted using a 100-mL Parr high-pressure batch reactor. The reactor was charged with 350 mg Pt/zeolite catalyst and 25 g alkane reactant. A glass stir bar was also added to the reactor. Figure 2.10 is a picture of the HI reactor setup. The reactor contents were agitated via mixing at a setting of 5 on the stir plate, purged with 250 psig H_2 five times, and once at 500 psig. After the 500 psig purge, the reactor was charged to the reaction pressure and sealed. After a 5-10 min waiting period to test for leaks, the furnace was raised and the reactor was heated at 10 °C/min to 300 °C. The reactor contents were stirred continuously at 240 rpm. After the desired reaction time, the reaction was quenched by lowering the furnace and cooling the reactor rapidly using a fan, water bath, and ice bath.

Figure 2.10: Batch alkane HI apparatus with stir plate, heating jacket and Parr batch reactor.

CBFA-derive alkane samples were hydroisomerized over approximately 350 mg 1 wt. % Pt/CaY at 300 °C at an initial reactor pressure of 500 psig. Deoxygenation of sample FA39A was done at two initial concentrations, once with 1.13 g FA39A and once with nearly 11 g FA39A. Deoxygenation of 11 g FA39A was done twice due to low conversion during the first experiment. Alkane products from the second 11 g FA39A deoxygenation experiment were mixed with alkane products from the deoxygenation with 1.13 g FA39A so that no additional reagent-grade C_{12} would need to be added to make up for lost mass. HI of FA39A-derived alkanes was conducted for 110 min. Alkanes produced from fed-batch deoxygenation of ASU sample NFA180.2-1 were hydroisomerized for 58 min. This reactant

mixture was made by mixing 11 g of alkane from NFA180.2-1 deoxygenation with 14 g reagent-grade C_{12}. Approximately 15 g alkanes from the fed-batch deoxygenation of Combo 1 (Run 1) were mixed with approximately 10 g reagent-grade C_{12} and hydroisomerized for 3 h.

The resulting alkane product from the second fed-batch deoxygenation of Combo 1 was hydroisomerized for 3 h. The condenser and reactor contents from the Combo 1 (Run 2) deoxygenation were mixed with 11 g C_{12}. This was done because HI reactions with reagent-grade alkanes were done with a total reactor mass of 25 g, and the resulting mass from the fed-batch deoxygenation experiment was just under 15 g. This reaction was run at 300 °C for 3 h. This process was repeated for HI of alkanes produced from Combo 1 (Run 2) because a low conversion was achieved during the first reaction. After the first alkane HI reaction, nearly 22 g of product was recovered. This mass was supplemented with a little over 3 g of C_{12} to bring the total reactant mass up to 25 g. The second reaction was quenched at a reaction time of 89 min.

Hydroisomerization Product Liquid-Phase Analysis

Liquid-phase HI products were analyzed on a Shimadzu GC-2010 equipped with an FID and EconoCap EC-1 capillary column (30 m x 0.32 mm x 1 µm). Analyses were run with a 15.6 psi head pressure. Early HI samples were analyzed with the following temperature program: hold at 30 °C for 5 min, ramp at 20 °C/min to 110 °C, ramp at 40 °C to 230 °C, hold for 3 min. This was later modified to extend the 40 °C/min ramp to 300 °C and the hold at 300 °C to 5 min. Later liquid-phase product samples were analyzed with the

following temperature program: hold at 30 °C for 5 min, ramp at 10 °C/min to 280 °C, hold at 280 °C for 5 min.

References

[1] J. P. Ford, J. G. Immer, and H. H. Lamb, "Palladium Catalysts for Fatty Acid Deoxygenation: Influence of the Support and Fatty Acid Chain Length on Decarboxylation Kinetics," *Topics in Catalysis,* vol. 55, pp. 175-184, May 2012.

[2] "Product Information LEWATIT® MonoPlus MP 64," ed, 2011.

[3] "DOWEX OPTIPORE L493 and V493," ed: Dow.

[4] C. D. Bannon, J. D. Craske, N. T. Hai, N. L. Harper, and K. L. Orourke, "ANALYSIS OF FATTY-ACID METHYL-ESTERS WITH HIGH-ACCURACY AND RELIABILITY .2. METHYLATION OF FATS AND OILS WITH BORON TRIFLUORIDE-METHANOL," *Journal of Chromatography,* vol. 247, pp. 63-69, 1982.

CHAPTER 3: Catalytic Deoxygenation of C12 and C14 Fatty Acids and Their Methyl and Ethyl Esters over 5 wt. % Pd/C

Introduction

The cyanobacteria fatty acids (CBFAs) secreted by *Synechocystis* sp. PCC 6803 consist primarily of LA (C12:0) (~80 wt. %) with MA (C14:0), PA (C16:0) and SA (C18:0) as minor constituents. Catalytic deoxygenation of LA and MA to *n*-alkanes over 5 wt. % Pd/C (E117) was investigated in order to gain insight into how CBFAs might be deoxygenated over the same catalyst. In this chapter, the effects of H_2 partial pressure and initial concentration on the semi-batch deoxygenation of LA over 5 wt. % Pd/C were investigated. These process variables affect alkane yields, CO_2 selectivity, initial rates, and batch productivity. The effect of initial LA concentration on deoxygenation was compared to recently published work on PA deoxygenation at increasing initial concentrations. An attempt was made to determine the reaction order with respect LA concentration.

The methyl and ethyl esters of LA are less reactive and hence more easily stored for later conversion to hydrocarbons than the free fatty acid. Moreover, these derivatives are prepared simply by reaction of the fatty acid with the respective alcohols. Catalytic deoxygenation of ML and EL over 5 wt. % Pd/C is also reported in this chapter. Deoxygenation of MS and ES were investigated for comparison to literature data on these compounds. The deoxygenation of ES is significantly slower than SA [1]. ES is deoxygenated to heptadecane over Pd/C via a SA intermediate with concomitant production of C_2H_6, CO, and CO_2 [2]. There appears to be no work in the literature on the catalytic deoxygenation of ML and EL.

Deoxygenation of LA: Effect of H_2 Partial Pressure and Initial Concentration

The effect of H_2 partial pressure was determined by holding the total reactor pressure constant and increasing the H_2 mole fraction in the gas feed from 1% to 20%. These reactions were conducted with the typical mass of catalyst (335 mg) and charge of LA (1.120 g, 5.6 mmol) at 300 °C and 15 bar for 4 h. The on-line QMS data for decarboxylation (loss of CO_2) and decarbonylation (loss of CO) of LA under these conditions is shown below in Figure 3.1. The decarboxylation rate declines significantly as the H_2 concentration increases; most of the decarboxylation activity has been lost when then H_2 concentration is increased to 10 mol. % H_2. An increase to 20 mol. % H_2 rendered the catalyst completely inactive for decarboxylation. LA decarbonylation increased as the H_2 content increased. At an H_2 concentration of 20 mol. %, deoxygenation occurred primarily through decarbonylation.

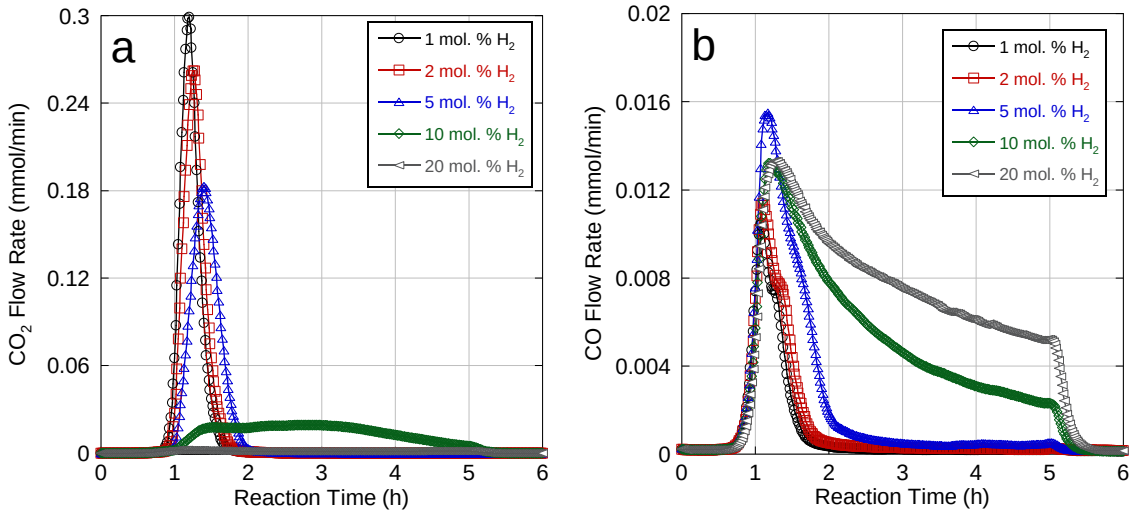

Figure 3.1: Semi-batch LA (a) decarboxylation and (b) decarbonylation over 5 wt. % Pd/C at an initial concentration of 4 mol. %, 300 °C, and 15 bar under 1 – 20 mol. % H_2.

The yields and CO_2 selectivities for each experimental run are shown below in Figure 3.2. These data are also provided in tabular form in the Appendix, Table A.1. As the H_2 partial pressure increased, both yields and the CO_2 selectivity of LA deoxygenation decreased. This change was small when the H_2 partial pressure was below 5%. When the H_2 mole fraction was doubled to 10%, neither the CO + CO_2 yield nor the alkane yield were significantly affected. However, the CO_2 selectivity of the reaction dropped by about 20%. When the H_2 partial pressure was doubled again, all three of these measurements of reaction efficacy dropped off significantly. Both yields were halved, and the CO_2 selectivity dropped to nearly one-seventh of its previous value. The discrepancy between *n*-C_{11} yield and CO + CO_2 yield cannot be explained by production of unsaturated hydrocarbon products, as GC-FID identified all products in the product mixture as *n*-alkanes. This difference could have been caused by an error in the calibration for the QMS response factor at low H_2 concentrations. Figure 3.2 below illustrates that in order to promote high yields and high CO_2 selectivity, the H_2 content should be kept at or below 5 mol. %.

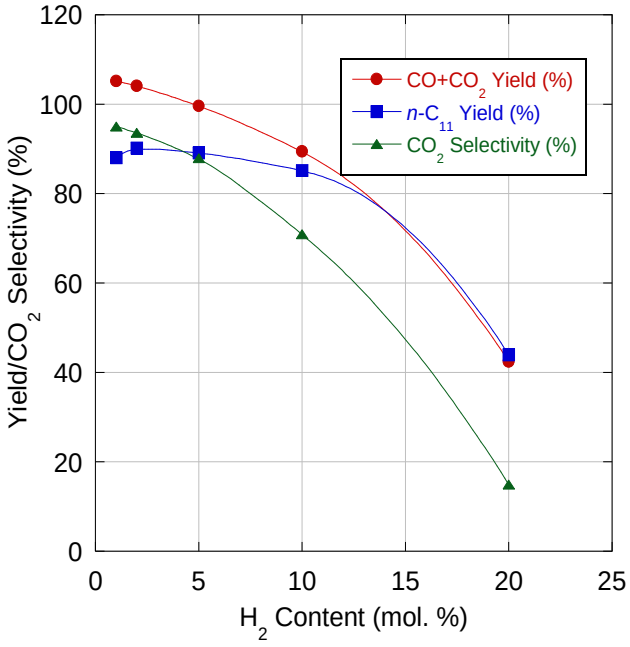

Figure 3.2: Effect of H_2 partial pressure on LA semi-batch deoxygenation yields and CO_2 selectivity at 300 °C and 15 bar over 5 wt. % Pd/C.

This point is further illustrated in the next two graphs. The first (Figure 3.3) is a plot of the initial CO and CO_2 production rates as a function of H_2 partial pressure. At the higher H_2 mole fractions (above 10%), the initial production rate of CO_2 is significantly depressed (<2 mmol/g_{cat}-h). At low H_2 mole fractions, the CO_2 initial rate increases sharply, but the initial decarbonylation rate remains relatively constant.

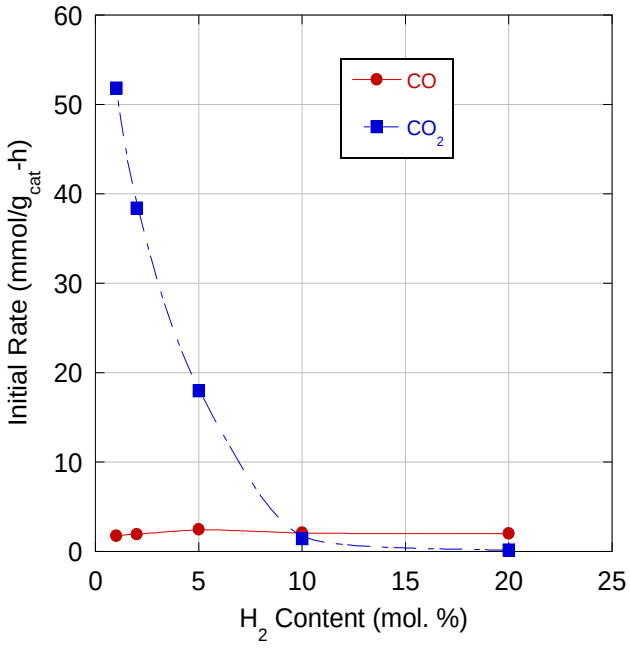

Figure 3.3: CO and CO_2 initial production rate as a function of H_2 partial pressure during semi-batch LA deoxygenation over 5 wt. % Pd/C at 300 °C and 15 bar.

The effect of initial LA concentration was studied under 5% H_2 by starting with the typical amount of LA and catalyst and then increasing the LA molar content while holding the total reactor mass (solvent and LA) constant. The concentration range tested was between 4 and 46 mol. % (5 and 50 wt. %) LA. All reactions were conducted for 4 h, with the exception of the experiment with 46 mol. % LA, which was conducted for 8 h. The on-line QMS results for these experiments are shown below in Figure 3.4 and are summarized in Table 3.1. The deoxygenation of MA at the same initial molar concentration over 5 wt. % Pd/C (335 mg) is also included in Table 3.1.

Figure 3.4(a) shows that as the initial LA concentration was increased, the initial decarboxylation rate decreased, as indicated by a decrease in slope at approximately 1 h of reaction time. It was also determined that there is an initial concentration at which the reaction switches from primarily decarboxylation to decarbonylation. It appears that this happens somewhere between 17 and 23 mol. %, as the difference between the green curve and the black curve is quite large. The CO_2 selectivity dropped to approximately one-quarter of its initial value by the time the initial concentration reached 46 mol.%. The catalyst was unable to fully convert the initial LA charge when the concentration was at or above 27 mol. %. This was indicated by continued CO_2 production until 5 h reaction time, which was typically the end of the reaction temperature soak. The lack of full conversion was also indicated by the sharp drop in CO_2 production as the reactor cooled from the reaction temperature. The sharp drop in CO_2 production was seen for the 46 mol. % data, but was not shown because the reaction time for the 46 mol. % reaction exceeds the time scale.

The range of the y-axis in Figure 3.4(b) is nearly half of that for Figure 3.4(a). As expected, the total amount of CO produced in each reaction increased as the initial LA concentration increased. Though this was the general trend, it should be noted that the CO peak reached a maximum when the initial LA concentration was 34 mol. %. The inability of the catalyst to fully convert LA at contents above 27 mol. % is also apparent here. CO was being produced until the end of the reaction time, and the rate of production dropped off significantly at the end of the reaction time. Incomplete LA conversion at higher concentrations is most likely due to inhibition of the decarboxylation pathway.

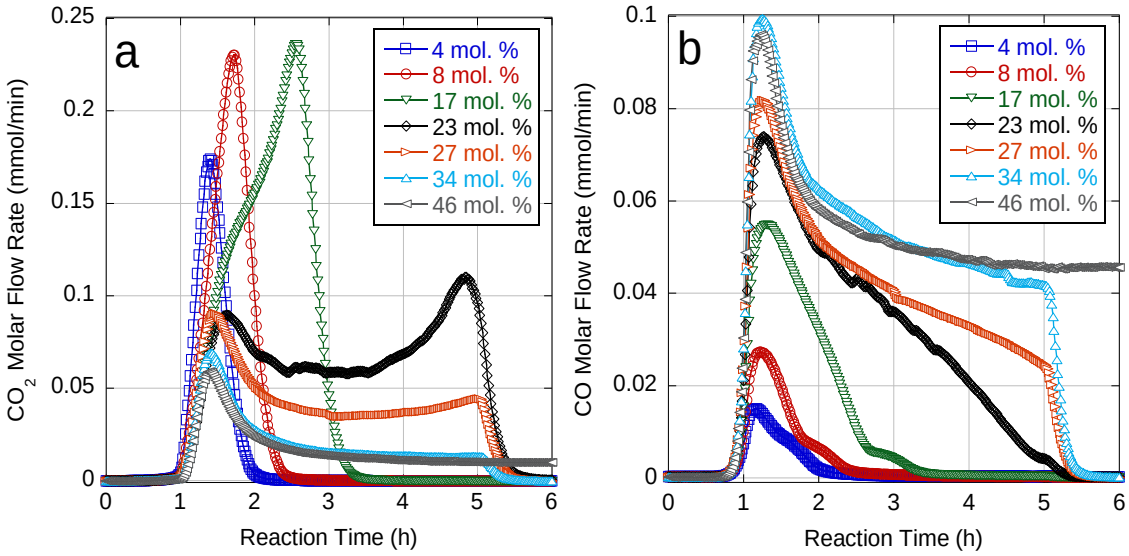

Figure 3.4: (a) Decarboxylation and (b) decarbonylation of LA concentration series over 5 wt. % Pd/C at 300 °C and 15 bar under 5% H_2.

Table 3.1: Summary of LA concentration series deoxygenation experiments and MA deoxygenation over 5 wt. % Pd/C at 300 °C and 15 bar under 5 mol. % H_2.

FA	**FA Conc. (mol. %)**	**$CO+CO_2$ Yield (%)**	***n*-C_{11} Yield (%)**	**CO_2 Selectivity (%)**	**mol H_2/mol $CO+CO_2$ Generated**
LA	4	99.6	89.1	87.9	-0.13
	8	89.0	98.0	87.5	-0.11
	17	87.9	89.1	81.4	-0.12
	23	90.0	84.7	66.7	-0.18
	27	62.9	68.9	50.4	-0.29
	34	44.3	43.2	27.7	-0.37
	46	53.9	58.1	22.3	-0.34
MA	4	90.6	91.2	89.8	-0.17

With the x-axis values in Figure 3.4, it is not readily apparent whether or not the initial CO production rate increased significantly with the increase in initial LA concentration. For these QMS plots, the x-axes were expanded, and the initial slopes determined. This analysis is shown in Figure A.1 and Figure A.2 in the Appendix. Figure 3.5 shows the results of this initial rate analysis. Also included in Figure 3.5 are data published by Ford, *et al*. on initial rates of PA deoxygenation over 5 wt. % Pd/C (E117) [4]. The data shown in Figure 3.5 is summarized in Table A.2 in the Appendix.

As expected from Figure 3.5(a), the initial decarboxylation rate decreased with increasing LA concentration. This initial CO_2 rate declined to a relatively steady level above an initial LA concentration of 20 mol. %. The effect of increasing initial LA concentration was more substantial for the initial CO rate, with the rate increasing nearly tenfold over the concentration range tested. Ford, *et al.* showed that, at low FA molar concentrations, increasing the length of the FA alkyl chain increased the initial decarboxylation rate [3]. Figure 3.5 shows that this relationship holds as the initial FA concentration increases. The work presented below also expands on the Ford, *et al.* work by showing that the linear increase in initial rate of decarbonylation with concentration (up to 40 mol. %) is independent of FA chain length (at least for LA and PA).

Extrapolating from the data set, if the LA mole content were to approach zero, it appears that the initial decarboxylation rate would approach infinity; however, at an LA concentration of 0 mol. %, the initial rate for both species would be zero. From this, we must infer that the initial decarboxylation rate reaches a maximum at a concentration between 4 mol. % and 0 mol. %.

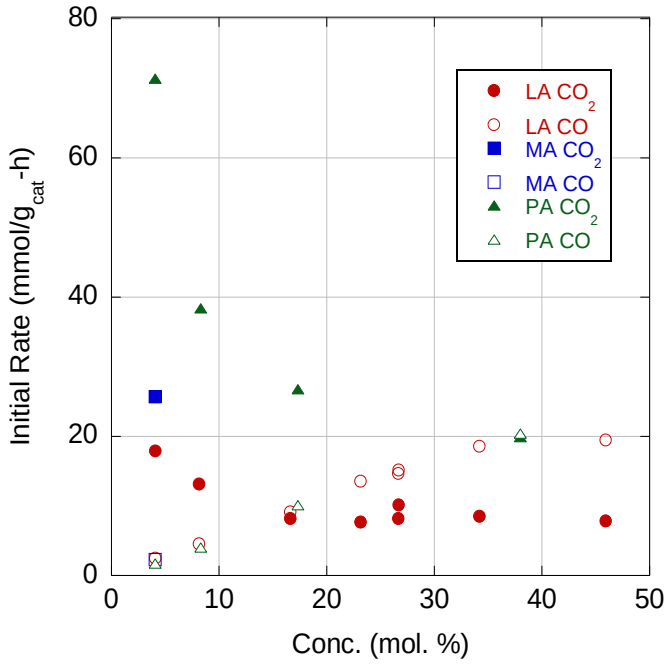

Figure 3.5: Initial rates (mmol/g_{cat}-h) of CO and CO_2 production from LA concentration series deoxygenation over 5 wt. % Pd/C at 300 °C and 15 bar under 5 mol. % H_2.

The variation in batch productivity (mmol/g_{cat}-h) for LA deoxygenation across the concentration series is illustrated below in Figure 3.6. Also included in Figure 3.6 is the batch productivity for PA deoxygenation over 5 wt. % Pd/C, as reported by Ford, *et al.* [4]. The data exhibit a volcano-like relationship between batch productivity and initial LA concentration, with the maximum batch productivity occurring at 17 mol. % LA. From 4 to 17 mol. %, the batch productivity increased. Between 17 and 27 mol. %, the batch productivity dropped off significantly. The significant drop in batch productivity between 17 and 27 mol. % LA is most likely due to a switch in primary deoxygenation pathway from

decarboxylation to decarbonylation. This batch productivity data also follows the chain length relationship shown by Ford, *et al.* [3].

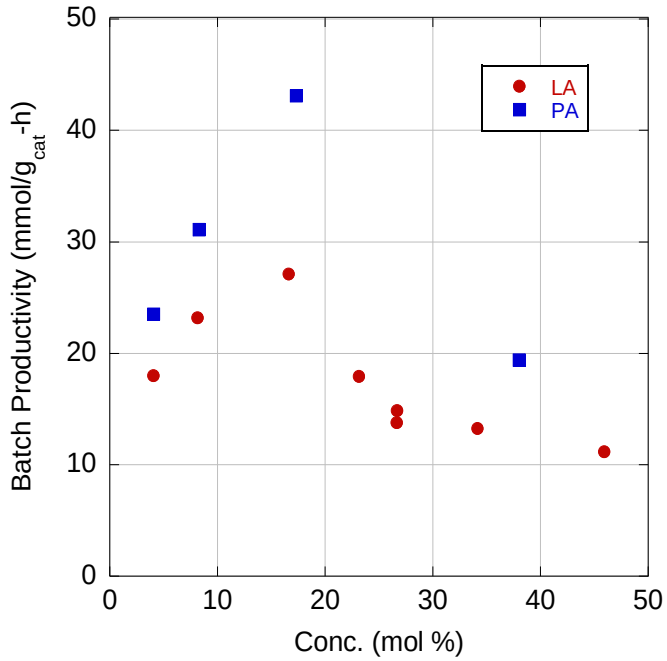

Figure 3.6: Batch productivity of LA and PA semi-batch deoxygenation over 5 wt. % Pd/C at 300 °C and 15 bar under 5 mol. % H_2.

The kinetics of LA deoxygenation also were explored using the integral method (for the overall rate of deoxygenation). The $CO+CO_2$ yields for all concentrations were determined at every half-hour and were plotted as a function of reaction time. This gave the 0^{th} order plot for LA deoxygenation. This data was also used to create a 1^{st} order plot, which is the natural log of 1 minus the $CO+CO_2$ yield plotted against the reaction time. Both of these plots are shown in Figure 3.7. From this figure, it is not clear whether or not LA

deoxygenation follows 0th order or 1st order kinetics, which means that the rate of $CO+CO_2$ generation could be a higher or fractional reaction order in LA. At lower concentrations (4 or 8 mol. %), neither of the two plots provide a linear relationship between their respective y-axis values and the reaction time. At higher concentrations (46 mol. %), both plots provide linear relationships between their y-axis values and the reaction time.

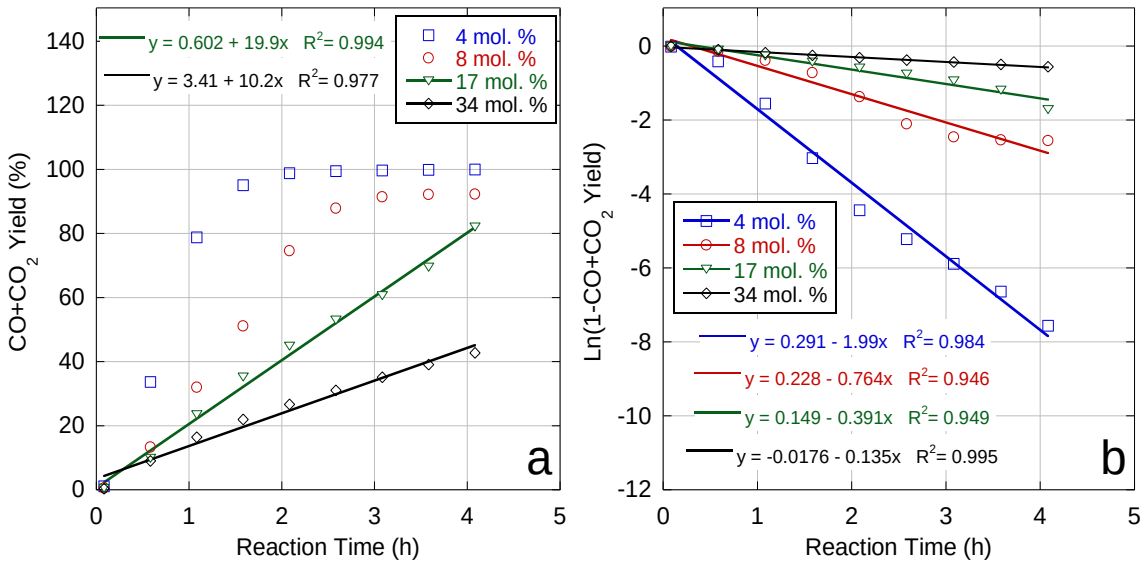

Figure 3.7: (a) 0th-order plot and (b) 1st-order plot of LA deoxygenation over 5 wt. % Pd/C at 300 °C and 15 bar under 5 mol. % H_2.

Deoxygenation of Fatty Acid Esters

The work presented in this section illustrates how deoxygenation is affected when the carboxyl functional group is changed from a carboxylic acid to an ester, and furthermore, how the length of the alkyl moiety on the ester group affects deoxygenation. A general

framework has been established by testing not only how the ester alkyl chain affects deoxygenation, but also how the length of the longer alkyl chain affects deoxygenation, much like with FAs. ML, EL, MS, and ES were all deoxygenated over 5 wt. % Pd/C (E117) in the fashion described at the beginning of this chapter.

Figure 3.8 shows the evolution of CH_4, CO and CO_2 during ML deoxygenation over 5 wt. % Pd/C at 300 °C and 15 bar under 5 mol. % H_2. Immediately below that in Figure 3.9 is a comparison of decarboxylation of LA and ML. CO, CO_2 and CH_4 are all produced during the course of ML deoxygenation. In Figure 3.8, all three curves reach a maximum at about 1.25 h and then exhibit what appears to be a 1st order decay. Deoxygenation of ML did not reach full conversion over the course of the reaction, as is shown by the steep decline in CO, CO_2, and CH_4 production at 5 h. ML deoxygenation occurred much more slowly than LA deoxygenation under the same conditions. Figure 3.9 illustrates this by showing that LA deoxygenation occurs with a higher initial decarboxylation rate and shorter reaction time required for full conversion.

The CO + CO_2 yield for ML deoxygenation was 53.7 %, and the *n*-C_{11} yield was 51.9%. The substitution of the ester group for the carboxylic acid group also caused the CO_2 selectivity to decrease to 74.9%. As shown in Figure 3.10, CH_4 production preceded CO and CO_2 production, suggesting a series reaction sequence in which a LA intermediate is formed and then deoxygenated to *n*-C_{11}. This series reaction scheme is supported by previous work on the deoxygenation of ES over Pd/C under 5 mol. % H_2, which showed that SA was produced before being deoxygenated to *n*-C_{17} [2].

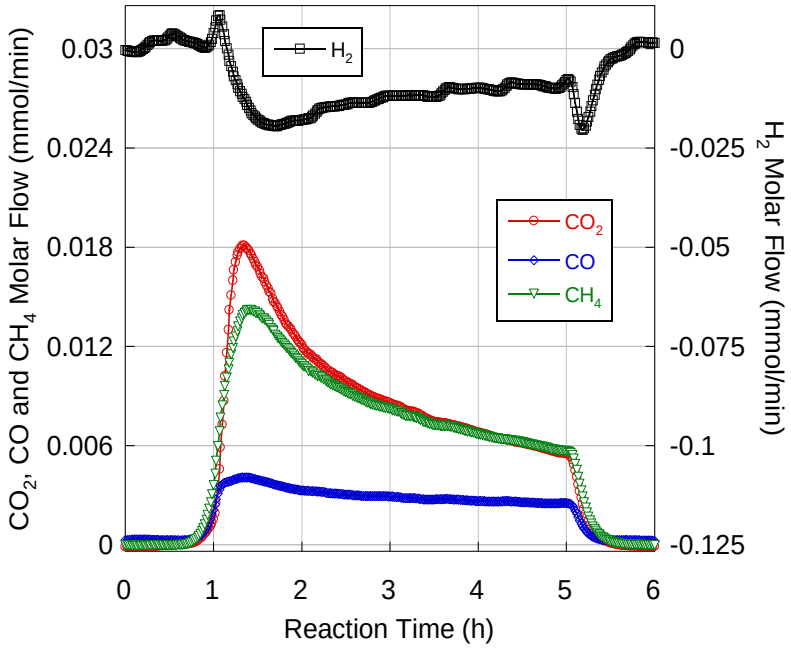

Figure 3.8: Molar production rate of CO_2, CO and CH_4 and consumption rate of H_2 during semi-batch ML deoxygenation over 5 wt. % Pd/C at 300 °C and 15 bar under 5 mol. % H_2.

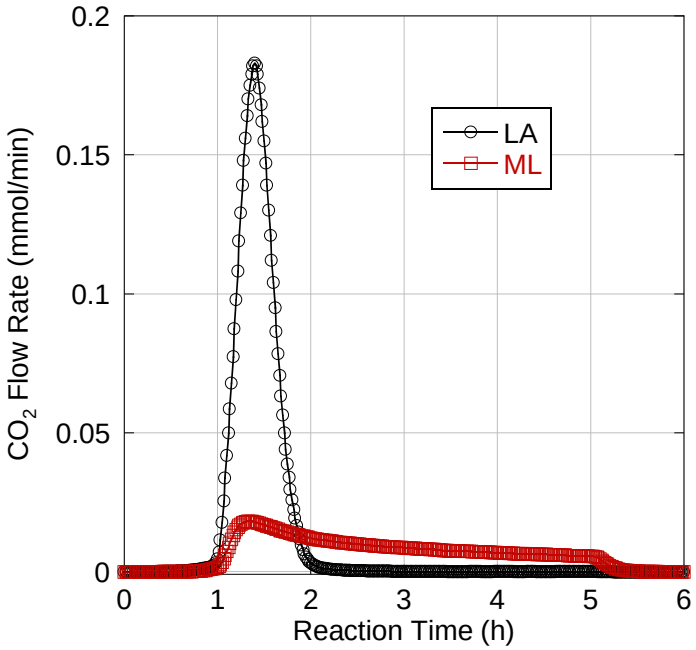

Figure 3.9: Semi-batch decarboxylation of 5.6 mmol LA and ML over 5 wt. % Pd/C at 300 °C and 15 bar under 5 mol. % H_2.

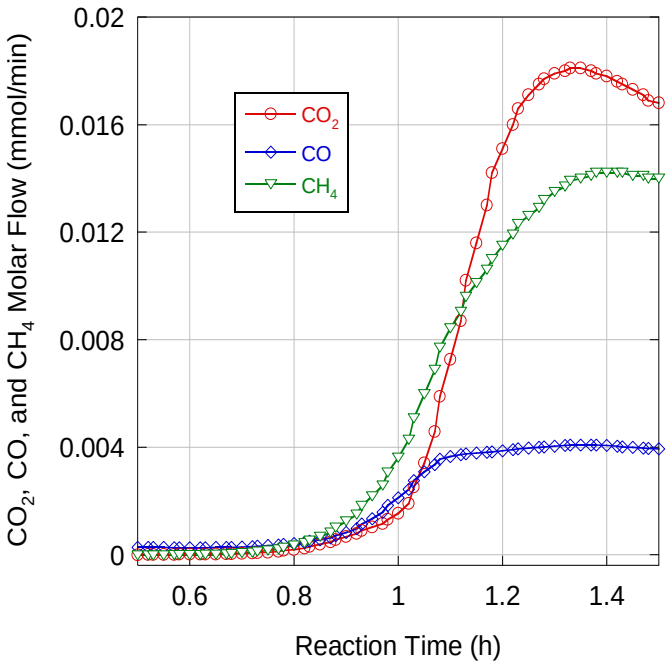

Figure 3.10: Expanded view of initial CO, CO_2, and CH_4 production from ML deoxygenation over 5 wt. % Pd/C at 300 °C and 15 bar under 5 mol. % H_2.

A set of reactions with the typical amount of reactant, solvent and catalyst were used with systematically varied reaction times in order to test the effect of reaction time on the deoxygenation of ML (shown in Figure 3.11). Results of this are summarized in Table 3.2. The data set showed that the experiments are extremely repeatable.

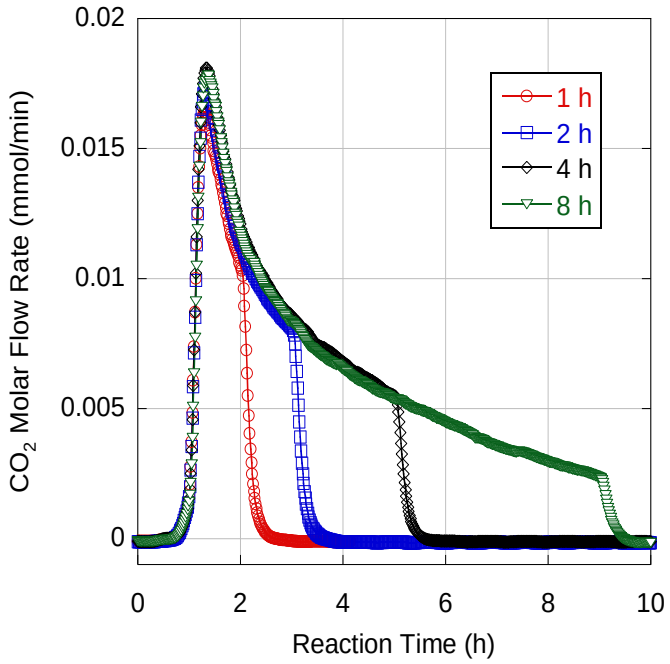

Figure 3.11: Semi-batch decarboxylation of ML over 5 wt. % Pd/C at 300 °C and 15 bar under 5 mol. % H_2 for 1 h, 2 h, 4 h, and 8 h.

The CO and CO_2 molar flow data from the original ML deoxygenation experiment was used to determine the yield every half-hour through the end of the reaction time. This was then used to create a 1^{st} and 0^{th} order plots to determine the reaction order for this reactant. This was also done for EL. The deoxygenation results for EL are shown in Figure 3.12 and look very similar to the results for ML deoxygenation. The only difference is that ethane (C_2H_6) production was not plotted. This is because the calibration mixture used to calibrate the QMS did not contain C_2H_6. EL was converted with higher yields than ML, but with an equivalent CO_2 selectivity.

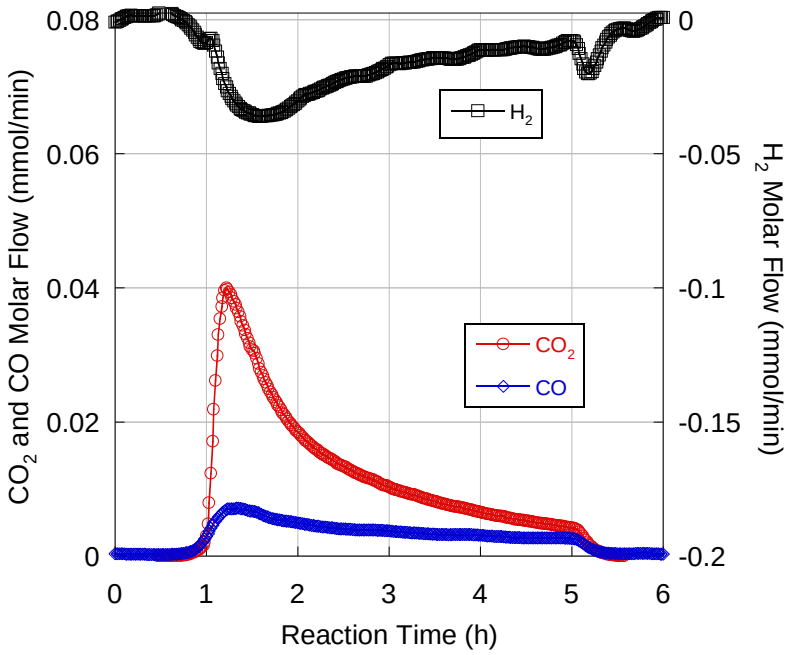

Figure 3.12: H_2, CO, and CO_2 evolution during semi-batch EL deoxygenation over 5 wt. % Pd/C at 300 °C and 15 bar under 5 mol. % H_2.

The 1st order plot of the data for ML and EL deoxygenation is shown in Figure 3.13. The data for this plot were obtained in several ways. The first way was using the overall CO + CO_2 yield data as a function of reaction time (shown in Figure 3.11). This set is marked "RT." The second data set marked "RT" was derived from the *n*-C_{11} yield from the deoxygenation experiments with increasing reaction time. The second way of obtaining this data was determining the CO+CO_2 yield every hour from the data from one 4 h reaction. These data are marked "S." The data show that both ML and EL follow 1st order kinetics at a concentration of 4 mol. %. The apparent rate constant for EL was slightly over twice that for

the apparent rate constant for ML. This may be due to the formation of a stable C_2 intermediate on the Pd surface during EL deoxygenation.

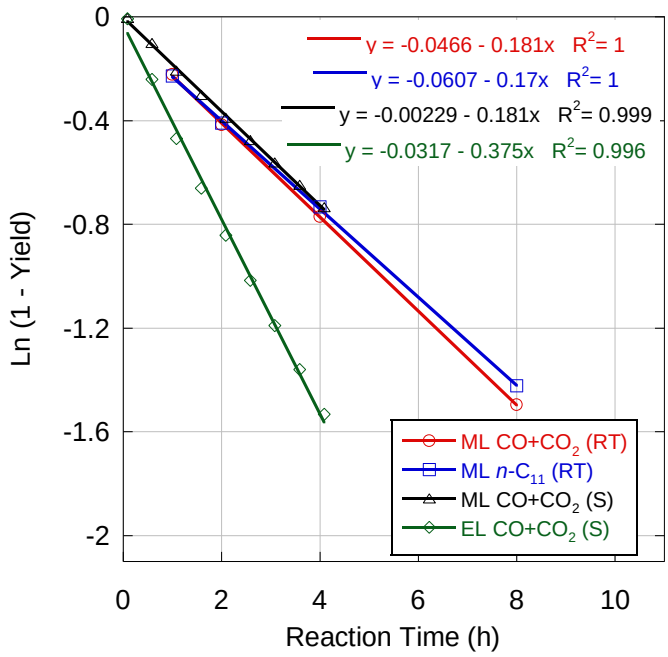

Figure 3.13: 1st order graph of ML and EL deoxygenation at over 5 wt. % Pd/C at 300 °C and 15 bar under 5 mol. % H_2. Data labeled RT were determined at different reaction times. Data labeled S were determined by calculating the $CO+CO_2$ yield every half hour for one 4 h reaction.

Table 3.2: Summary of semi-batch deoxygenation of 5.6 mmol ML and EL over 5 wt. % Pd/C at 300 °C and 15 bar under 5 mol. % H_2.

	ML				EL
Reaction Time (h)	1	2	4	8	4
$CO+CO_2$ Yield (%)	19.9	34.1	53.7	77.6	79.7
***n*-C_{11} Yield (%)**	20.4	33.6	51.9	75.9	76.8
CH_4 Yield (%)*	13.4	23.0	37.6	52.4	n/a
FAE Conversion (%)	29.7	43.5	64.2	84.6	86.3
CO_2 Selectivity (%)	77.4	76.5	74.9	71.0	76.4
mol H_2/mol $CO+CO_2$ Generated	-1.24	-1.09	-1.00	-1.22	-1.16

The effect of initial ML concentration also was tested; however, due to the slow reaction kinetics of ML deoxygenation, all experiments were conducted at 8 h reaction time. Figure 3.14 below shows the temporal CH_4 production exhibited by these experiments. As the ML concentration increased, the CH_4 maximum and the quasi steady-state CH_4 production rate increased. This figure looks very different from the concentration graph for LA. There were no major changes in the CH_4 curve shape. Table 3.3 summarizing the results of these experiments shows that the only major difference between the concentrations was the value of the yields. As the concentration increased, the $CO+CO_2$ yields, *n*-C_{11} yields and CH_4 yields all decreased with increasing ML initial concentration. While the $CO+CO_2$ yields and *n*-C_{11} yields were in good agreement, the CH_4 yields were all approximately 70% of these two yields. The discrepancy between these two yields could be explained by the generation of MeOH, resulting in dodecanal production. This dodecanal would then be deoxygenated to *n*-C_{11} and CO, creating one mole of CO without producing one mole of

CH_4. However, QMS data of the gas-phase products did not detect any MeOH (m/z 32), and n-C11 was identified as the only liquid-phase product via GC-FID.

The CO_2 selectivity actually increased as the ML concentration increased. This trend seems counterintuitive given the trend shown across the LA concentration range. However, it provides insight into how ML (and FAEs, in general) are deoxygenated. Gaseous data from ML deoxygenation indicated that CH_4 is produced immediately before CO and CO_2 are produced, meaning that FAE deoxygenation is a series of two reactions. The CO_2 selectivity data in Table 3.3 indicate that these two reactions occur at very different rates. Experiments shown above show that FAE deoxygenation occurs much more slowly than FA deoxygenation. The high CO_2 selectivity across all concentrations tested indicates that there is little build-up of LA in the reaction, meaning that FA deoxygenation occurs faster than ester hydrogenolysis. This hypothesis is also supported by the absence of LA in the product liquid-phase GC analyses from any of the experiments, even at reaction times shorter than 4 h. The sequential deoxygenation reaction pathway for the conversion of FAEs proposed in the work in this section was also exhibited during FAE conversion over other catalysts. Conversion of ML over NiMo/γ-Al_2O_3 occurred via a LA intermediate with *n*-C_{11} and *n*-C_{12} as the major products [5].

The initial rates were also calculated for this data series. It was shown that all three species (CO, CH_4, and CO_2) experienced an increase in initial rate with the increase in ML concentration. The rate at which CH_4 was initially produced exhibited the largest jump and more than doubled across the concentration series. The initial rate for CO increased very slightly across the concentration series. The CO_2 initial rate also increased, but reached a

maximum at 8 mol. %. These trends are consistent with the hypothesis that methane formation from ML conversion is rate limiting. The relationship between initial rates and ML concentration also points to quick conversion of any LA intermediate that may be produced during ML deoxygenation. It was posited above that the initial decarboxylation rate reaches a maximum between 0 mol. % and 4 mol. % LA. All of the initial decarboxylation rates from ML deoxygenation are less than the initial decarboxylation rate at an LA concentration of 4 mol. %, which indicates that LA concentrations are below 4 mol. %.

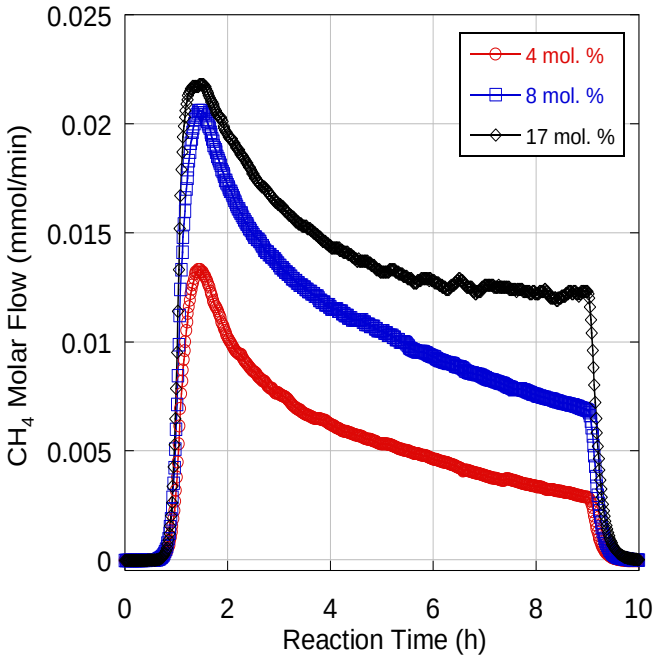

Figure 3.14: CH_4 produced by ML deoxygenation at concentrations of 4 mol. %, 8 mol. %, and 17 mol. % over 5 wt. % Pd/C at 300 °C and 15 bar under 5 mol. % H_2.

Table 3.3: Summary of ML concentration series deoxygenation.

	1xML	***2xML***	***4xML***
ML Conc. (mol. %)	4	8	17
$CO+CO_2$ Yield (%)	77.6	63.7	42.7
***n*-C_{11} Yield (%)**	75.9	61.4	42.5
CH_4 Yield (%)	52.4	48.4	31.9
ML Conversion (%)	84.6	71.1	49.9
CO_2 Selectivity (%)	71.0	76.7	80.9
mol H_2/mol $CO+CO_2$ Generated	-1.22	-1.04	-1.11
CH_4 Initial Rate (mmol/g_{cat}-h)	1.57	2.62	3.62
CO Initial Rate (mmol/g_{cat}-h)	0.624	0.755	0.805
CO_2 Initial Rate (mmol/g_{cat}-h)	2.70	3.41	3.20

The concentration series data also revealed more about the kinetics of FAE deoxygenation. More specifically, it revealed more about the reaction order of FAEs. Integral 0^{th} order and 1^{st} order kinetics plots were generated for this concentration series, as previously described. The results are illustrated in Figure 3.15. The figures show that all concentrations tested follow 1^{st} order kinetics, and apparent 0^{th} order kinetics are exhibited only at higher ML concentrations. This indicates that ML deoxygenation, and FAE deoxygenation, seems to follow Langmuir-Hinshelwood kinetics.

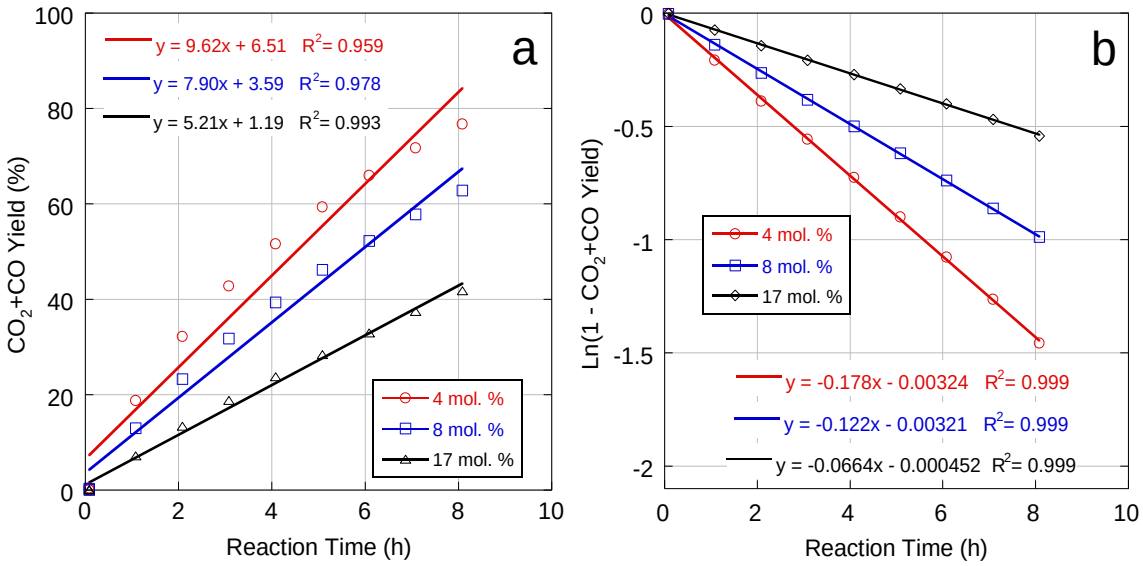

Figure 3.15: (a) 0^{th}-order plot and (b) 1^{st}-order plot of semi-batch ML deoxygenation over 5 wt. % Pd/C at 300 °C and 15 bar under 5 mol. % H_2 across a concentration range from 4 mol. % to 17 mol. %.

The reaction profiles for MS and ES deoxygenation are closely similar to those for ML and EL deoxygenation and are shown as Figure 3.16 and Figure 3.17, respectively. Table 3.4 also provides results for these experiments. ES was deoxygenated with higher yields than MS. The CO_2 selectivities from these reactions were almost identical.

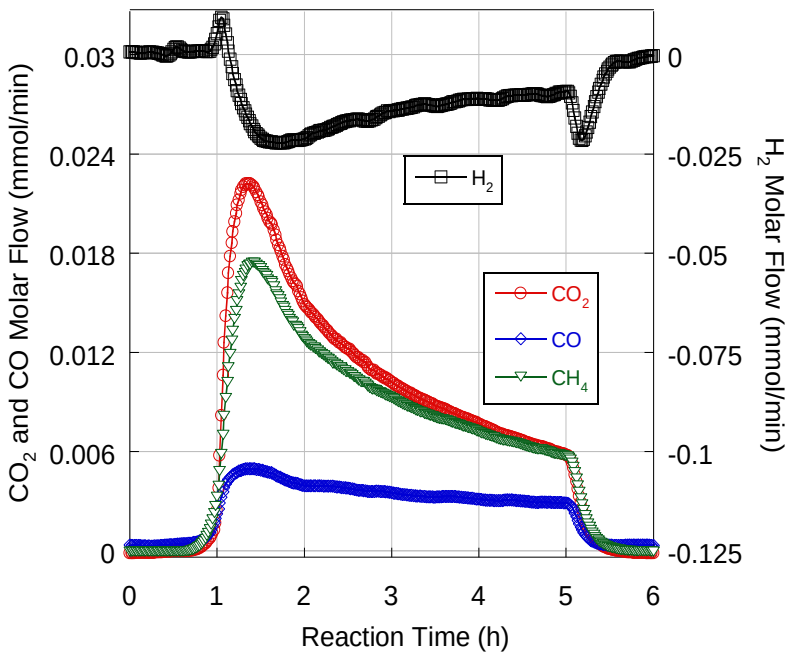

Figure 3.16: CO, CO_2 and CH_4 production (and H_2 consumption) during MS deoxygenation over 5 wt. % Pd/C at 300 °C and 15 bar under 5 mol. % H_2.

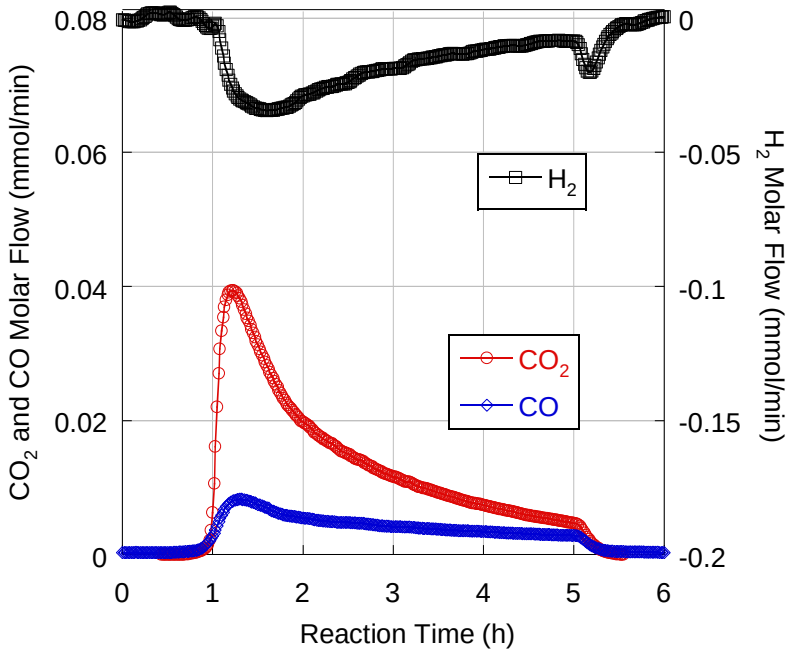

Figure 3.17: CO_2 and CO production and H_2 consumption produced via ES deoxygenation over 5 wt. % Pd/C at 300 °C and 15 bar under 5 mol. % H_2.

Table 3.4: Summary of MS and ES deoxygenation over 5 wt. % Pd/C at a concentration of 4 mol. %, 300 °C, and 15 bar under 5 mol. % H_2.

FAE	**$CO+CO_2$ Yield (%)**	**n-C_{17} Yield (%)**	**CH_4 Yield (%)***	**FAE Conversion (%)**	**CO_2 Selectivity (%)**	**mol H_2/mol $CO+CO_2$ Generated**
MS	66.9	63.6	43.8	74.8	75.2	-0.98
ES	85.8	80.3	-	89.6	75.6	-1.02

More important than the overall yield and CO_2 selectivities for these reactions are the apparent rate constants for 1st-order deoxygenation exhibited by FAEs. Figure 3.18 and

figure 3.19 are 1st-order plots comparing the deoxygenation of ML and MS and the deoxygenation of MS and ES, respectively. It has been shown that FA deoxygenation is influenced by chain length [3]. This was also demonstrated for FAE deoxygenation. In Figure 3.20, it can be seen that increasing the chain length from 12 to 18 carbons increased the apparent rate constant of CO and CO_2 production.

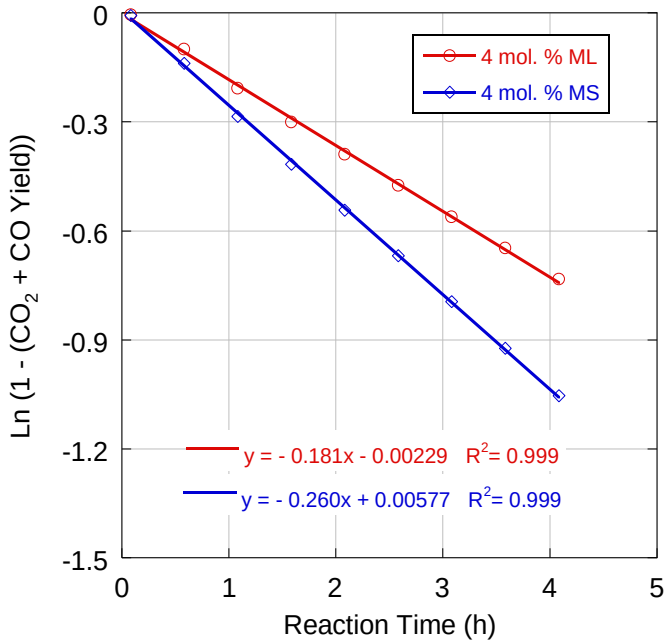

Figure 3.18: 1st-order plot of semi-batch ML and MS deoxygenation over 5 wt. % Pd/C at 300 °C and 15 bar under 5 mol. % H_2.

It was also determined that at longer chain lengths, the length of the ester alkyl group is also influential in determining the speed at which deoxygenation occurs. However, when the aliphatic chain of the FAE is longer, the effect of the ester alkyl chain length seems to be

mitigated. Previously in this section, it was shown that doubling the length of the ester alkyl chain more than doubles the apparent rate constant. However, the experiments with MS and ES deoxygenation show that doubling the ester alkyl chain only increases the apparent rate constant by a little over 70%. This shows that increasing the aliphatic chain length can be used to diminish the effects of the increase in ester alkyl chain length.

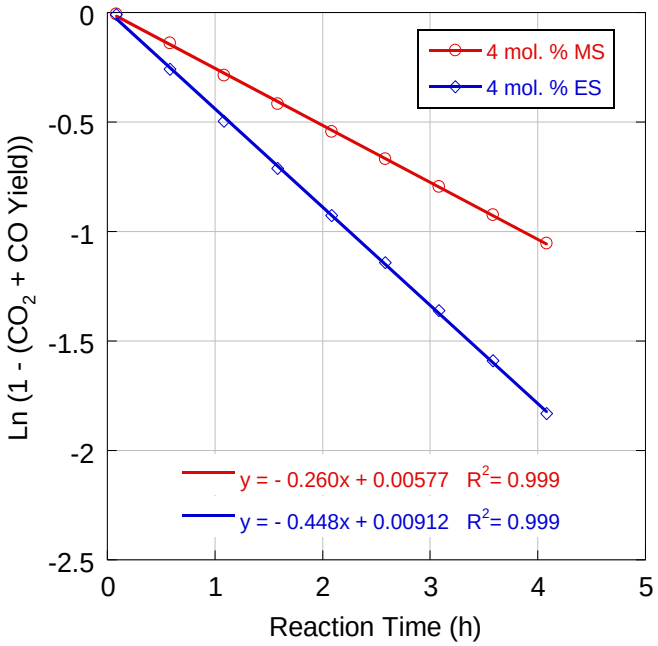

Figure 3.19: 1st-order plot comparison of MS and ES deoxygenation over 5 wt. % Pd/C at 300 °C and 15 bar under 5 mol. % H_2.

Summary

In this chapter, it was shown that increasing H_2 concentration in the gas feed stream from 1 mol. % to 20 mol. % causes nearly all metrics for LA deoxygenation ($CO+CO_2$ yield,

n-C_{11} yield, CO_2 selectivity, CO_2 initial rate, and batch productivity) to drop significantly. The only measurement of LA deoxygenation that did not decrease was the CO initial rate, which actually remained constant across all H_2 partial pressures. It was also determined that increases in LA concentration caused the $CO+CO_2$ yield, *n*-C_{11} yield, and CO_2 selectivity to decrease. It also caused the initial decarboxylation rate to increase and the initial decarbonylation rate to increase. The LA initial decarboxylation rate is lower than the PA initial decarboxylation rate, which follows the trend published in the literature showing that increasing FA chain lengths increased decarboxylation rates and overall CO_2 selectivity. The initial decarbonylation rates were actually identical across the concentration range. The batch productivity of LA deoxygenation reached a maximum at an LA concentration of 17 mol. %. This maximum is also lower for LA than it is for PA. 1^{st}-order and 0^{th}-order plots proved inconclusive when trying to determine the LA reaction order.

Deoxygenation of ML, EL, MS, and ES appear to occur in a series reaction scheme. During ML and MS deoxygenation, CH_4 production occurred before CO and CO_2 production. However, there was no liquid-phase evidence for either LA or SA during the experiments. This indicates that deoxygenation of FAEs occurs much slower than deoxygenation of FAs. More evidence of a two-step deoxygenation mechanism where the intermediate FA is a short-lived species was found during deoxygenation of ML at higher concentrations. When the initial ML concentration increased, the CO_2 selectivity did not change. This is contrary to the drop in CO_2 selectivity exhibited when the LA concentration was increased. It was also determined that FAE deoxygenation follows Langmuir-Hinshelwood kinetics and that apparent rate constants are controlled by both the long alkane

chain and the ester alkyl chain. When the long aliphatic chain on the FAEs increased from 12 carbons to 18 carbons, the apparent rate constant increased by a little over 40%. When the methyl ester moiety was substituted for an ethyl moiety, this apparent rate constant nearly doubled for both FAEs.

References

[1] E. W. Ping, R. Wallace, J. Pierson, T. F. Fuller, and C. W. Jones, "Highly dispersed palladium nanoparticles on ultra-porous silica mesocellular foam for the catalytic decarboxylation of stearic acid," *Microporous and Mesoporous Materials,* vol. 132, pp. 174-180, Jul 2010.

[2] A. T. Madsen, B. Rozmyslowicz, P. Maki-Arvela, I. L. Simakova, K. Eranen, D. Y. Murzin, *et al.*, "Deactivation in Continuous Deoxygenation of C-18-Fatty Feedstock over Pd/Sibunit," *Topics in Catalysis,* vol. 56, pp. 714-724, Jun 2013.

[3] J. P. Ford, J. G. Immer, and H. H. Lamb, "Palladium Catalysts for Fatty Acid Deoxygenation: Influence of the Support and Fatty Acid Chain Length on Decarboxylation Kinetics," *Topics in Catalysis,* vol. 55, pp. 175-184, May 2012.

[4] J. P. Ford, N. Thapaliya, M. J. Kelly, W. L. Roberts, and H. H. Lamb, "Semi-Batch Deoxygenation of Canola- and Lard-Derived Fatty Acids to Diesel-Range Hydrocarbons," *Energy & Fuels,* vol. 27, pp. 7489-7496, Dec 2013.

[5] K. C. Kwon, H. Mayfield, T. Marolla, B. Nichols, and M. Mashburn, "Catalytic deoxygenation of liquid biomass for hydrocarbon fuels," *Renewable Energy,* vol. 36, pp. 907-915, Mar 2011.

CHAPTER 4: CBFA Deoxygenation to *n*-Alkanes over 5 wt. % Pd/C

Introduction

Fatty acids (primarily, lauric acid (LA)) secreted from the cyanobacterium *Synechocystis* sp. PCC 6803 during growth in bench-top carboys at Arizona State University (ASU) were recovered using anion exchange and hydrophobic resins. The cyanobacteria-derived fatty acids (CBFAs) were tested for FA content by GC-FID and by liquid chromatography/mass spectrometry (LC/MS). Select samples were also submitted for elemental analysis by inductively coupled plasma-optical emission spectroscopy (ICP-OES). Typically, the crude CBFA samples contained ~80 wt. % LA and 100-150 ppm S with smaller concentrations of P, Na, Ca and Mg. β-hydroxymyristic acid (BHMA) was determined LC/MS to constitute almost 1-2 wt. % of the CBFAs. In a subsequent series of experiments, purification methods, including AC decolorization, adsorption chromatography, precipitation, and alkaline and acid hydrolysis, were employed to mitigate CBFA contamination by sulfolipids and proteins. As reported in this chapter, crude and purified CBFAs samples were deoxygenated over 5 wt. % Pd/C catalysts in semi-batch mode. BHMA was deoxygenated in semi-batch mode over 5 wt. % Pd/C, and a reaction network for deoxygenation of this model compound was established. The effect of the presence of BHMA on FA deoxygenation was also tested in semi-batch mode. Larger batches (10-30 g) of CBFAs were deoxygenated in semi-batch and fed-batch mode to produce *n*-alkanes for subsequent hydroisomerization to synthetic paraffinic kerosene.

Semi-batch Deoxygenation of Crude CBFAs

Early CBFA samples of obtained from ASU were primarily from the Vermaas Lab strain. Seven out of the eight samples obtained were recovered using the L493 (hydrophobic interaction) resin. FA02 was the only sample of this initial series to be recovered using the MP 64 anion exchange resin. Most of these were harvested from cultures with volumes of approximately 40 L. To assess the FA composition, a small portion of each sample was submitted for analysis by GC-FID. The GC-FID results, shown in Table 4.1, indicate that the average composition of the CBFAs is 80% LA, 7% MA and 3% PA. The total FA content is shown on the last line of Table 4.2. As evidenced by the data, none of the CBFA samples contained more than 85% FA by weight, with the average being 76%. FA10 had the lowest total FA content (698 mg FA/g sample). Both FA01 and FA02 had total FA contents >800 mg/g sample. The unknowns are likely to include hydroxy fatty acids (e.g., BHMA). LC/MS analysis (shown in Table 4.2) performed at ASU determined that BHMA was present in the CBFAs at a concentration between 1.5 and 2 wt. %. LC/MS analysis at ASU also was used to determine the total FA content of samples FA01-FA04: FA01 – 88.1%, FA02 – 103.1%, FA03 – 90.3%, FA04 – 104.9%. The only one of these total fat contents that agrees with the GC-FID analysis is the total fat content for FA01.

Table 4.1: Fatty acid analysis results for initial series of CBFAs. The designation Cn:m refers to the carbon number of the fatty acid (n) and the degree of unsaturation (m) (number of C-C double bonds in the alkyl chain).

	Amount (% of total fatty acids (w/w))						
Fatty Acid	**FA01**	**FA02**	**FA03**	**FA04**	**FA08**	**FA10**	**FA11**
C8:0	0	-	-	-	-	-	-
C 10:0	1	0	1	1	1	0	0
C 11:0	0	1	1	1	1	0	0
C 12:0	86	82	80	79	72	77	81
C 12:1*	1	-	1	1	1	1	1
C 14:0	5	6	6	7	7	6	9
C 14:1 cis	-	-	0	0	0	0	-
C 16:0	1	3	2	3	4	3	3
C 16:1 cis	0	1	1	1	2	1	1
C17:0	0	0	0	0	0	-	-
C 17:1 cis	-	-	0	0	0	-	-
C 18:0	0	0	0	0	1	0	0
C 18:1, cis	0	0	1	1	2	0	1
C 18:2 cis	0	1	2	2	2	1	0
C18:3 cis 6	1	2	2	2	1	7	0
C18:3 cis 9	-	0	-	0	-	-	-
C 20:1, cis	-	0	0	-	-	-	-
unknowns	4	3	2	2	6	3	4
Total fat (mg/g)	**843**	**801**	**738**	**755**	**711**	**698**	**771**

Table 4.2: LC/MS analysis of early ASU CBFAs.

	Amount (% of total fatty acids (w/w))	
Fatty Acid	**G***	**W***
C10:0	0.59	0.74
C12:0	86.02	81.27
C12:1	1.07	1.27
C14:0	6.75	6.37
C14:0-OH (BHMA)	1.83	1.51
C16:0	1.72	2.62
C16:1	0.67	1.82
C18:0	0.55	0.57
C18:1	0.66	1.79
C18:2	0.15	2.03
C18:3	0.00	1.10

*G and W denote the color of the CBFAs. G was chosen indicate a yellowish-green color. W indicates a white color.

ICP-OES analysis of one of the early CBFA samples received from ASU indicated that sulfur (S), a potent poison for noble metal catalysts, was present at a concentration of ~100 ppm. The results shown below (Table 4.3) indicate that FA04 also had a relatively high S concentration--over 50% higher than the previously analyzed sample.

Table 4.3: Elemental analysis of FA04 and a previous sample for S, P, Mg, Ca and Na concentrations.

			Contaminant Concentration (ppm)				
EATS ID	**CLIENT ID**	**Vial**	**Ca**	**Mg**	**Na**	**P**	**S**
GG5660	Fatty Acid	1st ASU Sample	17.8	8.57	190	9.11	95.2
HH1379	Fatty Acid	FA04	30.2	8.52	33.9	7.94	157
Method Detection Limit:			0.19	0.16	0.56	0.67	0.77
Limit of Quantification:			1.90	1.61	5.59	6.72	7.66

Semi-batch deoxygenation of the CBFAs to hydrocarbons over Pd/C was conducted at 300 °C and 15 bar under 5% H_2 using a 5 wt. % Pd/C. Two 5 wt. % Pd/C catalysts: Evonik E117 and BASF Escat^{TM}1971 were used. Catalyst characterization data and LA deoxygenation tests evidenced that E117 and Escat 1971 gave very similar results and could be used interchangeably for FA deoxygenation. The results of these experiments are shown below as Figure 4.1 and Table 4.4. In Figure 4.1, on-line quadrupole mass spectrometry (QMS) shows that the temporal CO_2 evolution curves during LA deoxygenation are closely similar, and that LA was fully converted after ~1 h. The main difference is the CO evolution, which is greater over E117. These similarities in LA deoxygenation activity are reasonable given that these catalysts have similar Pd particle sizes and surface areas. Both catalysts have total surface areas that exceed 800 m^2/g (855 m^2/g for E117 and 825 m^2/g for Escat 1971). Average Pd particles sizes for both catalysts are approximately 6 nm.

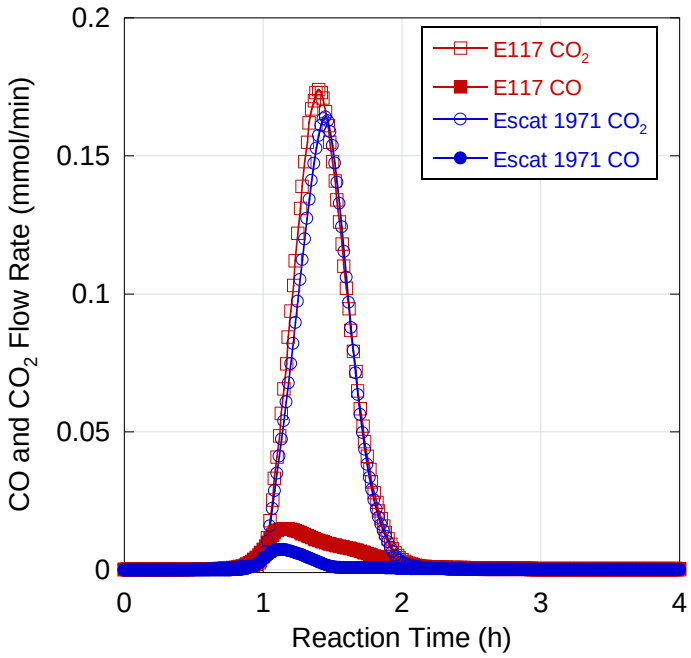

Figure 4.1: Semi-batch LA deoxygenation at a concentration of 5 wt. % over 5 wt. % Pd/C E117 and Escat 1971 at 300 °C and 15 bar under 5 vol. % H_2.

Table 4.4: Summary of LA deoxygenation over 5 wt. % Pd/C E117 and Escat 1971 at an initial concentration of 5 wt. %, 300 °C, and 15 bar under 5 vol. % H_2.

Catalyst	***E117***	***Escat 1971***
BET Surface Area (m^2/g)	855	825
Dispersion (%)†	17.8	18.2
CO+CO_2 Yield (%)	99.6	83.8
n-C_{11} Yield (%)	89.1	95.5
CO_2 Selectivity (%)	87.9	95.7
mol H_2/mol CO+CO_2 Generated	-0.13	-0.13

†Determined via volumetric CO chemisorption on a Micromeritics ASAP 2020c. Calculated with a Pd:CO ratio of 1.5:1.

The CBFAs were not deoxygenated as efficiently over 5 wt. % Pd/C catalysts as the LA model compound. The BASF Escat 1971 catalyst was used for three of the CBFAs in this set of experiments (FA01, FA02, and FA10), and Evonik E117 was used for the remainder. All reactions were conducted at 300°C for 4 h, except FA04, which had an 8 h reaction time. The CBFA deoxygenations gave $CO+CO_2$ yields ranging from 41.8 to 88.5%, alkane yields ranging from 45.1 to 79.7%, and CO_2 selectivities ranging from 7.1 to 91.4%. The differences in overall activity and selectivity to decarboxylation can be attributed to impurities in the CBFAs. The results in Table 4.5 also show that FA02 exhibited the highest $CO + CO_2$ yield, alkane yield, and CO_2 selectivity of all of the bio-derived samples. The yields and CO_2 selectivity were equivalent to those for LA deoxygenation over Escat 1971 and E117. In contrast, deoxygenation of FA10 gave the lowest $CO + CO_2$ yield, alkane yield, and CO_2 selectivity.

Lower FA content and higher S contamination levels (>100 ppm) in the CBFAs slowed deoxygenation kinetics and reduced Pd/C catalyst lifetime, when compared to the LA model compound. These trends are illustrated in Figure 4.2. Sample FA04 was typical of CBFA samples that showed slow deoxygenation kinetics associated with catalyst poisoning, and it contained 75-80% FA by weight and 150 ppm S. P contamination was <10 ppm, and at this level, P is not expected to affect catalyst lifetime. FA02 (recovered on MP 64) was converted to hydrocarbons more readily than FA01 (and the remaining CBFAs that were recovered using the hydrophobic L493 resin). Deoxygenation of FA03 resulted in complete conversion of FAs to hydrocarbons in less than 4 h reaction time with high CO_2 selectivity, as illustrated in Figure 4.2. This indicated that AC decolorization of CBFA samples was

effective in removing a significant portion of the remaining impurities (catalyst poisons). Comparison to the results for FA04 at 8 h reaction time (Table 4.5) also shows much higher alkane yield and much lower hydrogen consumption.

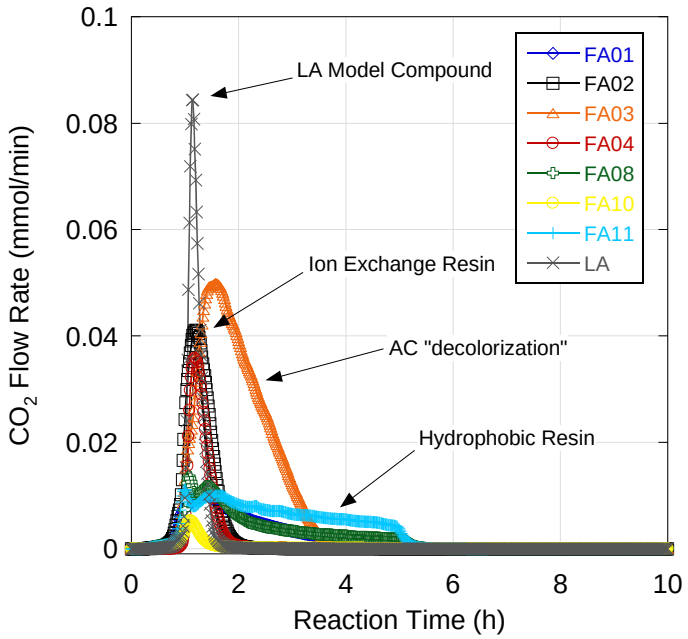

Figure 4.2: Decarboxylation of ASU CBFAs and model LA over 335 mg 5 wt. % Pd/C (E117 and Escat 1971) under 5 vol. % H_2 at 300 °C and 15 bar.

Table 4.5: Summary of deoxygenation results for the initial series of CBFA samples.

Sample	FA Content (%)*	FA Content (%)**	Mass (g)	FA Conc. (wt. %)	$CO+CO_2$ Yield (%)	Alkane Yield (%)	CO_2 Selectivity (%)	mol H_2/mol $CO+CO_2$ Generated
FA01	84.3	92.4	0.44	3.04	78.6	74.3	67.7	-0.46
FA02	80.0	88.3	0.38	2.67	88.5	79.7	91.4	-0.12
FA03[†]	-	87.5	1.36	6.09	87.4	90.9	90.0	-0.16
FA04	75.5	80.6	1.16	4.90	57.3	50.4	31.7	-0.88
FA08	71.1	81.7	0.80	3.41	60.8	54.0	62.3	-0.64
FA10	69.7	70.4	0.99	4.23	41.8	45.1	7.1	-0.65
FA11	77.1	78.1	1.18	4.99	68.4	51.1	61.1	-0.69
LA[a]	-	-	1.13	4.77	83.8	95.5	95.7	-0.13
LA[b]	-	-	1.13	4.77	99.6	89.1	87.9	-0.13

*Determined by Lisa Dean in NCSU Food Science Department.

**Determined by in-house GC-FID analysis and serves as basis for $CO+CO_2$ and alkane yield calculation.

[†]Decolorized using activated carbon prior to reaction.

[a]Deoxygenation over Escat 1971.

[b]Deoxygenation over E117.

ASU FA32 was recovered over L493 resin and deoxygenated under typical conditions over Pd/C E117. The results are shown below in Figure 4.3 and Table 4.6. Neither yield exceeded 40%. The CO_2 selectivity for this reaction was also extremely low. Due to the low yields and CO_2 selectivity obtained from FA32, the sample was sent back to ASU for AC decolorization (labeled FA32A after AC treatment). FA32A was analyzed for FA content by GC-FID, and the results are summarized in Table 4.7. FA analysis showed that FA32A was similar in composition and total fat content to previously tested samples. The AC treatment of FA32 was successful in improving deoxygenation performance, as demonstrated by large increases in yield and CO_2 selectivity at ~5 wt. % initial biomass concentration (Table 4.6).

Table 4.6: Summary of deoxygenation of ASU samples FA32 and FA32A.

Sample	**Mass (g)**	**Biomass Content (wt. %)**	**$CO+CO_2$ Yield (%)***	**Alkane Yield (%)***	**CO_2 Selectivity (%)**	**mol H_2/ mol $CO+CO_2$ Produced**
FA32	1.15	4.96	35.5	32.1	22.0	-1.07
FA32A	0.27	1.75	72.9	64.2	76.2	-0.12
FA32A	0.52	2.25	68.9	72.0	79.7	-0.29
FA32A	1.06	4.53	53.6	52.8	71.2	-0.32

*Calculated based on average FA profile as determined by Dr. Lisa Dean.

Table 4.7: Summary of FA32A fatty acid analysis.

Fatty acid	Amount (% of total fatty acids (w/w))
C 10:0	0.42
C 10:1	0.00
C 12:0	81.58
C 14:0	7.61
C 14:1 trans	0.00
C 14:1 cis	0.00
C 16:0	3.18
C 16:1 trans	0.00
C 16:1 cis	0.78
C16:3 cis	0.00
C16:4 cis	0.00
C 18:0	0.34
C 18:1, cis	0.35
C 18:2 cis	0.74
C18:3 cis 6	0.65
C18:3 cis 9	0.08
C 20:1, cis	0.15
unknowns	2.64
Total fat (mg/g)	**766.92**

Three semi-batch deoxygenation experiments with FA32A were conducted to examine the effects of initial biomass concentration on deoxygenation kinetics. Different initial masses of FA32A (0.27, 0.52 and 1.06 g) were charged to the reactor in each experiment and deoxygenated under standard reaction conditions. The CO_2 and CO QMS traces for these experiments are shown in Figure 4.3, and the results are summarized in Table 4.6.

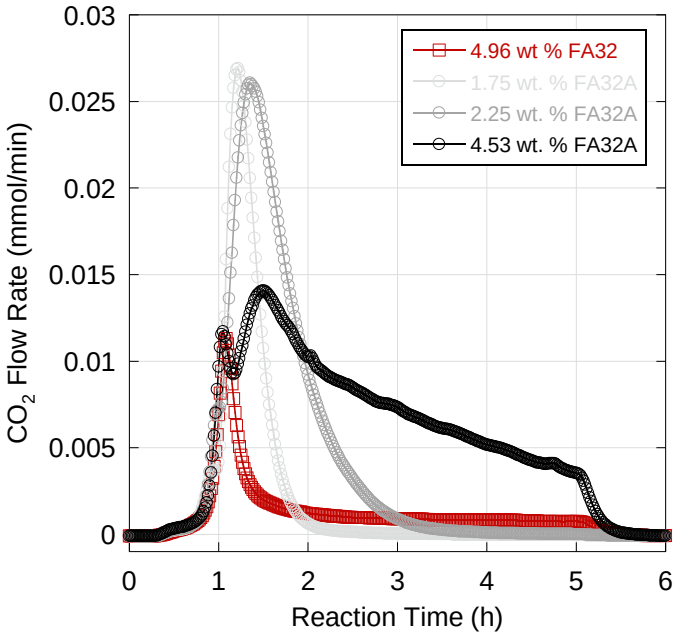

Figure 4.3: Deoxygenation of FA32 and FA32A at three different FA concentrations over 5 wt. % Pd/C under 5 % H_2 at 300 °C and 15 bar.

Figure 4.3 illustrates that at the lowest initial biomass concentration the decarboxylation pathway is dominant and deoxygenation is complete in ~1 h at 300°C. As the initial biomass concentration was increased, the CO_2 peak broadened and diminished in height and the CO peak (not shown) grew larger, indicative of a change in reaction pathway and catalyst deactivation. At the highest CBFA concentration (approximately the initial concentration used in a typical semi-batch LA deoxygenation), the reaction did not go to completion after 4 h at 300°C, as indicated by the decline in the CO_2 and CO signals when the reactor was cooled (at 5 h). Also, H_2 consumption increased as the biomass concentration increased. The correlation between biomass concentration and catalyst

deactivation is inferred to originate from feed impurities (sulfolipids and proteins) that are suspected catalyst poisons. Although FA32A was not submitted for elemental analysis via ICP-OES, evidence of relatively high (100-150 ppm) S concentrations in previous CBFAs supports the catalyst poisoning hypothesis.

Also of note in Figure 4.3 is the shape of the CO_2 peak for FA32 and FA32A at the highest initial concentrations. For FA32, the CO_2 production reached a maximum a little before 1 h, declined rapidly, and never recovered. The CO_2 trace for FA32A deoxygenation exhibits two maxima over the course of the reaction. The first of these coincided with the FA32 CO_2 maximum. It was suspected that the CO_2 peak appearing immediately before 1 h reaction time (just as the reactor reached 300°C) originated from BHMA deoxygenation. This hypothesis was investigated using model compounds, as described below.

BHMA Deoxygenation: Reaction Network and Effect on FA Deoxygenation

BHMA is a constituent of lipopolysaccharide, which is an endotoxin found in the cell membrane of gram-negative bacteria. BHMA was expected to be detected in CBFA samples received from ASU, as *Synechocystis* are gram-negative bacteria [1, 2]. LC/MS analysis of CBFAs confirmed that BHMA was present in concentrations between 1-2 wt. %. It was unknown if or how BHMA would be deoxygenated over Pd/C. Figure 4.4 shows the CO_2, CO and H_2 generated by this reaction at 300°C and 15 bar under 5 vol. % H_2.

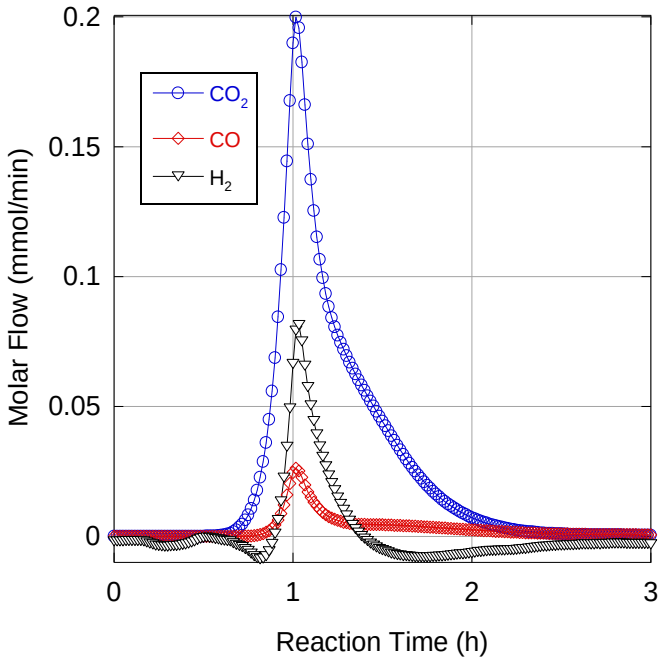

Figure 4.4: H_2, CO, and CO_2 evolution from BHMA semi-batch deoxygenation over 5 wt. % Pd/C at 300 °C and 15 bar under 5% H_2.

The deoxygenation of BHMA proceeded with a rapid production of CO_2 at an earlier reaction time than the maximum CO_2 production rate for the LA deoxygenation. The CO_2 + CO yield for this reaction was 95.7%, and the CO_2 selectivity was 88.3%. Post-reaction analysis of the condenser and reactor contents by GC-FID identified *n*-C_{13} and 2-C_{13}-ONE as major products. Minor products from the reaction were *n*-C_{11}, 2-C_{13}-OH, and an long-retention-time (presumably, high molecular weight) unknown. The GC-FID chromatograms are shown in Figure 4.5. The 2-C_{13}-ONE standard is in the top panel, the 2-C_{13}-OH standard is in the middle panel, and the reactor contents from BHMA deoxygenation are in the bottom panel.

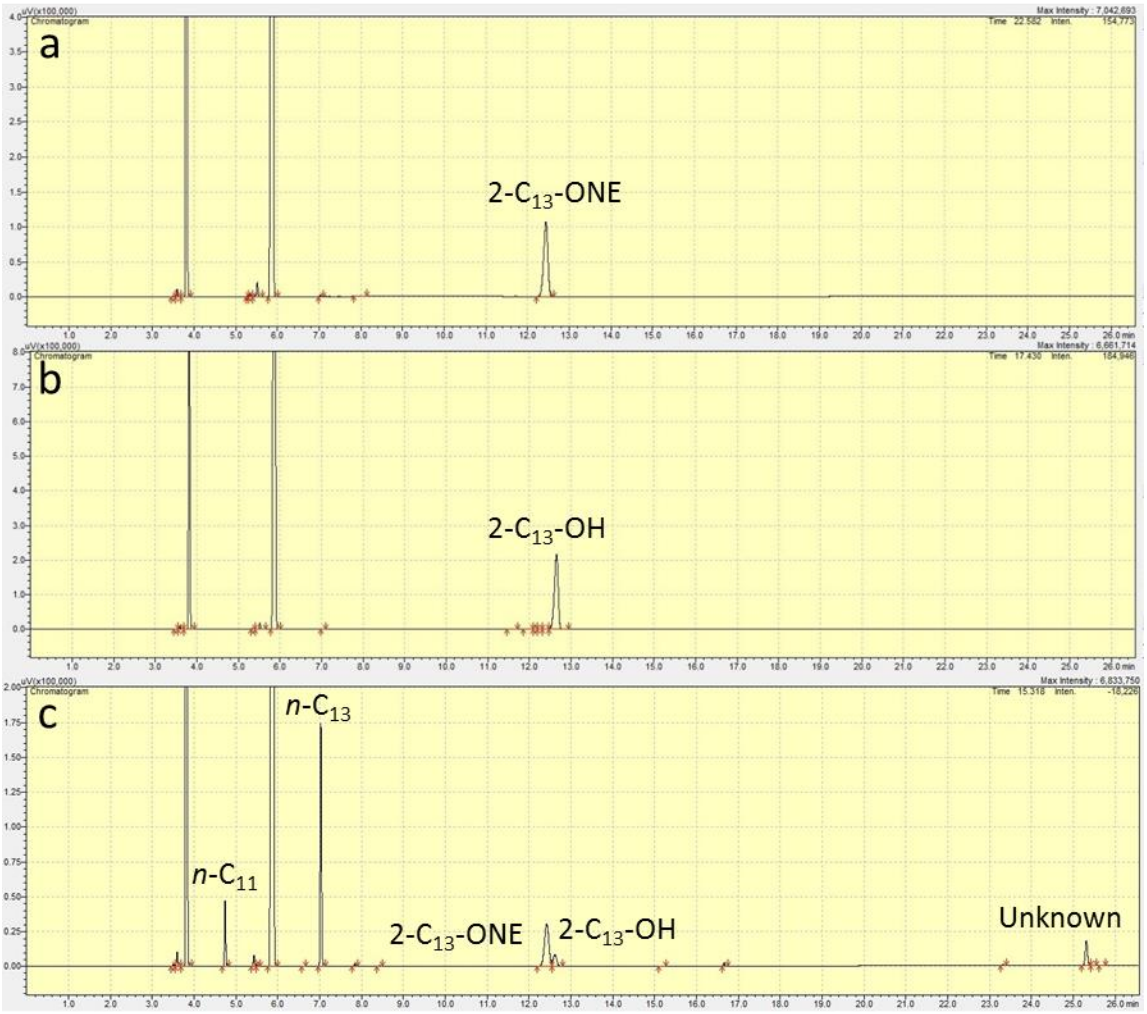

Figure 4.5: Chromatograms of standards and BHMA deoxygenation product with species identification: (a) 2-C_{13}-ONE, (b) 2-C_{13}-OH and (c) BHMA reactor contents.

Both 2-C_{13}-OH and 2-C_{13}-ONE were investigated for their ability to be deoxygenated to *n*-C_{13}. The results of these experiments and the BHMA deoxygenation experiments are shown in Table 4.8. Table 4.8 shows the number of moles of gaseous and liquid products formed by each reaction. The number of moles of unknown product were calculated by the

difference between the number of reactant moles and the number of product moles that could be accounted for with all other identified products. The table shows that BHMA was the only of the three reactants that led to significant *n*-C_{13} formation. Neither 2-C_{13}-ONE nor 2-C_{13}-OH were deoxygenated to *n*-C_{13} or *n*-C_{11} to any appreciable amount. In fact, 2-C_{13}-ONE was not converted to any extent at all. The *n*-C_{11} produced from these reactions is most likely from a series of reactions: hydrogenolysis to produce CH_4 and decarbonylation of the resulting dodecanal. The conversion of 2-C_{13}-OH was the reaction that produced the most unknown product, which suggests that the unknown may be a dimerized ether product. The liquid-phase data from all three reactions was used to create a reaction network, which is shown on the page after Table 4.8.

Table 4.8: Product moles of BHMA, 2-C_{13}-OH, and 2-C_{13}-ONE deoxygenation over 5 wt. % Pd/C at 300 °C and 15 bar under 5 vol. % H_2.

	Products (5.6 mmol Charge)								
	Gas (mmol)				***Liquid (mmol)***				
Feed	CO	CO_2	CH_4	H_2	*n*-C_{11}	*n*-C_{13}	2-C_{13}-ONE	2-C_{13}-OH	Unknown
BHMA	0.78	4.34	0.32	0.16	0.78	2.17	1.52	0.32	0.81
2-C_{13}-OH	0.40	0.09	0.25	3.68	0.62	0.22	3.23	0.22	1.31
2-C_{13}-ONE	0.31	0.06	0.23	-1.30	0.50	0.18	4.01	0.22	0.69

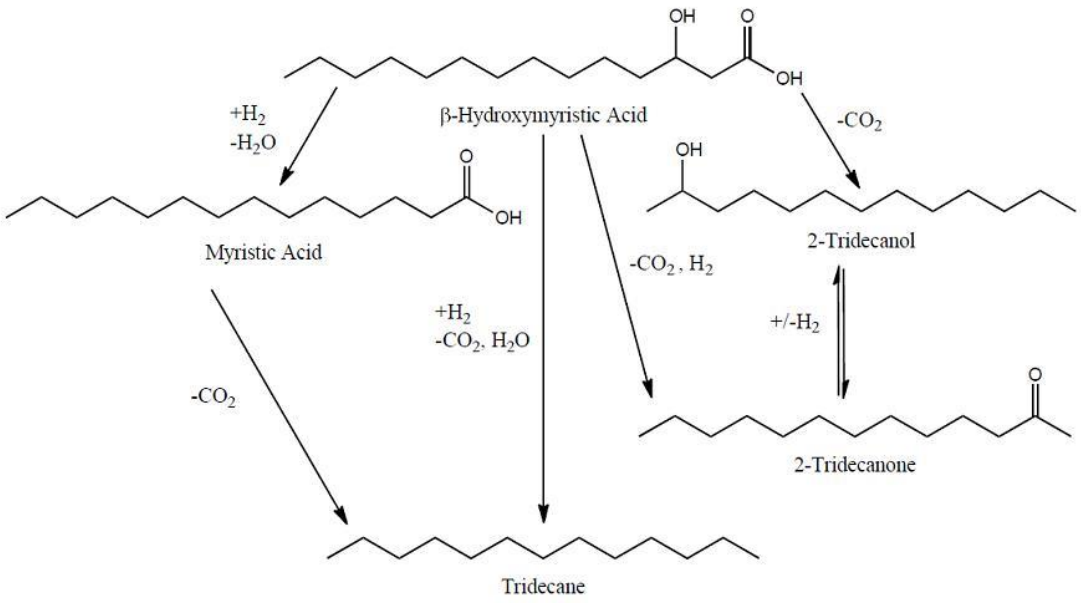

Figure 4.6: Suggested reaction network for BHMA deoxygenation over 5 wt. % Pd/C at 300 °C and 15 bar under 5 vol. % H_2.

Figure 4.6 shows that BHMA can be deoxygenated to *n*-C_{13}, 2-C_{13}-OH, or 2-C_{13}-ONE. It is unknown whether *n*-C_{13} is produced via direct full deoxygenation of BHMA, or through the MA intermediate shown on the left. MA was not detected in the liquid-phase products; however, FA deoxygenation has been shown to occur very rapidly when at low concentrations, meaning any MA produced during the reaction may have been converted to *n*-C_{13} very quickly. Pd is active for hydrogenation/dehydrogenation, producing an equilibrium between 2-C_{13}-ONE and 2-C_{13}-OH [3, 4]. Ketone deoxygenation over supported Pd can proceed via direct hydrogenolysis of the ketone, or hydrogenation to the alcohol and subsequent hydrogenolysis to the desired alkane product [5]. The ratio of 2-C_{13}-ONE to 2-

C_{13}-OH in the liquid products may explain the net hydrogen generation during BHMA deoxygenation. If 2-C_{13}-ONE generation proceeds via BHMA decarboxylation to 2-C_{13}-OH and subsequent 2-C_{13}-OH dehydrogenation, a mole of H_2 would be generated in the process. In an attempt to determine how BHMA would affect the deoxygenation of the CBFAs, LA/BHMA and MA/BHMA mixtures were deoxygenated under typical conditions. Figure 4.7 and Table 4.9 are the results from these experiments.

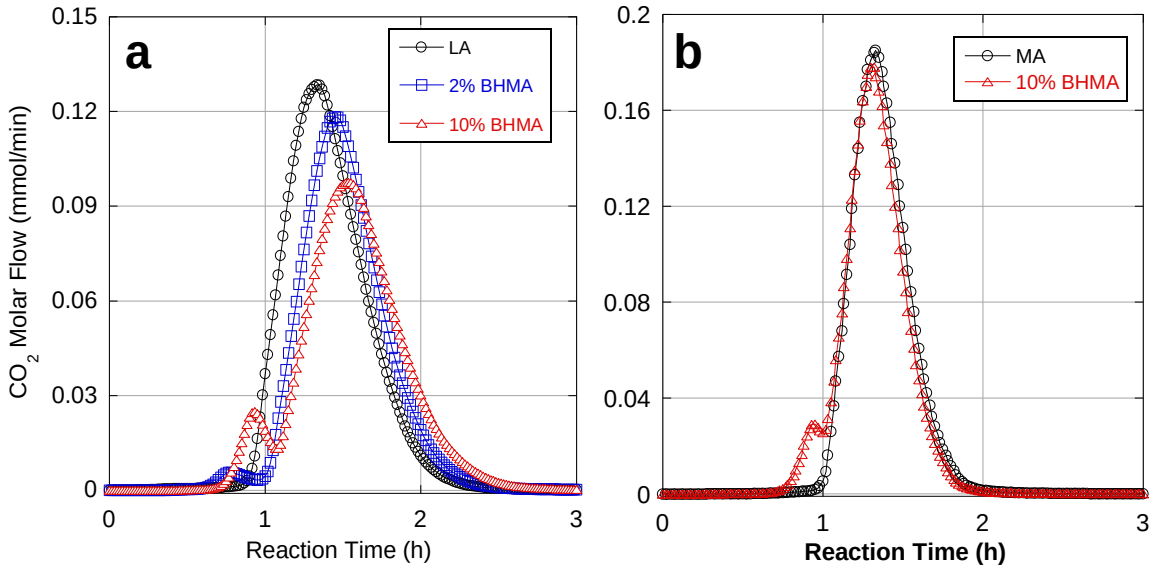

Figure 4.7: Decarboxylation of (a) LA/BHMA and (b) MA/BHMA mixtures over 5 wt. % Pd/C under 5 vol. % H_2 at 300 °C and 15 bar.

Table 4.9: Summary of LA/BHMA and MA/BHMA deoxygenation results.

Sample	FA Mass (g)	BHMA Mass (g)	$CO+CO_2$ Yield (%)	Alkane Yield (%)	CO_2 Selectivity (%)	mol H_2/mol $CO+CO_2$ Generated
BHMA	0.00	1.37	95.7	49.7	88.3	0.05
BHMA	0.00	1.36	91.6	52.7	84.8	0.03
LA	1.12	0.00	97.3	95.3	89.4	-0.02
2BHMA/98LA	1.11	0.02	84.1	45.6	90.9	-0.17
10BHMA/90LA	1.03	0.11	83.9	86.4	90.9	-0.07
MA	1.28	0.00	90.6	91.2	89.8	-0.17
10BHMA/90MA	1.15	0.10	90.3	86.8	90.1	-0.16

*Reaction conditions: T: 300 °C, P: 15 bar, H_2 Content: 5 vol. %.

From Figure 4.7, it was concluded that the presence of BHMA inhibits the conversion of the reaction mixture. As the BHMA concentration increased, the LA decarboxylation peak intensity dropped and the time required to convert most of the reaction mixture increased. The small initial CO_2 peak corresponded to the deoxygenation of BHMA and increased as the BHMA content increased. The deoxygenation of BHMA before LA suggests preferential adsorption of BHMA on the Pd surface. The effect of this preferential adsorption appears to be mitigated when MA is the FA reactant, as is evidenced by coincidental CO_2 peaks for both MA and 10BHMA/90MA. Table 4.9 confirms the full conversion of the model compounds and mixtures shown in Figure 4.7. For the BHMA samples, the disparity between the alkane yield and $CO+CO_2$ yield can be explained by the presence of 2-C_{13}-ONE and 2-C_{13}-OH products. All of the other alkane yields agree with their corresponding $CO+CO_2$ yields, with the exception of the 2BHMA/98LA sample. It is still unknown why the difference between the yields is so large for this sample. The CO_2

selectivity was also unaffected by the presence of BHMA, which is expected considering the CO_2 selectivity of BHMA deoxygenation. It is likely that the CBFA deoxygenation was being inhibited by the presence of both sulfur and BHMA in the biomass.

Semi-batch Deoxygenation of Recovered and Purified CBFAs

Another series of CBFA samples that (in most cases) were subjected to additional purification steps are listed in Table 4.10. Samples in this table were purified by one of 4 methods or combinations of these methods. One method was adsorption of impurities on AC as described in the previous section (denoted AC). The second method of purification was alkaline hydrolysis. The third method of purification was adsorption chromatography using a C-18 column (denoted C-18). In these experiments, different concentrations of methanol (MeOH) were used to elute the CBFAs from the column. The concentration of MeOH used for the elution step is also denoted in the table. Precipitation of FAs from solution was also investigated. Select samples were analyzed by ICP-OES, and the [S] and [P] results are included in Table 4.10.

Table 4.10: Purification procedures and ICP-OES [S] and [P] data for second series of CBFA samples.

Sample	Purification	[S] (ppm)	[P] (ppm)
FA39A	C-18; 75% MeOH	60	-
FA39B	C-18; 100 MeOH	89	-
FA101A	AC; C-18; 50% MeOH	-	-
FA101B	AC; C-18; 75% MeOH	65	<5
FA101C	AC; C-18; 75% MeOH	-	-
FA102A	AC	-	-
FA102B	C-18; 75% MeOH	73	5.3
FA110	C-18; MeOH	198	16
FA122	Crude	159	<21
FA122C	Precipitated	109	<20
MFA05	Crude	453	-
NFA05.1	C-18; 75, 80, 85% MeOH	75	8.2
NFA05.2	C-18; 75, 77.5, 80, 82.5% MeOH	12	-
NFA180.1-2	2 x Alkaline hydrolysis	-	-
Combo 1	4 x Alkaline hydrolysis; 4 x AC	29	-
Combo 2	Alkaline hydrolysis; 4 x AC	102	-

Table 4.11 shows the GC-FID FA compositions of select CBFAs in this series. The set presented below was determined to have the following average composition: 81.2% LA, 8% MA, 5.8% C16 FAs, and 1.7% C18 FAs. NFA05.1 was also analyzed via LC/MS. The LC/MS analysis found that NFA05.1 had the following FA composition: 69.6% C12, 9.8% C14, 12.9 C16 and 6.7% C18 FAs. LC/MS also determined that the total fat content of this sample was 908 mg/g, which was well above the 711 mg/g determined via GC-FID.

Though the FA profiles are similar, the total fat contents of these samples are quite different. The samples treated with both AC decolorization and C-18 adsorption

chromatography appear to have the lowest impurity concentrations. FA101A, FA101B, and FA101C all had total FA contents above 900 mg/g, which is unusual given historical total fat content. FA101B was determined to have a [S] of 65 ppm. Neither the AC decolorization nor the C-18 adsorption chromatography were sufficient alone to purify the samples. This is suggested by the low total fat contents shown in sample FA102A, which was purified only by AC, and FA102B, which was purified via C-18 adsorption chromatography. ICP-OES analysis confirmed this hypothesis by determining that FA102B contained 73 ppm S. Crystallization/precipitation also appears to be an insufficient purification method, as the total fat content of FA122C was only 749 mg/g. ICP-OES determined FA122C to contain 109 ppm S, indicating that crystallization was not efficient for purification. NFA180.1-2, treated by alkaline hydrolysis, had a total fat content of just under 900 mg/g.

Table 4.11: Summary of fatty acid analysis for CBFA samples recovered and purified according to methods shown in Table 4.10.

	Amount (% of Total Fatty Acids (w/w))								
Fatty Acid	***FA101A***	***FA101B***	***FA101C***	***FA102A***	***FA102B***	***FA110***	***FA122C***	***NFA05.1***	***NFA180.1-2***
C 10:0	0	0	0	1	1	0	0	0	0
C 10:1*	0	0	0	0	0	0	0	0	0
C 12:0	82	80	94	79	83	74	80	77	82
C 14:0	8	9	2	9	8	7	10	11	8
C 14:1 trans*	0	0	0	0	0	0	0	0	0
C 14:1 cis	0	0	0	0	0	0	0	0	0
C 16:0	2	3	1	6	3	6	3	4	3
C 16:1 trans*	0	0	0	0	0	0	0	0	0
C 16:1 cis	1	2	0	2	1	1	1	2	1
C16:3 cis*	0	1	1	0	0	0	1	0	1
C16:4 cis	0	0	0	1	1	2	1	1	0
C 18:0	0	0	0	0	0	0	0	0	0
C 18:1, cis	0	0	0	0	0	0	0	0	0
C 18:2 cis	1	1	0	1	0	2	1	1	1
C18:3 cis 6	0	0	0	0	1	2	2	0	0
C18:3 cis 9	1	1	0	0	0	0	0	0	0
C 20:1, cis	0	0	0	0	0	0	0	0	0
unknowns	3	2	1	0	0	3	1	3	1
Total fat (mg/g)	988	991	981	591	635	635	749	711	895

Samples shown in Table 4.10 were deoxygenated over 5 wt. % Pd/C under 5 vol. % H_2 at 300 °C and 15 bar. The results of these experiments are summarized in Table 4.12. A representative CBFA distribution (81% C12:0, 11% C14:0, 6% C16:0 and 2% C18:0 (w/w)) was used as the yield basis in these calculations. This distribution was determined by averaging a sample of obtained CBFA profiles shown in Table 4.11. The effluent CO_2 flow rates measured by on-line QMS during semi-batch decarboxylation of FA39A, FA101A, FA102B, NFA05.2, and NFA180.1-2 are shown in Figure 4.8. The CO_2 evolution trace measured during LA is shown for comparison. From Figure 4.8 it appears that only one of the purification methods mentioned above actually did a sufficient job of removing the sulfur-containing impurities. This was the C-18 adsorption chromatography that was conducted on NFA05.2. NFA05.2 contained only 12 ppm S, which is below the threshold for >90% CO_2 selectivity and >80% yield, as established below in Figure 4.9. The CO_2 selectivity for deoxygenation of NFA05.2 was 88.0%, which was the highest CO_2 selectivity obtained during CBFA deoxygenation at an initial concentration of 5 wt. %. Yields from deoxygenation of this sample were also high. There also appeared to be no BHMA present, as there is no shoulder before the LA decarboxylation peak.

This result conflicts with results from deoxygenation of other CBFAs purified via adsorption chromatography, such as FA39A and FA101A. FA101A was deoxygenated with high yields ($CO+CO_2$: 89.2%, alkane: 76.2%) and FA39A was deoxygenated with moderate yields ($CO+CO_2$: 66.2%, alkane: 70.0%). Both were deoxygenated with relatively the same CO_2 selectivity (78.7% for FA39A and 79.1% for FA101A). The low CO_2 selectivity during FA101A deoxygenation was unexpected, as the total fat content in the sample was

determined to be extremely high. FA102B, which was purified using adsorption chromatography, was also deoxygenated with moderate yields, which was expected due to the low total fat content.

The results from elemental analysis and deoxygenation suggest an optimum MeOH concentration range during adsorption chromatography where FAs are eluted and contaminants are not. FA39A, FA39B, FA101A, and FA102B were eluted with 75%, 100%, 50%, and 75% MeOH, respectively. NFA05.2 was eluted with a gradient of MeOH concentrations ranging from 75% to 82.5%, with increments of 2.5%. FA110 was also purified via adsorption chromatography; however it is unknown what concentration of MeOH was used to elute it. It was deoxygenated with a $CO+CO_2$ yield of 53.6%, an alkane yield of 34.4%, and a CO_2 selectivity of 16.1%. NFA05.2 had a [S] of only 12 ppm. The other CBFAs had [S] in the 60-90 ppm range, with the exception of FA110. FA110 was determined to have a [S] of 198 ppm.

Alkaline hydrolysis proved to be a slightly better purification method than AC decolorization or adsorption chromatography with MeOH concentrations out of the range set by NFA05.2. NFA180.1-2, which was purified by two rounds of alkaline hydrolysis, was deoxygenated with a $CO + CO_2$ yield of 93.2%, an alkane yield of 83.1%, and a CO_2 selectivity of 84.8%. These numbers are comparable to what was seen during NFA05.2 deoxygenation; however, the CO_2 trace shown in Figure 4.8 is much different for NFA180.1-2 than it is for NFA05.2. The CO_2 peak for NFA180.1-2 is much broader and approaches a lower maximum than the peak for NFA05.2, indicating slower deoxygenation kinetics.

BHMA also appeared to be a significant contaminant in this sample, as evidenced by the shoulder at approximately 1 h.

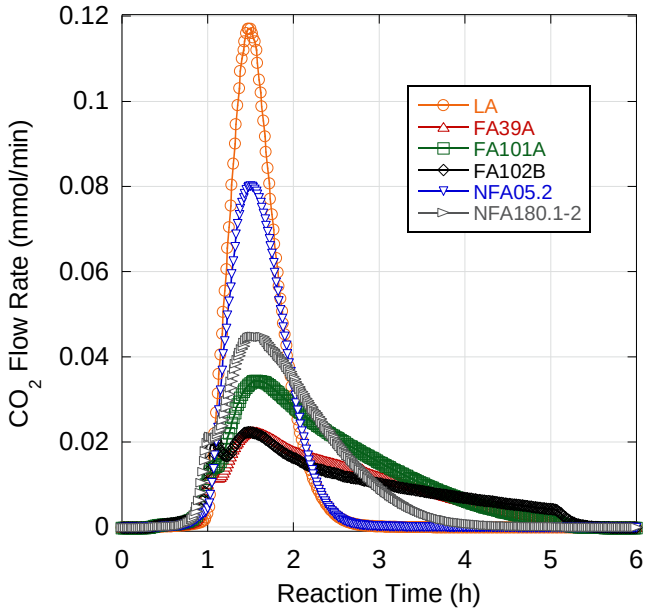

Figure 4.8: Decarboxylation of CBFA samples FA39A, FA101A, FA102B, NFA05.2, NFA180.1-2 and LA over 5 wt. % Pd/C at 300 °C and 15 bar under 5 vol. % H_2.

Table 4.12: Summary of recovered and purified CBFA deoxygenation over 5 wt. % Pd/C under 5 vol. % H_2 at 300 °C and 15 bar.

Sample	FA Mass (g)	FA Conc. (wt. %)	CO_2+CO Yield (%)†	Alkane Yield (%)†	CO_2 Selectivity (%)	mol H_2/ mol CO+CO_2 Produced
LA	1.13	4.78	93.3	94.2	89.1	-0.14
FA39A	1.13	4.79	66.2	70.0	78.7	-0.19
FA39B	1.13	4.78	53.7	54.1	65.3	-0.33
FA101A	1.13	4.75	89.2	76.2	79.1	-0.29
FA102A	1.00	4.28	43.9	36.8	24.5	-0.76
FA102B	1.12	4.75	76.0	62.2	70.2	-0.44
FA110	1.12	4.74	53.6	34.4	16.1	-0.64
FA122C	1.12	4.75	53.6	52.1	47.2	-0.46
MFA05	1.86	7.96	26.5	29.8	29.7	-0.65
NFA05.1	1.13	4.77	61.6	59.5	62.0	-0.69
NFA05.2	1.09	4.63	81.7	88.3	88.0	-0.23
NFA180.1-2	1.12	4.74	83.2	83.1	84.8	-0.09
Combo 1	1.14	4.82	81.0	78.8	84.1	-0.18
Combo 2	1.13	4.75	51.8	55.4	57.7	-0.47

Crystallization and acid hydrolysis proved to be effective but not sufficient (alone) for S impurity removal from CBFAs prior to conversion to hydrocarbons. Purification of FA122 via crystallization/precipitation was attempted. Deoxygenation of FA122C proceeded via decarboxylation and decarbonylation and converted only half of the initial CBFA charge. This result was consistent with the moderate drop in [S] between the crude FA122 and FA122C (Table 4.10).

When the MFA05/C_{12} solution from the acid hydrolysis experiment was deoxygenated, relatively low CO_2 selectivity and yields were observed. Using a GC-FID

fatty acid analysis of the reaction mixture, the CO_2+CO and alkane yields were determined to be 54.9% and 61.8%, respectively. The CO_2 selectivity (29.7%) was consistent with a [S] of 166 ppm (which was determined using Figure 4.9 shown below). The greater than 60% reduction in [S] (relative to the crude CBFAs) indicated that acid hydrolysis coupled with AC decolorization was effective at removing the bulk of S-containing impurities, e.g., sulfo-lipids and proteins; however, additional purification steps (e.g., adsorption chromatography) would be required to reduce the [S] to levels acceptable for continuous catalytic deoxygenation (<20 ppm).

ASU provided two pooled CBFA samples (Combo 1 and Combo 2) that had been purified using alkaline hydrolysis and AC treatments in series. Combo 1 underwent batch hydrolysis four times (4x); whereas, Combo 2 only underwent batch hydrolysis once. Each sample was treated subsequently with AC four times (4x). Combo 1 was deoxygenated much more efficiently than Combo 2. For Combo 1, yields were ~1.5 times higher than for Combo 2. These results indicate that repeated alkaline hydrolysis followed by AC decolorization can be nearly as effective (if not more so, depending on the metric) than C-18 adsorption chromatography at removing impurities from crude CBFAs. Triplicate ICP-OES analysis at ASU indicated that Combo 1 had a [S] of 131 ppm; however, there was an apparent outlier at a concentration of 337 ppm. Exclusion of this outlier brought the [S] down to approximately 29 ppm (consistent with the deoxygenation results). Combo 2 contained 102 ppm sulfur by ICP-OES.

Figure 4.9 illustrates the dependence of CO_2 selectivity and CO+CO_2 and alkane yields on the sulfur concentration [S] in the CBFA feedstock using data from samples tested

for [S] and in deoxygenation experiments at an initial concentration of 5 wt. %. The samples used for this figure are as follows: FA04, FA39A, FA39B, FA110, FA122C, NFA05.1, NFA05.2, Combo 1 and Combo 2. The red dots represent ICP-OES data obtained from Galbraith Labs. The blue squares represent data measured at ASU. The ICP-OES data obtained from both laboratories are in good agreement. Figure 4.9(a) shows that there is a highly-correlated inverse relationship between [S] and CO_2 selectivity. The relationship between the yields and [S] is qualitatively similar. From this data, it was determined that a [S] of less than 20 ppm is required to achieve a CO_2 selectivity approaching 90% and yields above 80% (similar to the results obtained with LA).

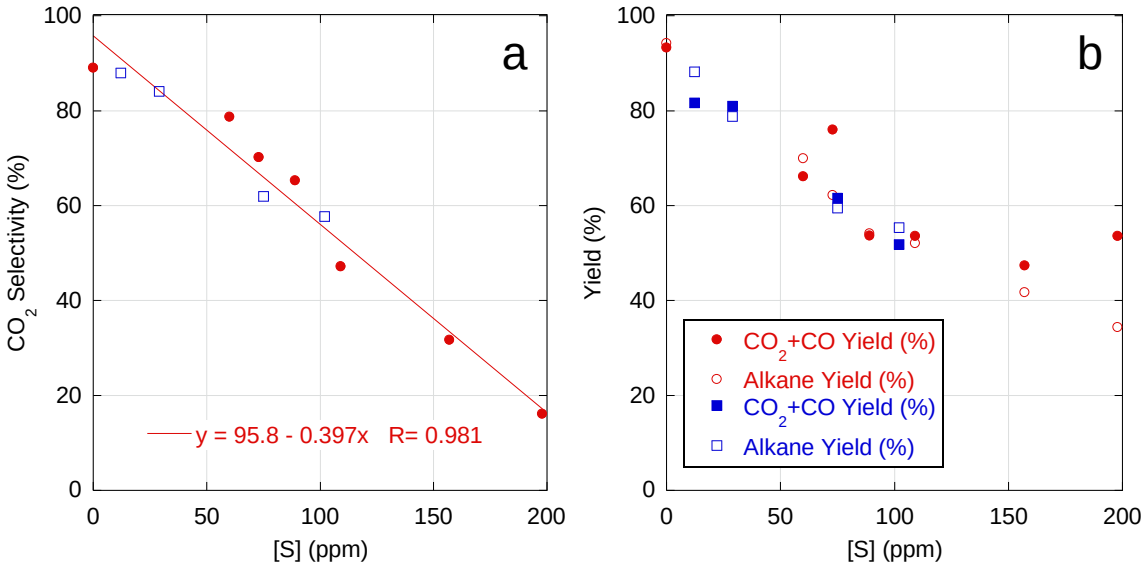

Figure 4.9: Deoxygenation (a) CO_2 selectivity and (b) yield dependence on [S] in CBFA samples. Data points plotted at 0 ppm [S] correspond to deoxygenation of reagent-grade LA.

Continuous Deoxygenation of CBFAs to Alkanes

Approximately 11 g of FA39A were deoxygenated over 1 g of Evonik E117 5% Pd/C under typical reaction conditions (5% H_2, 15 bar, 300°C). The reaction time was extended to 8 h in order to ensure that the reactions went (as nearly as practical) to completion. Figure 4.10 shows the QMS traces of the initial and reprocessing deoxygenation runs, and Table 4.13 is a summary of these results. The initial deoxygenation was carried out by reducing the 1 g of catalyst in 12.5 g of solvent, and then adding the 11 g of solid lipid biomass. The reprocess deoxygenation was carried out by collecting the condensate, separating the spent catalyst from the reactor contents, adding fresh catalyst to the reactor along with both the condensate and reactor contents, and then reacting the residual CBFAs. In Figure 4.10, it is shown that the initial deoxygenation occurred primarily via decarbonylation. This level of decarbonylation can be attributed to an increased initial FA concentration and increased impurity concentration. Over the course of 8 h, LA (model compound) with an initial concentration of 50 wt. % was deoxygenated over 335 mg Pd/C with a CO_2 selectivity nearly twice the CO_2 selectivity of this reaction, which indicates that impurities were most likely responsible for the level of decarbonylation exhibited with this CBFA sample. Reprocessing of this sample led to complete conversion at high CO_2 selectivity of the remaining CBFAs.

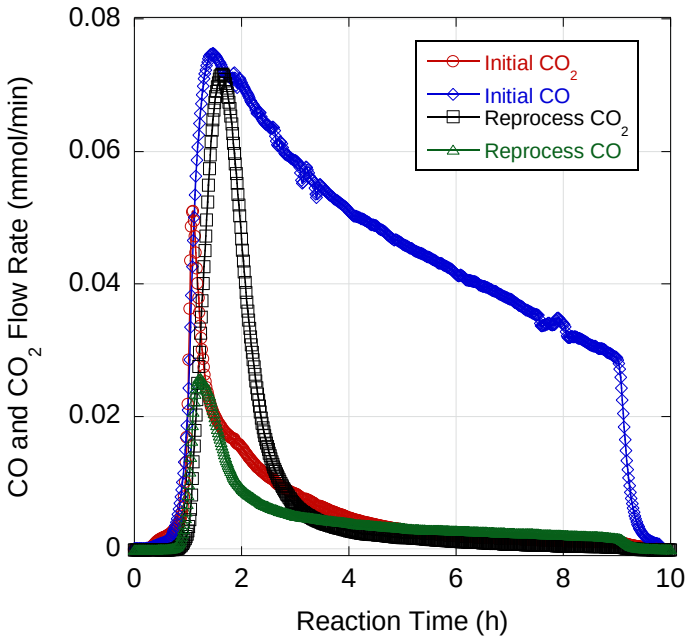

Figure 4.10: CO and CO_2 evolution from 10x FA39A deoxygenation over 1 g 5 wt. % Pd/C (E117) at 300 °C and 15 bar for 8 h.

Table 4.13: Summary of initial and reprocess deoxygenation experiments of 10x FA39A over 5 wt. % Pd/C under 5 vol. % H_2 at 300 °C and 15 bar.

Deoxygenation	***Biomass (g)***	***Biomass Conc. (wt. %)***	***CO+CO₂ Yield (%)***	***CO₂ Selectivity (%)***	***mol H₂/ mol CO+CO₂ Produced***
Initial	10.983	46.6	50.7	12.4	-1.21
Reprocess	-	-	13.8	64.6	-0.45

Fed-batch deoxygenation of larger batches of CBFAs obtained from ASU was done in order to obtain a product that could then be used in the final hydroisomerization step. Column washes from purification of NFA180.2-1 were pooled together (comprising ~8 g)

and deoxygenated using a continuous CBFA feed over 1 g of 5 wt. % Pd/C (E117). Using ICP-OES analysis from ASU, the [S] in the feed was determined to be approximately 26 ppm. The CBFAs were fed to the reactor at a liquid volumetric flow of 13 μL/min. The on-line QMS data for this run and a fed-batch deoxygenation of LA conducted under similar conditions are shown in Figure 4.11. The molar feed rate (LA basis) and timing (on/off) are indicated by the dashed black rectangles.

LA deoxygenation approached a short-lived quasi-steady-state after approximately 6 h. At this time on stream (TOS), CO + CO_2 yield and CO_2 selectivity were 89.8% and 91.8%, respectively. Decarboxylation activity declined with time on stream (TOS), and after about 10.5 h, the reaction switched over from decarbonylation to decarboxylation. Switchover occurred due to FA accumulation in the reactor with TOS under these reaction conditions (3% H_2, 23.4 bar). The increased reactor pressure was used to suppress evaporation of the C_{12} solvent and *n*-C_{11} product. In the previous chapter, it was shown that increased H_2 partial pressure can severely diminish catalyst decarboxylation activity. The switchover that was seen for LA in Figure 4.11(a) was most likely due to excess H_2. The H_2 content for the fed-batch deoxygenation of NFA180.2-1 was reduced to 2 % (vol.) to avoid this problem. During the fed-batch deoxygenation of NFA180.2-1 (2% H_2, 23.4 bar), the reaction did not begin until ~3 h time on stream (TOS) due to dead volume in the feed line. A quasi-steady state was achieved after ~7 h TOS. At this steady-state, the CO_2+CO yield was 73.3% and the CO_2 selectivity was 90.6%. Switchover was avoided during the course of the reaction, and FAs remaining in the reactor when feeding was stopped were rapidly consumed.

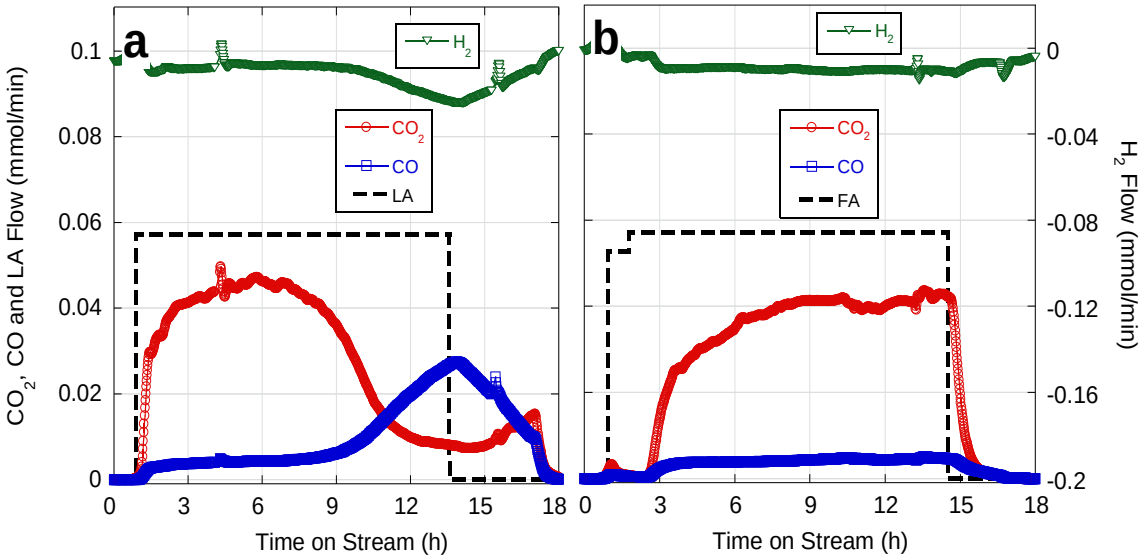

Figure 4.11: On-line QMS of fed-batch deoxygenation of (a) LA and (b) NFA180.2-1 at 300 °C and 23.4 bar over 5 wt. % Pd/C.

Combo 1 (~30 g) was converted to hydrocarbons in two fed-batch experiments that were conducted at 23.4 bar (under 2% H_2) to suppress evaporation of the solvent (C_{12}) and the *n*-C_{11} product. The volumetric feed rate in each experiment was 13 µL/min. The first fed-batch experiment with Combo 1 was carried out using 335 mg of 5 wt. % Pd/C; 1 g of 5 wt. % Pd/C (E117) was used in the second experiment. Figure 4.12 illustrates the on-line QMS data from these experiments.

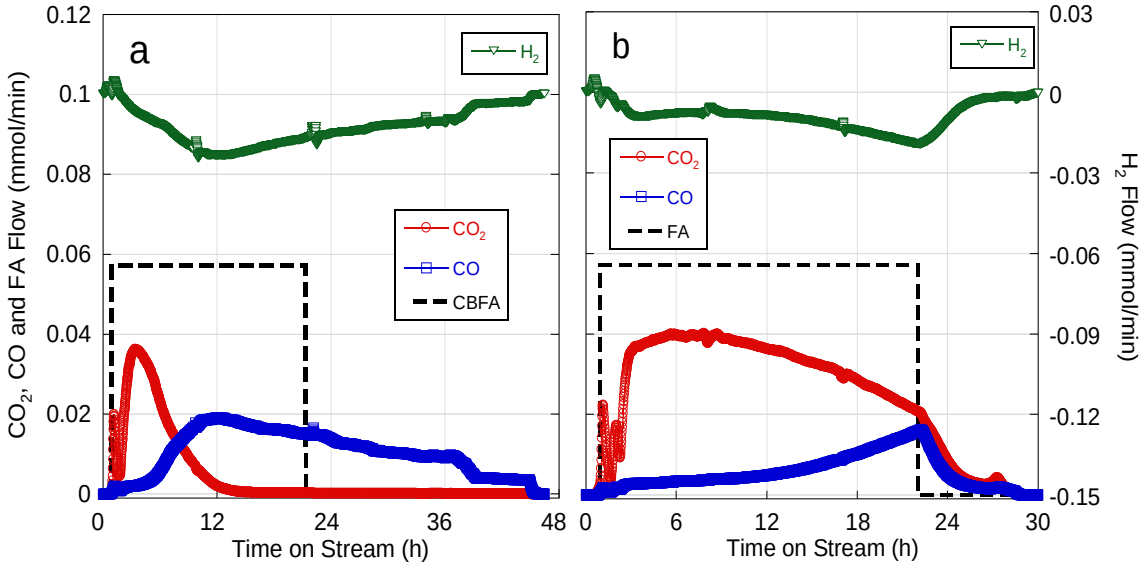

Figure 4.12: On-line QMS data for deoxygenation of Combo 1 (a) Run 1 (335 mg 5 wt. % Pd/C) and (b) Run 2 (1 g 5 wt. % Pd/C) at 300 °C and 23.4 bar under 2 vol. % H_2.

The catalyst mass used in Run 1 resulted in rapid loss of decarboxylation activity (presumably due to S poisoning) and a subsequent increase in the CBFA concentration. Decarbonylation was the dominant deoxygenation pathway after 12 h, and CBFA decarbonylation continued for many hours after feeding was stopped at ~22 h TOS. The sudden drop in the CO signal at around 36 h was most likely due to complete evaporation of solvent (and *n*-C_{11} product) from the reactor. In fact, there were no alkanes left in the reactor, only unreacted CBFAs, as is evidenced by solidification of the reactor contents upon cooling. The second fed-batch reaction (Combo 1, Run 2) proceeded much more efficiently and achieved a quasi-steady state after ~6 h TOS. Although there was a slow change in reaction pathway from decarboxylation to decarbonylation, switchover did not occur before

the feed was stopped after ~22 h, and the reaction went to completion. A summary of the quantitative results is given in Table 4.14.

Table 4.14: Summary of fed-batch CBFA deoxygenation over 5 wt. % Pd/C at 300 °C and 23.4 bar.

Sample	**Cat. Mass (g)**	**Approx. FA Mass (g)**	**CO_2+CO Yield (%)**	**HC Yield (%)**	**Alkane Selectivity (%)**	**CO_2 Selectivity (%)**
NFA180.2-1	1.004	8	66.0	55.2	-	89.4
Combo 1 (Run 1)	0.336	14	57.5	38.3	93.3	29.6
Combo 1 (Run 2)	1.002	14	73.4	73.5	99.2	81.6

Both NFA180.2-1 and Combo 1 (Run 2) exhibited moderate yields and high CO_2 selectivities. It was assumed that both of these reactions went to completion, as was evidenced by the sharp drop-off in QMS signals after injection was stopped. There was one slight difference between these two runs: a small percentage (0.8%) of the hydrocarbons in the Combo 1 (Run 2) products were alkenes (e.g., 1-undecene). Upon re-analysis, a much greater quantity of alkenes (6.7%) was found in the Combo 1 (Run 1) products, consistent with the high decarbonylation activity (low CO_2 selectivity) observed during this experiment. The ~74% alkane (hydrocarbon) yield observed for Combo 1 (Run 2) is consistent with the semi-batch results for this CBFA sample.

Summary

The overall goal of this project was to convert CBFAs to jet fuel in a two-step process: deoxygenation of the CBFAs over a Pd/C catalyst and subsequent isomerization of the alkane product over a Pt/zeolite catalyst. It was shown that effective removal of biologically derived impurities, such as sulfo-lipids, proteins and BHMA, is required to preserve Pd/C deoxygenation activity. A multitude of methodologies can be used to recover and purify CBFAs before they are deoxygenated. Some of the most efficient ways to remove impurities from the samples are AC decolorization, alkaline hydrolysis and adsorption chromatography. Combinations of these purification methods explored are also highly effective at impurity removal and should be employed rather than singular methods. Large batches of CBFAs were processed in higher concentrations over larger quantities in a semi-batch reactor. Reactions run in this manner required reprocessing to achieve complete conversion. These CBFAs were also converted in larger quantities via fed-batch reaction. However, larger quantities of catalyst were used in order to achieve high conversion of these CBFAs, as the purification methods presented in this chapter were not able to completely eliminate the presence of sulfur in the feedstock.

References

[1] M. Asayama, "Overproduction and easy recovery of target gene products from cyanobacteria, photosynthesizing microorganisms," *Applied Microbiology and Biotechnology*, vol. 95, pp. 683-695, Aug 2012.

[2] B. Szponar, L. Krasnik, T. Hryniewiecki, A. Gamian, and L. Larsson, "Distribution of 3-hydroxy fatty acids in tissues after intraperitoneal injection of endotoxin," *Clinical Chemistry*, vol. 49, pp. 1149-1153, Jul 2003.

[3] C. Keresszegi, T. Mallat, J. D. Grunwaldt, and A. Baiker, "A simple discrimination of the promoter effect in alcohol oxidation and dehydrogenation over platinum and palladium," *Journal of Catalysis*, vol. 225, pp. 138-146, Jul 2004.

[4] T. T. Pham, L. L. Lobban, D. E. Resasco, and R. G. Mallinson, "Hydrogenation and Hydrodeoxygenation of 2-methyl-2-pentenal on supported metal catalysts," *Journal of Catalysis*, vol. 266, pp. 9-14, Aug 2009.

[5] M. Bejblova, P. Zamostny, L. Cerveny, and J. Cejka, "Hydrodeoxygenation of benzophenone on Pd catalysts," *Applied Catalysis a-General*, vol. 296, pp. 169-175, Dec 2005.

CHAPTER 5: Hydroisomerization of CBFA-Derived Alkanes over Pt/Zeolite Catalysts

Introduction

The goal of this project was to produce jet fuel from alkanes produced via deoxygenation of CBFAs. In order to produce jet fuel from *n*-alkanes, they must be hydroisomerized, which can be accomplished by conversion over bifunctional Pt/zeolite catalysts. Military jet fuel (JP8, specifically) is comprised of mainly of normal long chain alkanes, but also includes aromatic and branched products [1, 2]. Hydroisomerization of the CBFA-derive alkanes changes the composition of the fuel (making it closer to the composition of jet fuel), which causes a decrease in the freezing point of the fuel. This decrease in freezing point is much needed, as temperatures in the upper troposphere can get as low at -40 °C [3]. The melting points of *n*-C_{11} and *n*-C_{12} are around -10 °C [4, 5]. The freezing points of JP5 and JP8 are -46 °C and -47 °C, respectively [1].

Normal alkane hydroisomerization/hydrocracking over Pt/zeolite catalysts is initiated by alkane dehydrogenation on the Pt surface [6, 7]. The alkenes desorb from the Pt surface and are protonated at the zeolite Brönsted acid sites. Once adsorbed to the zeolite acid site, the n-alkyl cation is branched via protonated cyclopropanes (PCPs) [8]. The *i*-alkyl cation can then undergo desorption as an *i*-alkene (which can then be hydrogenated over Pt to an iso-alkane) [6]. The long-chain carbenium ions can also undergo β-scission, which creates cracked products. Previous work with alkane and alkene isomerization over Pt/zeolite systems (specifically Pt/Hβ) has shown that the presence of the alkene in the reaction feed

promotes cracking and other unwanted side reactions, such as oligomerization and coking [9].

It has been shown that at moderate conversions (near 40%), long-chain alkanes can be almost exclusively isomerized over Pt/CaY [8]. Extremely high conversion is not necessarily desired as increases in alkane conversion over bifunctional zeolite catalysts generally leads to increased, if not total, cracking of the hydrocarbon reactants [8, 10]. The literature has also shown that the length of the alkane chain controls the rate at which it is hydroisomerized/cracked. It was determined that adsorption of the alkane to the zeolite crystal active sites is what determines the apparent rate of reaction. These rates of adsorption are higher for longer chain alkanes, which promotes conversion of longer alkanes [11].

Pt/Zeolite Characterization

Catalysts used in alkane hydrisomerization in this chapter (Pt/HY, Pt/NaY and Pt/CaY) were characterized for their Pt loading, surface area and metal dispersion via ICP-OES, N_2 physisorption and H_2 chemisoprtion. The results of these characterization techniques are summarized below in Table 5.3. Elemental analysis showed that all samples contained approximately 70-80% of their intended Pt loading. The entire set of catalysts was supposed to be 1 wt. %. H_2 chemisorption indicated that all catalysts samples had well-dispersed particles, with sizes ranging from 1.8 nm to 2.8 nm. N_2 physisorption indicated that Pt/NaY and Pt/HY had comparable surface areas, 925 and 900 m^2/g, respectively. Pt/CaY was determined to have a BET surface area of 706 m^2/g.

Table 5.1: Summary of Pt/zeolite characterization results.

Catalyst	Pt Loading (wt. %)	Support SiO_2:Al_2O_3	BET Surface Area (m^2/g)	Dispersion (%)	H/Pt (total)	H/Pt (strongly adsorbed)
Pt/HY	0.867	5.1	925	39.2	1.19	0.39
Pt/NaY	0.822	5.1	900	62.6	1.20	0.63
Pt/CaY	0.700	5.1	706	44.7	1.04	0.45

Hydroisomerization of n-Undecane

Liquid-phase batch hydroisomerization of n-undecane (*n*-C_{11}) was conducted using Pt/NaY, Pt/HY and Pt/CaY at 300°C. Figure 5.1 (below) is the temperature and pressure profile of two reactions of the set. The blue line is a representative temperature profile where the reactor was heated from room temperature to 300 °C at a rate of 5 °C/min. Shown in Figure 5.1 below are the pressure and temperature profiles of *n*-C_{11} hydroisomerization reactions over Pt/HY and Pt/CaY. The results of these experiments are shown in Table 5.2 and show that pressure profile for these catalysts are independent of their ability to isomerize instead of crack the alkane reactant. Figure 5.2 is a graph of *i*-C_{11} yield as a function of *n*-C_{11} conversion.

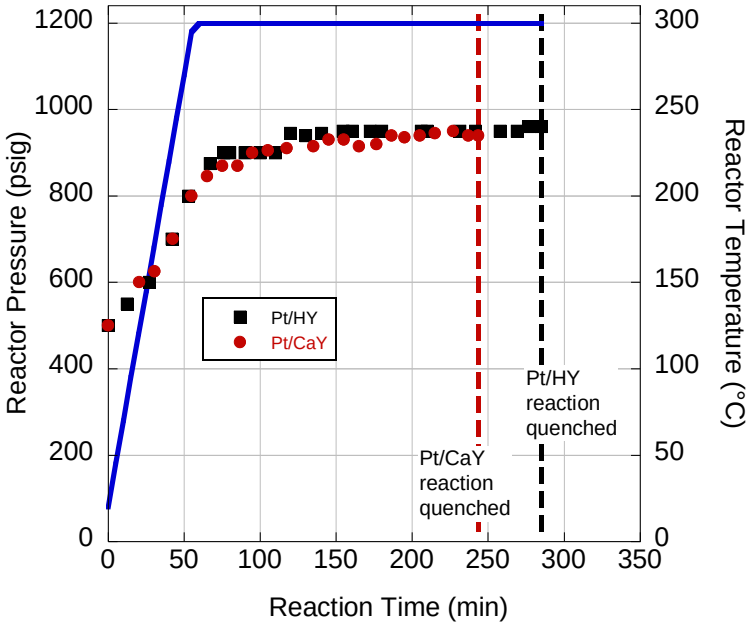

Figure 5.1: Reactor pressure and temperature as a function of reaction time.

n-C_{11} hydroisomerization occurred Pt/HY with two levels of conversion, depending on reaction pressure and time. When the total reactor pressure was doubled for Pt/HY with an approximate reaction time of 4 h, the conversion was actually suppressed, as expected. Kinetic analysis of *n*-C_{10} and *n*-C_{12} hydrisomerization over Pt/USY showed that increased H_2 pressure slows the rate of branched alkane production [12]. Pt/NaY exhibited negligible overall activity. Pt/CaY provided higher isomerization selectivity at high conversion (>50%) than Pt/HY. Figure 5.2 shown below shows the relationship between *i*-C_{11} yield and *n*-C_{11} conversion. The dashed 45° line represents perfect isomerization, where every mole of *n*-C_{11} converted is converted to an isomerized *n*-C_{11} product. Figure 5.2 shows exactly what is summarized in Table 5.2, which is that Pt/CaY is the most effective for batch long-chain

alkane hydroisomerization. Pt/NaY did not convert much of the *n*-C_{11} reactant; however, most of what was converted was converted to isomers. The low activity of Pt/NaY puts this data point near the origin. Hydroisomerization of *n*-C_{11} over Pt/HY occurred with either low or high conversion or lower isomer yields than Pt/CaY. The shape of the curve in Figure 5.2 is what is typically seen for long chain isomerization.

The *i*-C_{11} yield trend seen between the catalysts is most likely due to the acidity of the zeolite, which is dependent on the cation present. The identity of the cation in the zeolite structure directly contributes to the amount of H^+ in the structure, which directly contributes to the cracking activity of the catalyst [13]. All zeolite Y samples in this set of experiments were derived from NaY. In NaY, all of the Al^- sites are coordinated with one Na^+, which means that no H+ atoms are coordinated to the Al^- sites upon reduction of the Pt metal. When Na^+ is exchanged for Ca^{2+}, each Ca^{2+} is coordinated to two Al^- sites, which leaves a number of Al^- sites open for coordination with H^+ atoms when the Pt is reduced. Reduction of a Pt/NH_4Y catalyst (derived from ion exchange of Na^+ with NH_4^+) will result in Pt/HY and a high number of protons being coordinated to Al^- sites, causing the highest amount of cracking [14].

Table 5.2: Summary of batch hydroisomerization of *n*-C_{11} over Pt/zeolite catalysts.

Catalyst	Init. Press. (psig)	Final Press. (psig)	Reaction Time (min)	*n*-C_{11} Conversion (%)	*i*-C_{11} Selectivity (%)	*i*-C_{11} Yield (%)
Pt/HY	500	0	300	95.4	27.3	25.9
	500	0	240	96.3	24.3	23.4
	1000	940	230	9.2	95.8	8.7
	500	470	180	34.9	95.9	33.4
	500	150	159	89.6	47.8	42.8
	500	0	107	94.2	23.3	21.9
	500	475	60	8.3	97.8	8.1
Pt/NaY	1000	1000	180	0.4	87.8	0.4
Pt/CaY	500	490	180	58.9	92.7	54.6
	500	450	180	73.6	82.1	60.4
	500	160	92	89.8	61.4	55.1

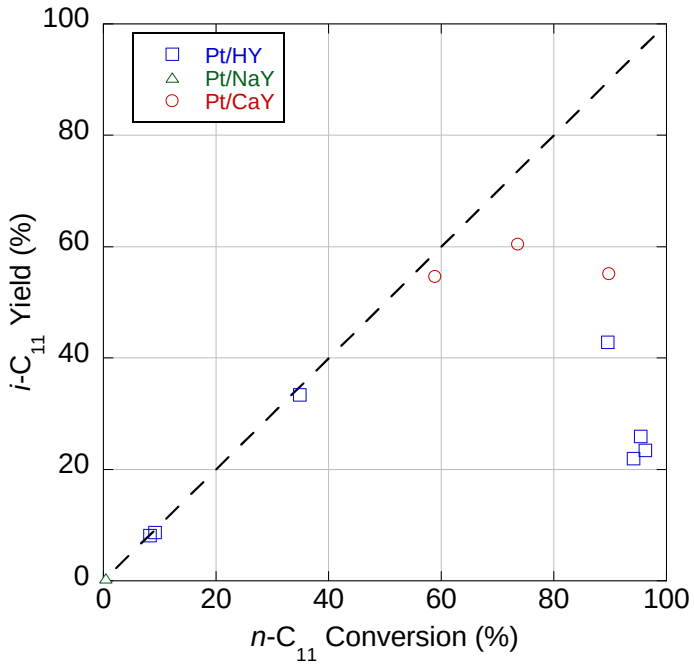

Figure 5.2: *i*-C_{11} yield as a function of *n*-C_{11} conversion during hydroisomerization over 350 mg Pt/Y zeolites (H, Ca, and Na) at 300 °C.

Hydroisomerization of n-C_{11}/n-C_{12} Mixtures and CBFA-derived Alkanes over Pt/CaY

All of the CBFA deoxygenation experiments presented in the previous chapter were conducted in a C_{12} solvent. Before converting any of the normal alkanes produced via CBFA deoxygenation, mixtures of *n*-C_{11} and *n*-C_{12} were converted over 350 mg Pt/CaY at 300 °C and 500 psig H_2. These model experiments were intended to give insight into how the presence of C_{12} would affect the hydroisomerization of *n*-C_{11}. After these experiments were completed, CBFA-derived alkanes were hydroisomerized over Pt/CaY. Samples deoxygenated at higher CBFA concentrations (FA39A) and in fed-batch mode (NFA180.2-1

and Combo 1) were used as feeds for hydroisomerization. The results of these experiments are shown in Table 5.3.

Table 5.3: Summary of *n*-C_{11}/*n*-C_{12} mixture and CBFA-derived alkane hydroisomerization over Pt/CaY at 300 °C and 500 psig H_2.

	Sample	*n*-C_{11}/*n*-C_{12}				FA39A Products	NFA180.2-1 Products	Combo 1 (Run 1) Products	Combo 1 (Run 2) Products HI 1	Combo 1 (Run 2) Products HI 2
	Final Pressure (psig)	200	450	250	450	490	175	450	450	450
	Reaction Time (h)	79	176	80	180	109	58	180	180	88
	Conversion (%)	87.6	60.2	89.6	63.6	19.6	94.9	22.9	35.9	-
	Isomer Selectivity (%)	60.2	90.1	54.4	79.1	94.9	31.9	86.0	91.9	-
Area Percent	***Cracking***	34.9	6.0	40.9	13.3	1.1	64.6	1.6	2.9	6.1
	C_{11}	30.0	26.7	29.3	29.1	2.7	6.0	3.8	7.7	9.3
	C_{12}	22.8	27.6	19.4	21.2	15.1	24.3	15.6	24.1	35.2
	C_{13}	-	-	-	-	0.2	0.0	0.2	0.4	0.5
	C_{15}	-	-	-	-	0.2	-	0.1	0.5	0.4
	C_{17}	-	-	-	-	0.4	-	0.0	0.3	0.2
	Heavy	-	-	-	-	-	-	1.4	-	-

The hydroisomerization experiments with the *n*-C_{11}/*n*-C_{12} mixture demonstrated that Pt/CaY was a hydroisomerization catalyst capable of high conversion and moderate selectivity to isomerized products independent of the conversion. All four reactions reached conversion of greater than 60%, with two reaching levels near 90% conversion. The selectivity of the catalyst to producing *i*-C_{11} products was between 26.7% and 30.0% for all four reactions. The selectivity of the catalyst to *i*-C_{12} products was slightly lower, with a range between 19.4% and 27.6%. The main difference between the four reactions was the selectivity of the reaction to cracking products. Two of the reactions, which happened quite quickly (reaction times near 80 min), produced cracking products with 30-40% selectivity. The other two reactions (both of which ran for 3 h) produced cracking selectivities less than 10%. This behavior is counterintuitive, as it is expected that longer reaction times (given the same initial conditions) would promote alkane cracking. This inconsistent behavior points to some sort of fundamental difference in the catalyst samples being used or the catalyst treatment before reaction.

The inconsistent nature of the Pt/CaY catalyst was exhibited once again during the hydroisomerization of alkanes derived from sample NFA180.2-1. This reaction was only run for 58 minutes, but it reached a conversions of 94.9% and a selectivity to cracked products of 64.6%. The remaining three out of four initial CBFA-derived alkane hydroisomerization experiments exhibited limited conversion, and thus limited total isomerized product yield. Hydroisomerization of the alkane products from deoxygenation of FA39A and Combo 1 (Run 1) produced conversions of approximately 20% and reaction selectivity to *i*-C_{11} products of 2.7% and 3.8%, respectively. Hydroisomerization of Combo 1 (Run 2) occurred

with a conversion of 35.9%, which increased the *i*-C_{11} selectivity to 7.7%. Of course the level of selectivity of the reaction to *i*-C_{11} products could be increasing due to an increased initial *n*-C_{11} concentration in the Combo 1 (Run 2) deoxygenation product mixture. However, *i*-C_{11} produced from this reaction accounted for 29.7% of the total C_{11} species present in the hydroisomerization product. This number was 17.5% for FA39A-derived alkane hydroisomerization and 18.1% for Combo 1 (Run 1)-derived alkane hydroisomerization. Products from Combo 1 (Run 2) alkane hydroisomerization were mixed with C_{12} (to make up for lost mass during reaction and collection) and converted again over Pt/CaY. After this reaction, the *i*-C_{11} content in the product mixture increased to 9.3%. As a percentage of the total C_{11} species in the reactor, it increased to 44.7%.

Summary

In this chapter, it was shown that Pt/CaY was an extremely good catalyst for liquid-phase batch conversion of long-chain alkanes produced via deoxygenation of CBFAs to their isomerized analogs. The increased isomerization activity was posited to come from moderate acidity of the Pt/CaY catalysts. It was acidic enough to catalyze the reaction, but not so acidic that it cracked a majority of the converted normal alkanes. It was also shown that mixtures of these long-chain alkanes could be hydroisomerized over Pt/CaY without much difference in reaction time scale or process variables. As stated previously, the goal of this entire project was to convert large batches of CBFAs into jet fuel using the two-step process of deoxygenation and isomerization. The products of CBFA-derived alkane hydroisomerization reactions presented in this chapter represent the closest this project came to producing actual jet fuel from a pure *n*-C_{11} reactant produced via CBFA deoxygenation.

This was a significant step toward producing a carbon-neutral jet fuel. The final product of the entire process of growing the cyanobacteria, recovering and purifying the CBFAs, deoxygenating the CBFAs and, finally, isomerizing the CBFA-derived alkanes is shown below.

Figure 5.3: Green jet fuel produced from deoxygenation of FA39A over Pd/C and subsequent isomerization of FA39A-derived alkanes over Pt/CaY.

References

[1] N. R. Council, "Permissible Exposure Levels for Selected Military Fuel Vapors," 1996.

[2] B. L. Smith and T. J. Bruno, "Composition-explicit distillation curves of aviation fuel JP-8 and a coal-based jet fuel," *Energy & Fuels,* vol. 21, pp. 2853-2862, Sep-Oct 2007.

[3] "Standardized Temperature Profile," ed, 2010.

[4] "Undecane," ed.

[5] "Dodecane," ed.

[6] *Guidelines for Mastering the Properties of Molecular Sieves: Relationship between the Physicochemical Properties of Zeolitic Systems and Their Low Dimensionality*. New York: Plenum Press, 1990.

[7] K. C. Park and S. K. Ihm, "Comparison of Pt/zeolite catalysts for n-hexadecane hydroisomerization," *Applied Catalysis a-General,* vol. 203, pp. 201-209, Oct 2000.

[8] J. Weitkamp, "ISOMERIZATION OF LONG-CHAIN N-ALKANES ON A PT/CAY ZEOLITE CATALYST," *Industrial & Engineering Chemistry Product Research and Development,* vol. 21, pp. 550-558, 1982.

[9] H. Y. Chu, R. P. Rosynek, and J. H. Lunsford, "Skeletal isomerization of hexane over Pt/H-beta zeolites: Is the classical mechanism correct?," *Journal of Catalysis,* vol. 178, pp. 352-362, Aug 1998.

[10] H. F. Schulz and J. H. Weitkamp, "ZEOLITE CATALYSTS - HYDROCRACKING AND HYDROISOMERIZATION OF N-DODECANE," *Industrial & Engineering Chemistry Product Research and Development,* vol. 11, pp. 46-&, 1972.

[11] J. F. Denayer, G. V. Baron, W. Souverijns, J. A. Martens, and P. A. Jacobs, "Hydrocracking of n-alkane mixtures on Pt/H-Y zeolite: Chain length dependence of the adsorption and the kinetic constants," *Industrial & Engineering Chemistry Research,* vol. 36, pp. 3242-3247, Aug 1997.

[12] M. Steijns and G. F. Froment, "HYDROISOMERIZATION AND HYDROCRACKING .3. KINETIC-ANALYSIS OF RATE DATA FOR NORMAL-DECANE AND NORMAL-DODECANE," *Industrial & Engineering Chemistry Product Research and Development,* vol. 20, pp. 660-668, 1981.

[13] J. W. Ward, "NATURE OF ACTIVE SITES ON ZEOLITES .I. DECATIONATED Y ZEOLITE," *Journal of Catalysis,* vol. 9, pp. 225-&, 1967.

[14] B. C. Gates, J. R. Katzer, and G. C. A. Schuit, *Chemistry of Catalytic Processes*: McGraw-Hill, 1979.

CHAPTER 6: Summary and Conclusions

LA was deoxygenated over 5 wt. % Pd/C catalysts to simulate deoxygenation of high-purity CBFAs over the same catalysts. Semi-batch deoxygenation reactions were carried out in the liquid phase at 300 °C and 15 bar. The effects of H_2 partial pressure (1-20 mol. %) and initial LA concentration (4-46 mol. %) on deoxygenation were investigated. Gas-phase product analysis via on-line QMS showed that increasing H_2 partial pressure inhibited LA decarboxylation, resulting in large decreases in *n*-undecane yield, CO_2 selectivity, and the initial decarboxylation rate. The initial decarboxylation rate remained constant for all H_2 partial pressures tested. Higher initial LA concentrations were also found to inhibit the decarboxylation pathway; a linear increase in the initial decarbonylation rate with initial LA concentration up to ~34 mol. %. Higher initial LA concentrations did not result in a change in the initial decarbonylation rate consistent with Langmuir-Hinshelwood (saturation) kinetics. Comparison of the initial rate data for LA and PA deoxygenation as a function of molar concentration indicated that, in contrast to the initial decarboxylation rate, the initial decarbonylation rate is independent of FA chain length.

These trends in yield, CO_2 selectivity, and initial rates can be explained by surface coverage-dependent FA adsorption. FA adsorption will be affected by the availability of vacant surface sites, which could alter the deoxygenation pathway. The decarboxylation of butanoic acid over Pd(111) was explored theoretically by Lamb, Sremaniak, and Whitten [1]. In this work, 3 different pathways for butanoic acid decarboxylation on the (111) surface of a Pd nanoparticle were investigated. The most thermodynamically favorable of these pathways involves the dissociative adsorption of butanoic acid to H and butanoate, which occupies 3

Pd atoms. Two of these atoms are occupied by the butanoate species, which adsorbs perpendicular to the Pd surface. The α-carbon (which is the carbon atom adjacent to the carbonyl carbon) of this adsorbed butanoate species is then dehydrogenated, requiring another site. Pre-adsorbed H then inserts in the C-C bond between the α-carbon and –COOH carbon. Propane and CO_2 are the final products [1].

Propanoic acid decarbonylation and decarboxylation on Pd(111) has also been investigated using density functional theory (DFT) calculations and microkinetic modeling [2, 3]. The most energetically favorable pathway for decarbonylation of propanoic acid is initiated with the adsorption of the intact molecule to one Pd atom via its carbonyl O. The adsorbed propanoic acid then undergoes dehydrogenation at the α-carbon. At low H_2 partial pressures (0.01 bar), the adsorbed species ($CH_3CHCOOH$) then undergoes β-carbon dehydrogenation to produce CHCHCOOH. This species is then dehydroxylated to produce CHCHCO, whose C-CO bond is cleaved to produce CHCH and CO. Decarboxylation at the same H_2 pressure is initiated when propanoic acid is adsorbed via the carbonyl O, the α-carbon is dehydrogenated, and the –OH is dehydrogenated. The α-carbon is then fully dehydrogenated, allowing for the removal of CO_2 from the molecule. At 0.01 bar H_2 pressure, decarbonylation is predicted to be the dominant pathway, with a TOF nearly one order of magnitude larger than that for decarboxylation. At higher H_2 partial pressures, the decarbonylation pathway shifts to dehydroxylation of the acid prior to dehydrogenation of the β-carbon. However, dehydrogenation of the β-carbon must occur in order for C-CO bond cleavage to occur. At intermediate (1 bar) and high (30 bar) H_2 partial pressures, the TOF for both the decarbonylation and decarboxylation reactions are on the same order of magnitude.

The increase in H_2 partial pressure also reduced the TOFs by 2-3 orders of magnitude. The massive reduction in TOF with increased H_2 partial pressure was attributed to overestimated energies of adsorption due to the DFT functional used. Decreases in TOF were expected to occur at higher H_2 partial pressures due to decreased dehydrogenation activity. [3].

When the total surface coverage is low (due to decreased H_2 partial pressure and FA initial concentration), it may be possible for the initial FA adsorption event to occur dissociatively, as described above in the butanoic acid work. This type of adsorption would facilitate decarboxylation, leading to higher initial decarboxylation rates, CO_2 selectivities and yields. As the surface coverage increases, due to the increased H_2 and FA concentrations, the way in which the FA adsorbs may change. Larger open Pd ensembles may not be available for dissociative adsorption, and thus the molecule must adsorb via its carbonyl O atom, initially occupying a single site. As proposed in the theoretical work presented above, FA adsorption in this manner favors decarbonylation at lower H_2 partial pressures and made it competitive with decarboxylation at higher H_2 partial pressures. The one phenomenon that this change in adsorption does not explain is the chain length effect on the initial decarboxylation rate. The studies shown above only include α- and β- carbon dehydrogenation as plausible steps towards deoxygenation, which should make the difference in deoxygenation between a 12-carbon FA and an 18-carbon FA negligible. The results shown in this work indicate that decarbonylation most likely occurs through dehydrogenation of α- and β-carbons only, as there was no difference in initial decarbonylation rate due to the FA chain length.

The effect of replacing the carboxylic acid functional group with an ester group on deoxygenation over Pd/C was also investigated. ML, EL, MS , and ES were all deoxygenated in semi-batch mode in the liquid-phase at 300 °C and 15 bar under 5 vol. % H_2. The FAEs were deoxygenated via ester hydrogenolysis to form a FA intermediate, which was then quickly deoxygenated via decarboxylation and decarbonylation to the corresponding alkane. The ester hydrogenolysis step was inferred to occur much more slowly than the FA deoxygenation step. The effect of increasing initial ML concentration was conducted in the same manner as the LA concentration series, with a maximum initial ML concentration of 17 mol. %. Unlike the set of experiments with increasing LA concentration, it was found that the CO_2 selectivity of ML deoxygenation was unaffected by increases in initial ML concentration. The independence of CO_2 selectivity from initial ML concentration indicated that any LA produced via ester hydrogenolysis of ML was quickly removed from the reactor via deoxygenation. Liquid-phase analysis via GC-FID confirmed the absence of LA in the reaction medium, even at shorter reaction times (1 to 2 h). Though no FAs were identified in the liquid-phase product, the literature supports the hypothesis that deoxygenation occurs via FA intermediates [4]. For both sets of FAEs, the 1^{st}-order apparent rate constant increased when the ester was changed from methyl to ethyl. This increase in apparent rate constant indicates that the $–OC_2H_5$ group more readily undergoes hydrogenolysis. Decomposition of methyl acetate over Pd(111) has been shown to occur via dehydrogenation of the acetate moiety (making $CCOOCH_3$) and subsequent C-O acyl-alkoxy bond cleavage. Initial dehydrogenation of the methoxy end of methyl acetate occurred much more slowly due to an increased activation energy [5]. Doubling the ester group chain length from one to two

carbons may induce dehydrogenation on the alkoxy moiety, which would then lead to cleavage of the O-CH_xCH_3 bond.

LC/MS analysis of CBFAs determined that BHMA was present in concentrations of up to 2 wt. %. Semi-batch deoxygenation experiments demonstrated that BHMA was deoxygenated over Pd/C to *n*-C_{13}, 2-C_{13}-OH, and 2-C_{13}-ONE. Neither 2-C_{13}-OH nor 2-C_{13}-ONE were deoxygenated further over Pd/C to *n*-C_{13} in any appreciable extent; however, 2-C_{13}-OH was dehydrogenated to 2-C_{13}-ONE and produced an unknown product, which is postulated to be a heavy ether. These two species (2-C_{13}-OH and 2-C_{13}-ONE) were shown to be stable products that did not contribute to the overall alkane yield from CBFA deoxygenation. Deoxygenation of BHMA/FA mixtures demonstrated that BHMA is deoxygenated prior to LA and MA deoxygenation, which may be attributed to preferential adsorption of BHMA onto the Pd surface. The presence of BHMA in LA caused the decarboxylation peak to be delayed. This was not true for MA, as the MA decarboxylation peaks with or without BHMA present in the mixture occurred as the same reaction time.

CBFAs produced by *Synechocystis* sp. PCC 6803 were recovered over an anion exchange resin and a hydrophobic resin. Deoxygenation of CBFAs recovered with an anion exchange resin occurred much more readily than CBFAs recovered with a hydrophobic resin. However, neither of these methods was sufficient alone to produce a CBFA feedstock with a low enough sulfur concentration for continuous deoxygenation (because of sulfur poisoning of the Pd/C catalyst). AC adsorption, acid hydrolysis, alkaline hydrolysis, crystallization, and adsorption chromatography were all employed as CBFA purification methods. Adsorption chromatography (when using the optimum MeOH concentration range of 75 –

82.5%) was effective at removing large quantities of sulfur-containing impurities from the crude CBFAs; the sulfur concentration [S] of this sample was 12 ppm. Deoxygenation of CBFAs purified using this methodology produced the highest CO_2 selectivity. Alkaline hydrolysis and subsequent AC adsorption also proved to be efficient for removal of S-containing impurities, yielding a [S] of 29 ppm. Deoxygenation of these CBFAs resulted in the second highest CO_2 selectivity of the set. The CO_2 selectivity and yields from semi-batch deoxygenation of CBFAs were inversely proportional to [S] with high linear correlation coefficients. From these correlations, it was determined that a [S] of <20 ppm was necessary to achieve CO_2 selectivities approaching 90% and yields above 80%.

Larger quantities of purified CBFAs were deoxygenated in semi-batch and fed-batch modes. The resulting alkanes from these reactions were hydrisomerized over Pt/CaY to produce a synthetic paraffinic kerosene (SPK) with a composition similar (sans aromatics) to that of jet fuel, which is comprised of a mixture of C_{10}-C_{14} hydrocarbons (including both normal, branched and cyclic alkanes and aromatics) [6]. The hydrisomerization step was the final step in the process of producing carbon-neutral jet fuel from a non-food biomass resource. The CBFA purification processes and subsequent deoxygenation and hydrisomerization reactions over heterogeneous catalysts described above could be optimized for large-scale implementation of SPK production, thus alleviating some of the economic and environmental impacts of fossil fuel usage. One major improvement to this process could be the usage of a more sulfur-tolerant catalyst, such as sulfided $NiMo/Al_2O_3$, which has been shown to deoxygenate rapeseed oil via hydrodeoxygenation to a mixture of normal and iso alkanes [7].

References

[1] H. H. Lamb, L. Sremaniak, and J. L. Whitten, "Reaction pathways for butanoic acid decarboxylation on the (111) surface of a Pd nanoparticle," *Surface Science,* vol. 607, pp. 130-137, Jan 2013.

[2] J. M. Lu, S. Behtash, and A. Heyden, "Theoretical Investigation of the Reaction Mechanism of the Decarboxylation and Decarbonylation of Propanoic Acid on Pd(111) Model Surfaces," *Journal of Physical Chemistry C,* vol. 116, pp. 14328-14341, Jul 2012.

[3] J. M. Lu, S. Behtash, M. Faheem, and A. Heyden, "Microkinetic modeling of the decarboxylation and decarbonylation of propanoic acid over Pd(111) model surfaces based on parameters obtained from first principles," *Journal of Catalysis,* vol. 305, pp. 56-66, Sep 2013.

[4] A. T. Madsen, B. Rozmyslowicz, P. Maki-Arvela, I. L. Simakova, K. Eranen, D. Y. Murzin, *et al.*, "Deactivation in Continuous Deoxygenation of C-18-Fatty Feedstock over Pd/Sibunit," *Topics in Catalysis,* vol. 56, pp. 714-724, Jun 2013.

[5] L. Xu and Y. Xu, "Activation of methyl acetate on Pd(111)," *Surface Science,* vol. 604, pp. 887-892, Jun 15 2010.

[6] B. L. Smith and T. J. Bruno, "Composition-explicit distillation curves of aviation fuel JP-8 and a coal-based jet fuel," *Energy & Fuels,* vol. 21, pp. 2853-2862, Sep-Oct 2007.

[7] R. Sotelo-Boyas, Y. Liu, and T. Minowa, "Renewable Diesel Production from the Hydrotreating of Rapeseed Oil with Pt/Zeolite and NiMo/Al2O3 Catalysts," *Industrial & Engineering Chemistry Research,* vol. 50, pp. 2791-2799, Mar 2 2011.

APPENDIX

Table A.1: Summary of yield, CO_2 selectivity, initial rate and batch productivity data from LA semi-batch deoxygenation over 5 wt. % Pd/C at 300 °C and 15 bar with systematic variation of H_2 partial pressure.

H_2 Content (vol. %)	**$CO+CO_2$ Yield (%)**	***n*-C_{11} Yield (%)**	**CO_2 Selectivity (%)**	**CO Initial Rate (mmol/ g_{cat}-h)**	**CO_2 Initial Rate (mmol/ g_{cat}-h)**	**Batch Efficiency (mmol/ g_{cat}-h)**
1	105	88.0	95.0	1.77	51.3	31.2
2	104	90.2	93.6	1.95	38.4	27.1
5	99.6	89.1	87.9	2.46	18.0	19.3
10	89.4	85.2	70.9	2.07	1.45	4.37
20	42.4	43.9	14.9	2.01	0.162	1.64

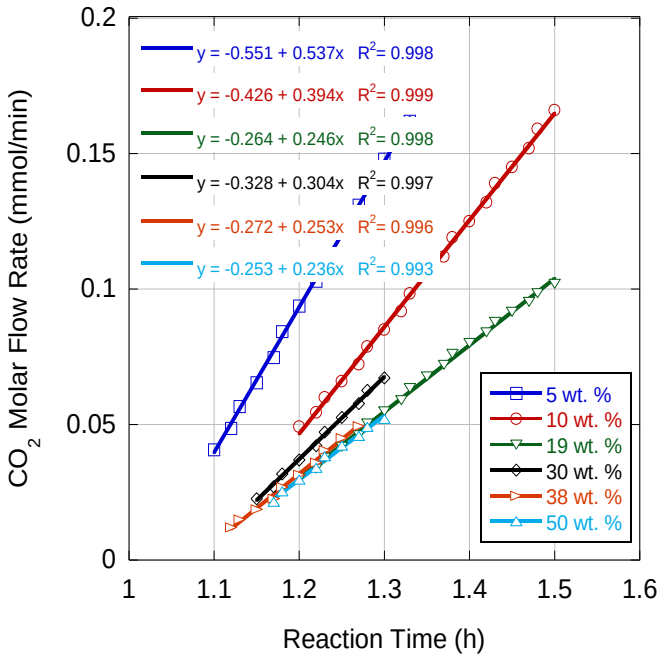

Figure A.1: Initial rates of CO_2 production from LA concentration series deoxygenation.

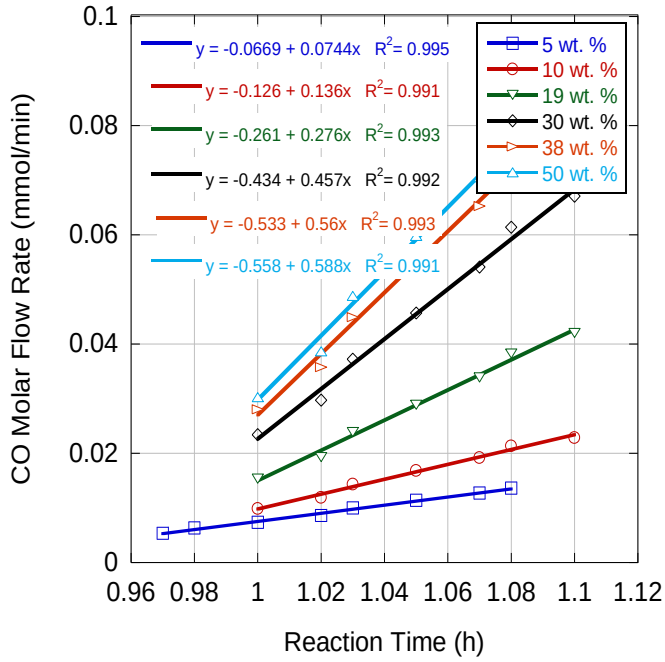

Figure A.2: Initial rates of CO production from LA concentration series deoxygenation.

Table A.2: Summary of CO and CO_2 initial rate and batch productivity analysis from LA, MA, and PA deoxygenation over 5 wt. % Pd/C (E117) at 300 °C and 15 bar under 5 vol. % H_2.

FA	**FA Conc. (mol. %)**	**CO Initial Rate ($mmol/g_{cat}$-h)**	**CO_2 Initial Rate ($mmol/g_{cat}$-h)**	**Batch Productivity ($mmol/g_{cat}$-h)**
LA	4	2.46	17.9	18.0
	8	4.51	13.1	23.2
	17	9.14	8.19	27.1
	23	13.5	7.67	17.9
	27	15.1	10.1	14.8
	27	14.6	8.18	13.7
	34	18.6	8.51	13.2
	46	19.5	7.83	11.1
MA	4	2.29	25.7	-
PA	4	1.74	71.4	23.5
	8	4.02	38.4	31.1
	17	10.1	26.8	43.1
	38	20.4	19.9	19.4